– Integrated Master in Chemical Engineering –

Numerical simulation of transport phenomena in a bacteria trapping device

by

Patrícia da Costa Moura

Faculty of Engineering, University of Porto

Research performed at

Laboratory of Protection and Physiology, EMPA

St. Gallen, Switzerland

Supervisor at EMPA: **Dr. Tiago Sotto Mayor**

Supervisor at FEUP: **Prof. João Campos**

Porto, February 2016

Acknowledgements

First and foremost, I would like to acknowledge Dr. Tiago Sotto Mayor for the guidance and invaluable advice provided throughout my thesis. I am also thankful to him for encouraging autonomous work. I would like to thank my supervisor at the University, Professor João Campos.

I am grateful to EMPA for the financial support and the opportunity to take part in this enriching experience.

Last but not the least, I want to thank my family and friends for the continuous support and companionship, despite being almost two thousand kilometres away.

Abstract

In the past two decades, microfluidic devices have been widely improved and developed in a variety of chemical and biological applications, such as crystallization, micro/nano-particle synthesis, polymer engineering, immunology and clinical diagnosis. This project focussed on a new microdevice for application in the biology field, to aid in experimental studies of bacteria growth. The device aims at trapping bacteria in a confined space, continuous supply of nutrients and removal of metabolic products, growth of bacteria in monolayer and easy observation of bacteria metabolic responses to medium changes. For its fabrication, the selection of the optimal parameters should be carefully pondered according to the experimental limitations, e.g. pressure drop/flow rate limits of the micropump, precision of the available manufacturing methods and biological requirements of bacteria motion in a confined channel.

In this project, computational fluid dynamics (CFD) was used to investigate the parameters affecting motion and trapping of bacteria in the device, as well as the conditions that promote a better nutrient distribution. A 2D numerical computation model was developed and validated against literature data.

The results indicate that bacteria trapping is enhanced by narrower feed channel, shorter microchannels, longer devices and higher ratio between the average velocities of the feed and waste inlet streams. They also show that changes in the inlet average velocity of the feed channel and in the microchannel density does not produce a significant effect on bacteria trapping.

Keywords: CFD, Microfluidics, Hydrodynamic trapping, Bacteria

Resumo

Dispositivos em microescala têm vindo a ser amplamente desenvolvidos nas últimas duas décadas, para uma variada gama de aplicações na área da química e da biologia, como por exemplo, cristalização, síntese de micro e nano partículas, engenharia de polímeros, imunologia e diagnóstico clínico. Este projecto foca-se num novo dispositivo para aplicação na área biológica, para auxiliar em estudos experimentais sobre crescimento de bactérias. O dispositivo visa a captura das bactérias em espaços confinados, acesso contínuo a nutrientes e remoção de produtos metabólicos, crescimento em monocamada e observação facilitada das respostas metabólicas das bactérias a alterações do meio. Para a sua manufactura, os parâmetros óptimos devem ser cuidadosamente escolhidos de acordo com as limitações experimentais, nomeadamente a queda de pressão ou o caudal limite das micro-bombas, precisão dos métodos de fabrico disponíveis e restrições do movimento de bactérias num canal confinado.

Neste projecto, recorreu-se à técnica de *computational fluid dynamics* (CFD) para estudar quais os parâmetros do dispositivo que promovem a captura das bactérias, bem como as condições que promovem uma melhor distribuição dos nutrientes. Um modelo computacional em 2D foi desenvolvido e validado comparando com dados presentes na literatura.

Os resultados mostram que a captura das das bactérias é potenciada por canais de alimentação mais estreitos, microcanais mais curtos, dispositivos mais longos e maior razão entre as velocidades médias das duas correntes de entrada. Além disso, mostram que alterações na velocidade média de entrada no canal de alimentação e na densidade de microcanais não produzem efeitos significativos na captura das bactérias.

Palavras-chave: CFD, Microfluidica, Captura hidrodinâmica, Bactérias

Table of contents

List of Figures

List of Tables

Nomenclature

A	Cross-sectional area of the channel	[m^2]
AR	Aspect ratio of the channel (= H/W)	[-]
C_c	Concentration of species c	[$mol.m^{-3}$]
D_c	Diffusion coefficient of species c in a solvent	[$m^2.s^{-1}$]
D_h	Hydraulic diameter of the channel (= $4A/P_w$)	[m]
d_p	Particle diameter	[m]
$\vec{f}$	Vector of the total body forces applied to the fluid elements	[N]
$\vec{F}$	Vector of the total forces applied to the particle	[N]
$\vec{F}_D$	Drag force vector	[N]
$\vec{F}_{ext}$	Total external force vector	[N]
$\vec{F}_g$	Gravitational force vector	[N]
H	Channel height	[m]
L	Channel length	[m]
L_{in}	Length from the inlet to the 1st microchannel wall	[m]
L_m	Microchannel length	[m]
L_{out}	Length from the last microchannel wall to the outlet	[m]
L_{sp}	Space between microchannels	[m]
m_p	Particle mass	[kg]
n_i	Number of grid points	[-]
N_p	Number of particles	[-]
N_μ	Number of microchannels	[-]
P	Pressure	[Pa]
Pe	Péclet number	[-]
P_w	Wet perimeter	[m]
Re	Reynolds number	[-]
R_p	Particle radius	[m]
sp	Space between particles	[m]
St	Stokes number	[-]
t	Time	[s]
U	Fluid velocity magnitude	[$m.s^{-1}$]
$\vec{U}$	Fluid velocity vector	[$m.s^{-1}$]
U_{aver}	Average fluid velocity	[$m.s^{-1}$]
$\vec{U}_p$	Particle velocity vector	[$m.s^{-1}$]
VR	Velocity ratio (=U_f/U_w)	[-]
W	Channel width	[m]
x, y, z	Coordinate values in space	[m]
η	Fluid kinematic viscosity	[$m^2.s^{-1}$]
μ_f	Fluid dynamic viscosity	[Pa.s]

ρ_f	Fluid density	[kg.m^{-3}]
ρ_p	Particle density	[kg.m^{-3}]
τ_p	Particle characteristic time (= $\rho_p d_p^2 / 18\mu_f$)	[s]

Subscripts

in	Inlet
out	Outlet
f	Feed channel
w	Waste channel
m	Microchannel

1. Introduction

Bacterial growth has been studied for many years, from batch to continuous flow processes. Understanding bacterial growth is very important and useful in clinical applications, namely the way it can affect diagnosis and treatment of infections. Microfluidics has been a novel area in the study of bacteria growth by developing devices capable of trapping bacteria in confined spaces. However, there are still some limitations on the existing devices. In order to gain further insight on bacterial growth and general behaviour, the development of new microdevices is important.

1.1. Scope of the project

The goal of this project is the development of a new bacteria trapping microdevice. The purpose of this device is to allow continuous supply of nutrients and removal of metabolic products, trapping of bacteria in a confined space to prevent new formed cells to overlap (and affect imaging analysis), monitoring a controlled number of bacteria per microdevice region (cells arranged in a chain rather than clustered together) and observing metabolic responses to changes in the environment (by introduction of different media streams without affecting trapping).

1.2. EMPA

As an institution of the ETH domain, EMPA (Swiss Federal Laboratories for Materials Science and Technology) is an interdisciplinary research institute which main focus is to meet the requirements of industry and the needs of the society, and link applications-oriented research to the practical implementation of innovative ideas. EMPA employs around one thousand scientists, engineers, general staff and students. The current project was developed in the Laboratory for Protection and Physiology (401), in collaboration between *Heat and Mass transfer* and *Functional membranes* group.

1.3. Contribution of the study

This thesis will contribute to the design of a bacteria trapping microdevice, by giving a first insight about its performance.

A numerical model was developed and implemented to simulate transport phenomena in the microfluidic device (Figure 2.4), considering fluid flow, bacterial motion and transport of nutrients. Systematic studies were performed for different device geometries and operating conditions, in order to investigate parameters that affect bacteria trapping, namely feed channel width (W_f), device length (L_μ), microchannel density (N_μ/L_μ), microchannel length (L_m), feed to waste inlet velocity ratio (VR) and average inlet velocity of the feed channel (U_f). The distribution of nutrients was also analysed regarding two trapping strategies.

1.4. Layout of the thesis

This thesis is structured in five sections. Section *2 Context and State of the art* gives general background information on bacteria growth, microfluidics and computational fluid dynamics, presents the main equations on fluid flow, mass transfer and particle motion, and the main assumptions on device configuration/performance. The numerical model developed during this project is thoroughly described in Section *3 Computational modeling* and validated in Section *4 Validation*, by implementing it to simple problems. In Section *5 Results and discussion*, first numerical results on the microdevice are shown and discussed: study of bacteria trapping in a base model device and the effects of changing size parameters and operating conditions; discussion on possible trapping strategies; and analysis of mass transfer (feeding and removal of secreted products). The main conclusions and prospect for future work are discussed in section *6 Conclusions*.

2. Context and State of the art

Bacterial growth, which consists in the cell division of a bacterium into two daughter cells, has been studied for many years, being batch procedures the most utilized. One of those techniques is using a Petri dish, which consists of a plate with fixed initial amount of nutrients, for bacteria to growth. In this media, bacteria multiplies until one necessary growth factor becomes depleted (usually the amount of nutrients). If no additional nutrients are added, no further growth takes place and a stationary phase is reached. After that, bacteria start dying due to the lack of nutrients and the accumulation of its own metabolic products (death phase).

Solutions to the problem of nutrient shortage were early found in macroscale by implementing a continuous flow technique (Herbert et al., 1956). However, this technique provides average results of bacteria population and therefore there is no control on single bacteria and their individual behaviour. For that reason, a growing number of new strategies/devices for bacteria trapping have been developed, through microfluidics, to achieve precise control of bacteria position, i.e. confine the bacteria for easy monitoring.

Microfluidics is a research area that consists on the manipulation of fluids in channels with dimensions of the order of micro- or nanometres. This field is very attractive compared to the macroscale because it offers a thorough control of the fluid flow and particle motion. In the past two decades, many techniques have been improved and developed for a wide range of chemical and biological applications, e.g. crystallization (Puigmartí-Luis, 2014; Whitesides, 2006; B. Zheng et al., 2004), polymer engineering (Kuhn et al., 2011; Peyman et al., 2009; Puigmartí-Luis et al., 2011), micro-particle synthesis (Faustini et al., 2013; Hyun et al., 2014; Nightingale and de Mello, 2010), immunology (Boedicker et al., 2008; Junkin and Tay, 2014; S. Kim et al., 2010; Nie et al., 2007; Wu et al., 2009) and clinical diagnosis (Mckay, 2011).

Strategies for trapping particles were reported by Nilsson *et al.*(2009) including those which apply acoustic, electric, magnetic and optical fields. Despite the importance of these techniques, the particles must have specific characteristics to be trapped. In the other hand, combination of flow properties with geometry configurations have been used for quantum dots synthesis (Nightingale et al., 2013), phase-change materials synthesis (Hyun et al., 2014) and protein crystallization (Gerdts et al., 2006; B. Zheng et al., 2004) through droplet formation (creation of an immiscible layer between a fluid/mixture and a carrier fluid); for controlled formation of polymer fibres (Kuhn et al., 2011; Puigmartí-Luis et al., 2011, 2010) via flow focusing (use of shear stress of two fluids co-flowing in a straighter channel to create a controlled interface); and for single-particle monitoring (M Tanyeri et al., 2011; M Tanyeri and Schroeder, 2013; Xu et al., 2013) and multiple particle/cell trapping (Choi et al., 2008; Hur et al., 2011).

More recently, microfluidics has been used to locate bacteria colonies in controlled areas/chambers of microdevices (e.g. Figure 2.1a), in order to monitor their evolution (Grünberger et al., 2012; Westerwalbesloh et al., 2015). Eun et al. (2011) developed a technique to encapsulate bacteria in agarose microparticles, in which bacteria grow into colonies (Figure 2.1b). In order to analyse single cell behaviour Tanyeri et al. (2010), Choi et al. (2008) and Kim and Klapperich (2010)

advanced strategies to trap single bacterium, by using hydrodynamic forces, wells and physical traps, respectively. Banaeiyan et al. (2013) also tested a continuous flow trapping method (Figure 2.1c) but with mammalian cells (which are up to ten times bigger than bacteria).

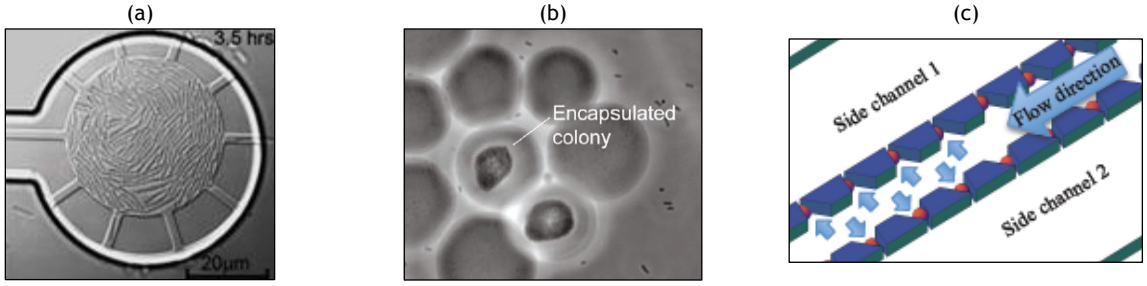

Figure 2.1 – Cell trapping in microfluidic devices: (a) multi-trapping of bacteria and colonial growth inside a chamber (Grünberger et al., 2012); (b) trapping of single bacteria by encapsulation and colony formation inside the particle (Eun et al., 2011); (c) trapping of single mammalian cells in orthogonal microchannels (Banaeiyan et al., 2013).

In the framework of this Master thesis, a preliminary idea of a new microdevice for trapping bacteria was developed. The purpose of such a device is to offer solutions in the biology field, in a single device: continuous supply of nutrients and efficient removal of metabolic products secreted by bacteria (i.e. avoid nutrient shortage and waste accumulation); bacteria growth in monolayer to enable clear image analysis (for example through microscopy) without being affected by overlapped bacteria; monitor individual behaviour while allowing new-formed bacteria to be close to the mother cell; and observe metabolic responses to changes in the medium (in order to recreate environmental variations). Before manufacturing any device one should understand which configuration/conditions promote its performance, in this case that lead to the optimization of bacteria trapping.

Computational fluid dynamics (CFD) is a fundamental tool in engineering to perform numerical analysis on fluid flow. As small devices are being more and more developed and applied in different areas (e.g. chemistry, biology …) it is important to learn how the fluid flow behaves in these microscale geometries, which can be done through CFD based software (as the FEM platform used in the current project). CFD was already applied for many microfluidic applications, namely, electrophoretic transport (Charhrouchni et al., 2013; Low et al., 2014), flow in sudden expansions (Tsai et al., 2006), mixing strategies (Jeon and Shin, 2009; Sarkar et al., 2014), particle motion (Xu et al., 2013) and droplet formation (Li et al., 2012; Vladisavljević et al., 2014; Wehking et al., 2015). Numerical results, besides supporting the understanding of fluid flow in a microdevice, allow obtaining data with low cost when compared to multi device fabrication and testing. Moreover, numerical simulation enables studying a wide range of parameters (that represent different devices/operating conditions) and go beyond the conditions available experimentally (e.g. test critical values/extreme conditions).

In fluid dynamics conservation of mass, momentum and energy must be considered in order to describe velocity, pressure and density fields. The continuity equation, which describes the conservation of mass (Kirby, 2010), is given by:

$$\frac{\partial}{\partial t}\int_{v} \rho_{\mathrm{f}}\,\mathrm{d}V = -\int_{S} \left(\rho_{\mathrm{f}}\vec{U}\right).\hat{n}\,\mathrm{d}A \qquad \textbf{Equation 2.1}$$

where ρ_{f} is the fluid density, t is the time, $\vec{U}$ the fluid velocity vector, dV the differential volume upon the control volume v , $\hat{n}$ the unit outward normal along the surface S and dA the differential area upon the surface S.

In microfluidics flow velocity is much smaller than the velocity of sound, so the fluid is considered incompressible (Bruus, 2011). In that case, i.e. when the density of the fluid is constant through space and time, the previous equation can be written simply as:

$$\nabla.\vec{U} = 0 \qquad \textbf{Equation 2.2}$$

In order to drive a fluid through a microchannel one needs a driving force such as pressure gradient, capillary effects or electric fields. Pressure-driven flow is achieved by imposing a pressure difference between the inlet and the outlet of the channel. To formulate the momentum conservation in a pressure-driven flow, Navier-Stokes equations are used:

$$\frac{\partial}{\partial t}\int_{v} \rho_{\mathrm{f}}\vec{U}\,\mathrm{d}V = -\int_{S} \left(\rho_{\mathrm{f}}\vec{U}\vec{U}\right).\hat{n}\,\mathrm{d}A + \int_{S} \vec{\vec{\tau}}.\hat{n}\,\mathrm{d}A + \int_{v}\sum_{i}\vec{f_i}\,\mathrm{d}V \qquad \textbf{Equation 2.3}$$

where $\vec{f_i}$ represents a body force vector and $\vec{\vec{\tau}}$ the surface stress tensor.

For an incompressible fluid the momentum equation can be rewritten in a differential form known as Cauchy momentum equation (Equation 2.4). In the particular case of a Newtonian fluid Equation 2.5 is valid (Kirby, 2010).

$$\rho_{\mathrm{f}}\frac{\partial\vec{U}}{\partial t} + \rho_{\mathrm{f}}\vec{U}.\nabla\vec{U} = \nabla.\vec{\vec{\tau}} + \sum_{i}\vec{f_i} = -\nabla P + \nabla.\vec{\vec{\tau}}_{visc} + \sum_{i}\vec{f_i} \qquad \textbf{Equation 2.4}$$

where ∇P represents the pressure forces and $\nabla.\vec{\vec{\tau}}_{visc}$ the viscous forces.

$$\underbrace{\rho_{\mathrm{f}}\frac{\partial\vec{U}}{\partial t}}_{\substack{Unsteady\\ acceleration}} + \underbrace{\rho_{\mathrm{f}}\vec{U}.\nabla\vec{U}}_{\substack{Convective\\ acceleration}} = \underbrace{-\nabla P}_{\substack{Pressure\\ gradient}} + \underbrace{\nabla.\eta\nabla\vec{U}}_{Viscosity} + \underbrace{\sum_{i}\vec{f_i}}_{\substack{Body\\ forces}} \qquad \textbf{Equation 2.5}$$

where η is the kinematic viscosity of the fluid.

In microscale, low-Reynolds numbers Re (Equation 2.6) are typical which enhances the laminar flow regime, i.e. the streamline pattern is ordered and regular.

$$\mathrm{Re} = \frac{\rho_\mathrm{f} U_\mathrm{aver} D_\mathrm{h}}{\mu_\mathrm{f}} \qquad \textbf{Equation 2.6}$$

where μ_f is the fluid dynamic viscosity, D_h is the hydraulic diameter and U_{aver} is the fluid average velocity.

As devices become smaller (and Reynolds number much inferior than 1), the viscous forces dominate over inertial forces and the influence of convection and gravity can be neglected. In these conditions, for stationary flow, Poisson equation is obtained:

$$\nabla P = \nabla . \eta \nabla \vec{U} \qquad \textbf{Equation 2.7}$$

This kind of flow, when driving through a tube/channel is known as Poiseuille flow (Bayraktar and Pidugu, 2006; Hardt and Schönfeld, 2007). When the cross-sectional area of the channel is rectangular (Figure 2.2), Equation 2.8 truncated at the third term (i = 5) gives a good approximation of the velocity profile in the streamwise direction (White, 1974, p. 120).

$$U_x(y,z) = \frac{4H^2 \Delta P}{\pi^3 \mu_f L} \sum_{i=odd}^{\infty} \frac{1}{i^3} \left[1 - \frac{\cosh\left(i\pi \frac{y}{H}\right)}{\cosh\left(i\pi \frac{W}{2H}\right)} \right] \sin\left(i\pi \frac{z}{H}\right) \qquad \textbf{Equation 2.8}$$

where U_x is the velocity in the streamwise direction, y the coordinate along channel width W, z the coordinate along channel height H, L the device length and ΔP the pressure difference between inlet and outlet of the channel.

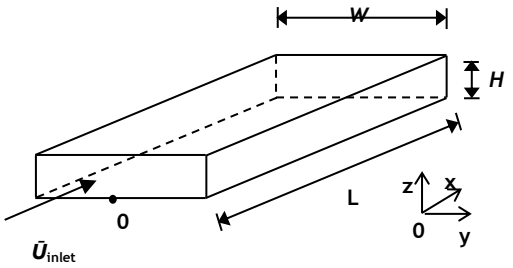

Figure 2.2 – Schematic view of a channel with length *L* and rectangular cross section with width *W* and height *H*.

The heat-transfer equation is responsible for guaranteeing the conservation of energy in a system. The power required to drive a fluid through a channel at a certain velocity generates viscous heating. In microfluidics, the viscous heating effect can be neglected due to large surface area to volume ratio that allows a quick dissipation of the heat. However, when electrical fields are applied, electrical energy is converted into thermal energy which causes resistive heating (Joule effect) that creates a more significant temperature shift in the fluid than viscous heating. In that case, one should take into account the heat transfer to prevent possible damages in the devices or any changes of flow properties (Becker and Locascio, 2002; Horiuchi and Dutta, 2004).

Distribution of nutrients and metabolic products is also important to accurately predict whether bacteria in the microdevice have access to a sufficient amount of nutrients or if the metabolic products do not exceed the limit amount after which they become detrimental to the bacteria.

In microscale the fluid streamline pattern is usually ordered and regular (laminar flow) enabling mass transfer to occur mainly by diffusion. For the limit of diluted solutions and low thermal gradients, Fick's first law (Equation 2.9) and Fick's second law (Equation 2.10) are applicable, in stationary and transient problems, respectively (Kirby, 2010).

$$\vec{J}_{\mathrm{diff,c}} = -D_{\mathrm{c}} \nabla C_{\mathrm{c}} \qquad \textbf{Equation 2.9}$$

where $\vec{J}_{\mathrm{diff,c}}$ is the flux of a species c by diffusion, D_{c} the diffusion coefficient of that species in a solvent, and ∇C_{c} the gradient of species concentration.

$$\frac{\partial C_{\mathrm{c}}}{\partial t} = \nabla.\left(D_c \nabla C_{\mathrm{c}}\right) - \nabla.\left(\vec{U} C_{\mathrm{c}}\right) \qquad \textbf{Equation 2.10}$$

For analysis of mass transport in the fluid, the species behaviour can be observed through the Péclet number (Pe), which is defined by the ratio between convection and diffusion effects (Equation 2.11).

$$\mathrm{Pe} = \frac{U_{\mathrm{aver}} D_{\mathrm{h}}}{D_{\mathrm{c}}} \qquad \textbf{Equation 2.11}$$

2.1. General assumptions

2.1.1. Carrier fluid

In this study pressure-driven flow is assumed and the system is considered isothermal. The most common media utilized to keep bacteria alive is an aqueous solution of phosphate buffer saline solution, PBS (Choi et al., 2008; Figueroa-Morales et al., 2015; Wu et al., 2009). Therefore, water (ρ_{f} = 1000 kg·m^{-3}, μ_{f} = 0.001 Pa·s) was the selected fluid to flow in the channels/device.

2.1.2. Bacteria morphology

Bacteria are microorganisms with typical size of 0.5-5.0 micrometres. There are diverse types, relating to the shape, being the most usual coccus, spirillum and bacillus which are spherical, spiral and rod-shaped, respectively, as seen in Figure 2.3. A frequently studied bacteria type is Escherichia coli which usually have a rod-shape configuration with length ranging from 1.5 to 5.5 μm and diameter from 0.5 to 1.0 μm (Nanninga, 1998), and multiple appendages, as flagella (Vigeant and Ford, 1997). Therefore, the motion of this kind of bacteria is influenced by the shear rate in the fluid flow, but also by flagella motion (i.e. swimming of bacteria). These microorganisms consist mostly of water so their density is

Figure 2.3 – Common shapes of bacterial cells: rod-shape, spherical and spiral (from left to right).

similar to that of water. For that reason, a density of 1040 kg.m^{-3} was selected[1]. In this study, one considered spherical bacteria with 1 μm diameter, and flagella motion was neglected. The flexibility of the cell membrane was also neglected which allows approximation of bacteria to rigid spherical bodies/particles.

To determine the evolution of the position of a particle in a continuous pressure-driven incompressible fluid flow the following equations (Kirby, 2010, p. 34) must be solved: conservation of mass (Equation 2.2) and conservation of momentum (Equation 2.5) for the fluid and Newton's second law (Equation 2.12) for the particle.

$$\sum \vec{F} = m_{\mathrm{p}} \frac{d\vec{U}_{\mathrm{p}}}{dt} \qquad \textbf{Equation 2.12}$$

where $\vec{F}$ is the vector of each force applied to the particle, m_{p} the mass of the particle and $\vec{U}_{\mathrm{p}}$ the vector of its velocity.

To evaluate particle motion in a fluid flow one should use the dimensionless Stokes number, defined as the ratio between the characteristic time of the particle τ_{p} and the characteristic time of the flow τ_{f}, given by (Wu et al., 2009):

$$\mathrm{St} = \frac{\rho_{\mathrm{p}} {d_{\mathrm{p}}}^2 / 18 \mu_{\mathrm{f}}}{D_{\mathrm{h}} / U_{\mathrm{aver}}} \qquad \textbf{Equation 2.13}$$

where ρ_{p} is the particle density and d_{p} the particle diameter.

This dimensionless number describes how quickly a particle adjusts to the changes in the surrounding flow. Low values of Stokes number (St << 1) are characteristic of particles that follow the fluid streamlines, in contrast to large Stokes numbers in which particles keep their original velocity direction instead of adjusting its trajectory to the fluid streamlines.

2.1.3. Device configuration

Microfluidic channels can be manufactured in polydimethylsiloxane (PDMS), silicon, thermoplastics, glass, stainless steel and ceramics. However the last three materials are too hard to form some elements of the device (e.g. valves). Despite silicon mechanical stability and resistance to high temperatures, this material is expensive and opaque to visible and ultraviolet light (which is inconvenient to imaging analysis). PDMS is the most common material in microfluidics since it is an optically-transparent soft elastomer[2], ductile, highly flexible, chemically and thermally stable, biocompatible and non-toxic (Skurtys and Aguilera, 2008; Whitesides, 2006). The PDMS surface is hydrophobic so it is difficult for polar solvents to wet the surface. Generally, PDMS devices undergo surface treatments, for example plasma oxidation, that transforms the hydrophobic surface in a hydrophilic one. This allows wetting of the polar solvent on the wall of the device and implies no-slip

[1] Value previously used by Kim and Klapperich (2010). Similar values (1.075 to 1.101 kg·m^{-3}) were used by Wu et al. (2009).
[2] It is easier to fabricate micro-systems in elastomers than in rigid materials.

boundary condition, i.e. a null velocity of the fluid element in contact with the walls. In this study a hydrophilic surface is assumed.

Figure 2.4a illustrates the device design. It consists of two main channels, one to release bacteria and provide nutrients, feed channel (left channel on Figure 2.4a), and other with a carrier fluid to assist trapping and removal of secreted products, waste channel (right channel on Figure 2.4a). Figure 2.4b shows the parameters selected to characterize the device dimensions and Table 2.1 presents the parameters values for a base model microdevice.

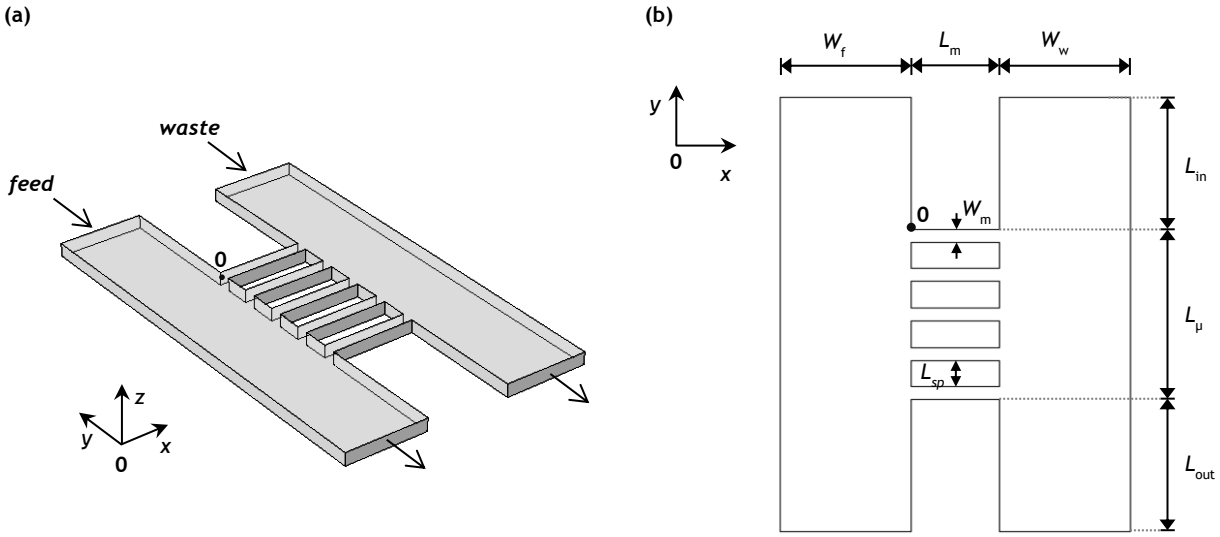

Figure 2.4 – 3D (a) and 2D (b) scheme of the microdevice and respective coordinate system.

Table 2.1 – Parameters of a microdevice model, its values and units.

Parameter	Description	Value	Unit
H	Device height	1.5	μm
W_f	Feed channel width	30	μm
W_w	Waste channel width	30	μm
W_m	Microchannel width	1.5	μm
L_{in}	Length from the inlet to the 1st microchannel wall	50	μm
L_{out}	Length from the last microchannel wall to the outlet	15	μm
L_{sp}	Space between microchannels	3	μm
L_m	Microchannel length	10	μm
N_μ	Number of microchannels	50	-
L_μ	Device length/length with microchannels	222	μm
N_μ/L_μ	Microchannel density	0.22	μm^{-1}

3. Computational modeling

3.1. Hardware and software

The machine used in this study[1] had 15 GB RAM. Simulations were performed in COMSOL Multiphysics 5.1, using 10 processors in each simulation.

3.2. Geometry

Figure 2.4 shows a base model of a microdevice for trapping bacteria. 2D numerical simulations were performed for the middle height plan of the device (*x*0*y*) to study design and working parameters.

3.2.1. Sub-domains

The geometry[2] is shown in Figure 3.1. It consists of two main channels and a selected number of orthogonal microchannels (N_μ) in which bacteria should enter. The previous channels are further referred to as *feed channel*, *waste channel* and *microchannel* M_1, M_2, …, $M_{N\mu}$, respectively.

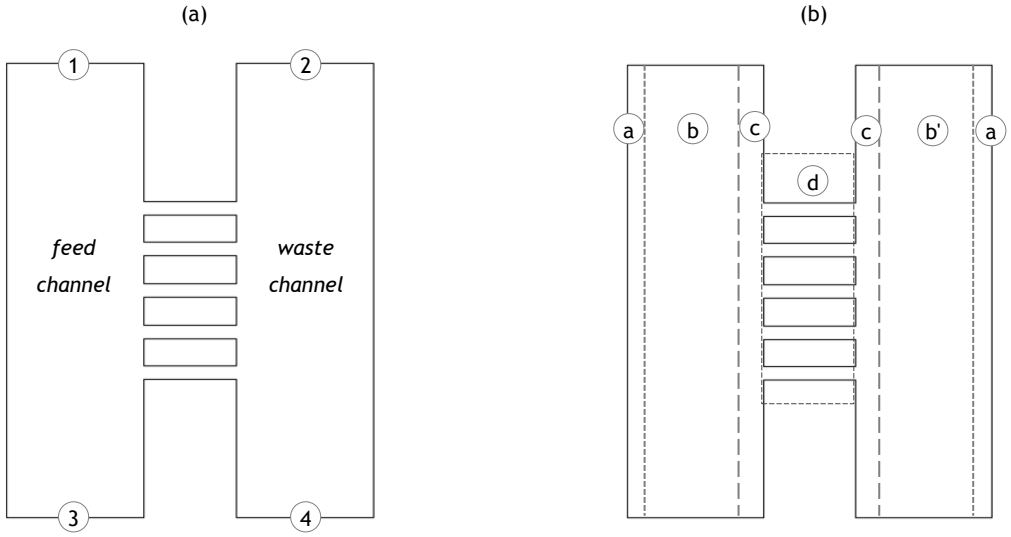

Figure 3.1 – 2D representation of the middle height plan of the microdevice model. (a) Geometry boundaries: 1-inlet of the feed channel, 2-inlet of the waste channel, 3-outlet of the feed channel, 4-outlet of the waste channel. (b) Different areas created for mesh refinement.

3.2.2. Boundaries

The device has one inlet and one outlet for each main channel, marked with numbers in Figure 3.1a. The remaining boundaries correspond to the channel walls.

Feed and waste channels inlet boundaries (1 and 2) were defined through inlet average velocities U_f and U_w and the outlet boundaries (3 and 4) defined through null relative pressure. Due to the

[1] Cases V, VI for W_f = 3 and 5 μm and Cases VII and VIII for L_μ = 447 μm were performed in a machine with 30 GB RAM.
[2] Please refer to Annex A – Geometry.

hydrophilic nature of the channels' surface, null velocity in the walls was assumed (no-slip boundary condition).

Two settings regarding contact of particles with the boundaries were imposed: when they collide with channel walls particles were set to freeze and when they reach the outlet they disappear. On the waste channel outlet, particles were also set to freeze to allow automation of bacterium counting[1].

3.3. Modules

When particle diameter is similar to the channel width, particle motion affects and is affected by fluid flow (Al Quddus et al., 2008; Dechadilok and Deen, 2006). In this study, in the microchannels, particles/bacteria (d_p = 1 µm) occupy approximately 70% of the channel width (W_m = 1.5 µm). However, given the need to run an extensive series of parametric analyses to explore different possibilities about the design and operating conditions of the device, preference was given to the computationally less expensive approach. Thus, a one-way approach was selected, i.e. fluid flow was assumed not to be affected by the presence of the bacteria. This selection is further clarified in Annex B.

As fluid flow does not change in time, two study steps were considered[2]: one stationary step, that solves the fluid flow, and a time dependent step that determines bacteria trajectory.

Considering values of Reynolds number much smaller than 1, the modeling of fluid flow was established by the COMSOL module *Laminar flow*. In this module one assumed incompressible Stokes flow (Re « 1) in shallow channels with a finite height. This way, the shear stress acting on fluid flow, caused by the proximity of the upper and lower walls of the device, is considered.

Figure 3.2 - Positioning of particles at the feed channel entrance. The 1st bacteria, the one on the right, is spaced by *sp*/2 µm from the channel wall, and the following bacteria are spaced by *sp* µm. The last bacteria (on the left) is also distanced from the channel wall *sp*/2 µm.

Bacteria motion, which does not affect fluid flow, was achieved by implementing the module *Particle tracing for fluid flow*. This module solves the trajectory of a number of particles N_p neglecting particle-particle interactions, thus the numerical results correspond to the trajectory of single bacteria released independently[3]. In this case 25 bacteria, equally separated from each other and aligned in the *x*-direction (Figure 3.2), were released from the feed channel inlet boundary ($y = -L_{in}$). A parameter *sp* was set[4] to describe the initial (t = 0) location of the bacteria. The 1st bacterium is located at *sp*/2 micrometres from the wall closer to the microchannels and the last

[1] Strategy presented in Annex E – Particle motion.

[2] This approach is less time consuming than solving both modules in a single time dependent study.

[3] As seen in section 5, this model allows determining the percentage trapped bacteria, which is the ratio between the number of bacteria that enter the microchannels and the number of released bacteria. This value is equivalent to the percentage of the feed channel width in which the placed bacteria will enter the microchannels within an uncertainty of $1/(2N_p)$ x 100 %.

[4] Space between bacteria correspond to the ratio between feed channel inlet and the number of released particles ($sp = W_f/N_p$).

bacterium is located at *sp*/2 from the opposite wall. The bacteria are separated from each other by *sp* micrometres.

Particle tracing module allows two types of particle formulations: massless that, as the name suggests, does not consider particle mass; and Newtonian, the one selected in this study, that implements Newton's second law to determine particle motion. Hence, the total force applied in the particle is defined by the sum of the drag force, given by $\vec{F}_D = \left(\frac{1}{\tau_p}\right) m_p(\vec{U} - \vec{U}_p)$, the gravitational force (equal to zero since simulations are carried out at a specific height) and other external forces[1] (also equal to zero).

3.4. Parametric analysis

The aim of this study is to understand which parameters/variables enhance the entrance of bacteria on the microchannels. Hence, the effects of velocity ratio (U_f/U_w), feed channel inlet average velocity (U_f), feed channel width (W_f), length with microchannels (L_μ), microchannel density (N_μ/L_μ) and microchannel length (L_m) were analysed (see Table 3.1). Table 3.2 shows the parameters assumed constant (except where mentioned otherwise) throughout the numerical simulations.

Table 3.1 – Parameter values for each parametric Case analysed. Device length and microchannel density were defined by changing the number of microchannels and the space between them (presented in Table H.1).

Case	$VR = U_f/U_w$ [-]	U_f [mm·s^{-1}]	W_f [µm]	L_μ [µm]	N_μ/L_μ [µm^{-1}]
I	100, 50, 20, 10, 5, 2, 1	1	30	42	0.22
II	100, 50, 20, 10, 5, 2, 1	1	30	222	0.22
III	100, 50, 20, 10, 5, 2, 1	1	10	42	0.22
IV	100, 50, 20, 10, 5, 2, 1	1	10	222	0.22
V	100	1	30, 20, 10, 5, 3	222	0.22
VI	2	1	30, 20, 10, 5, 3	222	0.22
VII	100	1	30	19.5, 42, 87, 222, 447	0.22
VIII	2	1	30	19.5, 42, 87, 222, 447	0.22
IX	100	1	30	150	0.22, 0.33, 0.44
X	100	1	10	150	0.22, 0.33, 0.44
XI	100	1, 0.5, 0.3, 0.1, 0.05	30	42	0.22
XII	100	1, 0.5, 0.3, 0.1, 0.05	10	42	0.22
XIII	2	1, 0.5, 0.3, 0.1, 0.05	30	42	0.22
XIV	100	1	30	42	0.22
XV	100	1	10	42	0.22
XVI	20	1	30	42	0.22
XVII	20	1	10	42	0.22
XVIII	1	1	30	42	0.22
XIX	1	1	10	42	0.22

Table 3.2 – Constant parameter values, for the microdevice, fluid and particle, throughout the simulations (except where mentioned otherwise).

Device						Fluid		Bacteria		
H [µm]	L_{in} [µm]	L_{out} [µm]	W_w [µm]	W_m [µm]	L_m [µm]	ρ_f [kg·m^{-3}]	μ_f [Pa·s]	ρ_p [kg·m^{-3}]	R_p [µm]	N_p [-]
1.5	50	15	30	1.5	10	1000	0.001	1040	1	25

The parametric studies performed are labelled from Case I to Case XIX. In total, 70 combinations of parameters were simulated. The model was prepared to automatically update geometry, equations and mesh when changes in input parameters occur. However, the version of COMSOL used

[1] Other forces might be originated by magnetic, electric or Brownian effects. No magnetic or electrical fields are applied; non-Brownian particle is considered (particle much bigger than fluid molecules).

in this study does not allow introduction of parameters in particle release settings. Therefore, manual update of particle tracing module is required when bacteria initial position varies.

3.5. Meshing

Two types of parametric studies were executed: changes in operating conditions (U_f, VR) and changes in device geometry (W_f, L_μ, N_μ/L_μ, L_m). Grid independence test[1] was executed, for a fixed geometry (W_f = 30 μm, N_μ = 5, L_{sp} = 3 μm), for the case where bigger gradients are expected (U_f = 1 mm·s^{-1}, VR = 100). An unstructured mesh with triangular elements was employed, with increased density in the vicinity of the channel walls. The geometry was divided in several areas according to the refinement need (Figure 3.1b). In each zone, the maximum element size is controlled by W_f, W_w, W_m, n_f, n_w and n_m as described in Table 3.3. W_f, W_w and W_m represent the feed channel, waste channel and microchannel widths, respectively, and n_f, n_w and n_m represent the minimum number of points created by the grid elements, in each area. The maximum element size applied on the wall boundaries is also presented in Table 3.3. The presented ratios were used in all the simulations in order to guarantee grid independence of the numerical results for the Cases where device configuration changes. Values of n_f, n_w and n_m were kept constant (and equal to 15).

Table 3.3 – Maximum element size values used in the different zones (Figure 3.1b) for domain meshing.

Mesh refinement zones	Maximum element size
Area a	2 x W_m/n_m
Area b	W_f/n_f
Area b'	W_w/n_w
Area c	1.5 x W_m/n_m

Mesh refinement zones	Maximum element size
Area d	W_m/n_m
Feed channel walls	0.95 x W_f/n_f
Waste channel walls	0.95 x W_w/n_w
Microchannels walls	0.95 x W_m/n_m

3.6. Time discretization

For the time-dependent part of the simulations, a time step of 0.1 ms was found[2] to be suitable to describe particles trajectory. The total solution time for each simulation is set according to the feed channel inlet average velocity and device length. The former time step refers to data-saving time stepping. The solver time step was defined as *strict* through the *Generalized-alpha* method[3], in order to force the solver to take time steps that end in the solution times, and take additional steps in between, if necessary (COMSOL, 2013).

3.7. Discretization and convergence criteria

The aforementioned unstructured meshes were used for discretization of the domain. Second-order elements and linear elements were used for velocity and pressure fields, respectively, for fluid discretization. The relative tolerance for fluid velocity and pressure calculation was set to 10^{-5} and the absolute tolerance for particle position to 10^{-6}.

[1] Please refer to Annex C – Grid independence test.
[2] Please refer to Annex D – Time-step dependence test.
[3] Suitable for transport problems (COMSOL, 2013).

Additionally, values of mass imbalance[1] (Equation G.2) were determined in order to check conservation of mass. Reynolds number (Equation G.6) and Stokes number (Equation G.7) were monitored for the main channels and for microchannel $M_1^{(2)}$, in order to ensure the applicability of the model simplifications for the flow and bacteria motion, in all the simulations.

3.8. Model simplification

In this study, Stokes number is much lower than 1, i.e. trajectory of particles is the same as the flow streamline[3] (Wu et al., 2009). Therefore, solving only the stationary step for fluid flow gives the necessary information about bacteria positioning. For the purpose of knowing how many bacteria enter/pass the microchannels, the mentioned approach (selected in this study) implies manually counting of the streamlines, but with lower calculation times[4].

In the following sections, one should keep in mind that no particles/bacteria are introduced in the domain. Wherever mentioning the percentage of released bacteria that enter the microchannels, it corresponds, in fact, to the percentage of the fluid streamlines that leave the feed inlet and enter the microchannels.

3.9. Model for the nutrients transfer studies

For the mass transfer studies, numerical simulations were performed in a device similar to the base model (Table 2.1) but with just 3 microchannels (L_μ = 10.5 μm). In the middle of each microchannel a circumference was considered to account for the presence of a spherical bacterium. In the initial moment all the domain had null concentration. In the feed inlet boundary, a concentration $C_{glucose,feed}$ was set.

In total, four simulations were performed: two to determine solutions along time (for feed to waste velocity ratios of 1 and 100) and two to determine the corresponding steady state solutions. The model applied consists in two steps: one stationary to solve the fluid flow and one time-dependent/stationary to solve the transfer of glucose along time/at steady state. For the transient step, a time range of 700 ms and a solution time step of 2.5 ms were selected. The section of the model applied for the parametric studies which solves the fluid flow is maintained equal. To solve the mass transfer of glucose one selected the *Transport of diluted species* module which determines the concentration field of a diluted solute in a solvent by diffusion and convection phenomena. Defining the diffusion coefficient of the solute in the solvent is required to solve diffusion.

The discretization of the domain was defined by unstructured meshes similar to the ones described in section 3.5 with increasing refinement (i.e. smaller mesh elements) near the bacteria surface (Figure 3.3). The maximum element size of those elements was set to 0.025 μm. Second-order elements were used for concentration discretization. By assuring an adequate discretization, numerical/artificial diffusion does not influence the numerical results.

---

[1] Relative difference between inlet and outlet total mass flow rates.

[2] On the following microchannels de pressure drop is inferior and consequently the average velocity is also inferior. Re and St are proportional to the average fluid velocity. Therefore, if the microchannel M1 fulfils the requirement, the following microchannels will too.

[3] Please refer to Annex E – Particle motion.

[4] For other studies an evaluation between simulation time and post-processing effort must be done (Annex E).

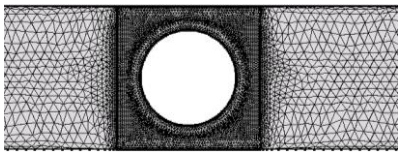

Figure 3.3 – Representation of the mesh elements in a microchannel with a bacterium. Mesh elements near the bacterium are smaller than in the remaining microchannel domain.

The absolute tolerance for concentration calculations was set to 10^{-4}. The values of mass imbalance (Equation G.2) and molar imbalance (Equation G.3) were determined in order to check conservation of mass and species quantity. Reynolds number (Equation G.6) was also monitored for the main channels and for microchannel M_1, in order to ensure the applicability of the model simplifications.

4. Validation

In order to ensure that the obtained results are accurate and representative of the reality, one should compare the results with experimental/numerical solutions. As the microdevice in study was not yet fabricated[1], no experiments were done. Therefore the computational model was validated by applying it to cases that represent the studied phenomena and comparing the obtained results to theoretical, experimental or numerical data. Validation was performed in two steps: validation of fluid flow; and validation of transfer of nutrients in a continuous flow.

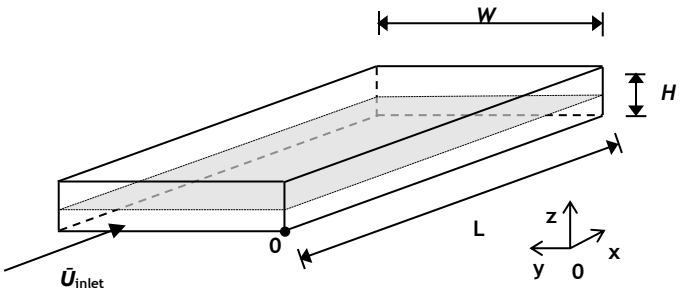

Figure 4.1 – Schematic view of a channel with constant (and rectangular) cross section and highlighted middle height plan (parallel to x0y). Dimensions and coordinate system associated.

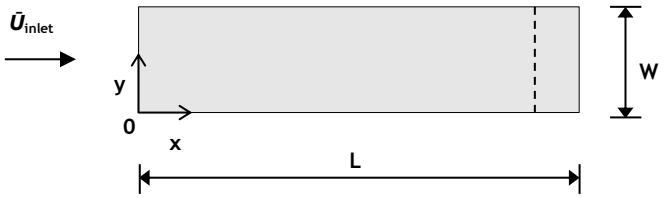

Figure 4.2 – Geometry used in the 2D simulations of a rectangular microchannel. Dimensions and coordinate system associated.

To validate the 2D model for the fluid flow, one conducted a numerical study on laminar pressure-driven flow through a simple microchannel. This geometry was selected because the base geometric elements of the current microdevice are microchannels with constant cross-sectional area. Figure 4.1 illustrates the configuration of the studied channel, featuring length *L* and rectangular cross-section with aspect ratio $AR = H/W$, in which *H* represents the shorter dimension (channel height) leading to $0 < AR \leq 1$. Figure 4.2 shows the employed geometry which corresponds to the top view of the middle height plan ($z = H/2$). Numerical simulations were performed in several (1.5 μm high) devices with different aspect ratios, i.e. ratios between channel height and channel width, equal to 0.05, 0.075, 0.15, 0.3, 0.5 and 1. The values of *AR* were defined according to the range of channel widths studied during the project for the present microdevice (*W* = 30, 20, 10, 5, 3 and 1.5 μm). The numerical results were compared with a 3D theoretical correlation (Equation 2.8) for fluid flow in rectangular ducts (Nguyen and Wereley, 2002, p. 35; White, 1974, p. 120). Figure 4.3 shows the velocity along normalized *y* direction, i.e. along channel width, for a fully developed flow in steady state, for selected aspect ratios. Figure 4.4 gives the maximum error between maximum

[1] One of the final applications of this project is to assist the selection of the device configuration.

velocity determined by Equation 2.8 and maximum velocity obtained by the 2D numerical simulations with the present model.

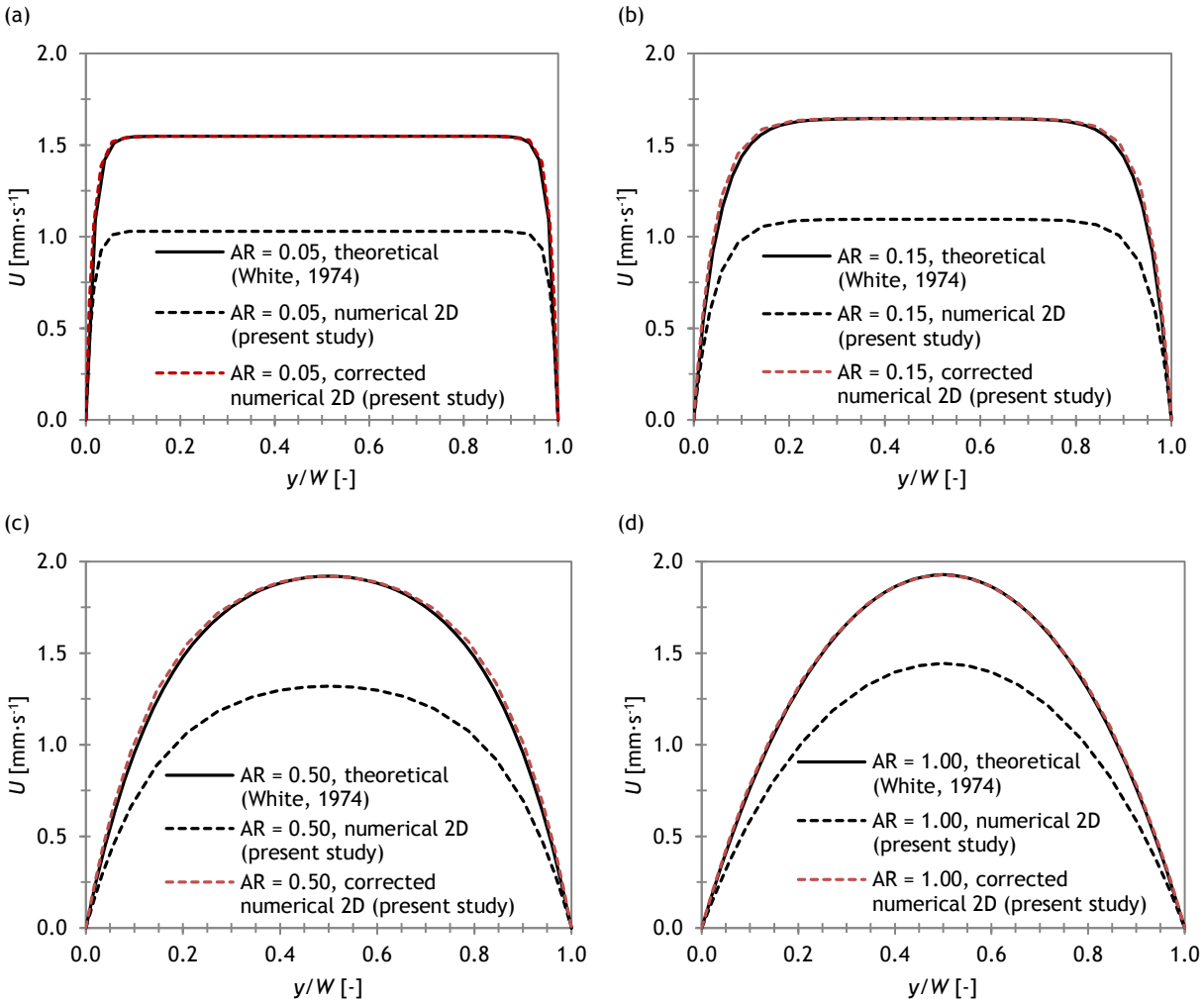

Figure 4.3 - Comparison of theoretical and numerical velocity profiles along channel width, at $x = L$, for aspect ratios ($AR = H/W$) equal to (a) 0.05, (b) 0.15, (c) 0.50 and (d) 1.00.

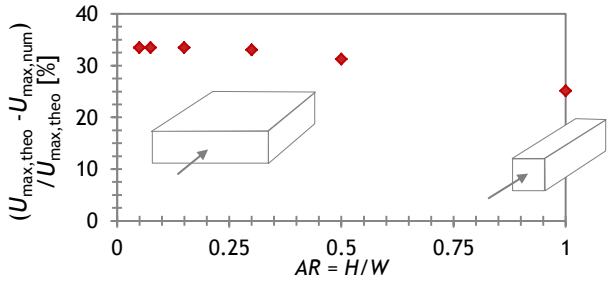

Figure 4.4 - Relative difference between numerical and theoretical maximum velocity for aspect ratios from 0 to 1.

When a 2D simulation is performed for fluid flow in a rectangular plan using this FEM platform, the velocity field calculations are based on an infinitely high channel. Adding a drag force term (by selecting the option *shallow channel approximation*), as done in the current model, indicates that the channel has a rectangular cross section (i.e. finite height). However, as seen in Figure 4.3 and Figure 4.4, the present model underestimates the velocity by 25 to 33%, when H = 1.5 μm. Nonetheless, the velocity profile curves tendency is identical, trend that can be seen by multiplying the nu-

merical velocities by $U_{max,theo}/U_{max,num}$ (Figure 4.3, corrected numerical 2D lines). For high velocity ratios, i.e. when channel width is similar to channel height, the velocity profile tends to a parabolic curve (Figure 4.3d). In the other hand, for low velocity ratios, i.e. for channel widths larger than channel height, the velocity profile acquires a flat configuration (constant velocity along channel width except very close to the walls).

The correlation to which the numerical data was compared (Equation 2.8) was widely validated in the past by experimental and numerical data. In this section one analysed the works of Zheng and Silber-Li (2008), who evaluated the streamwise velocity profiles experimentally by micro particle image velocimetry (μ-PIV) technique, and of Kashaninejad et al. (2012), who obtained numerical results for the velocity profiles using a 3D finite element method. 2D numerical simulations were performed in two channels, according to the previously mentioned literature, with the following features: a 19.1 μm high, 27.9 mm long channel, with aspect ratio AR = 0.35 and imposed pressure drop along the channel of 34000 Pa (X. Zheng and Silber-Li, 2008); and a 20 μm high, 1 mm long channel, with aspect ratio AR = 1/3 and imposed pressure drop along the channel of 500 Pa (Kashaninejad et al., 2012). For the latest device numerical results for a 3D simulation were also obtained, adapting the applied model in this project to three dimensions.

Figure 4.5a shows the velocity profiles for the middle height plan ($z = H/2$ = 9.55 μm) obtained through the theoretical correlation given by Equation 2.8, through the μ-PIV measurements[1] performed by Zheng and Silber-Li (2008) and through the 2D numerical simulations using the current model. Figure 4.5b shows the velocity profiles along channel width (for $z = H/2$ = 10 μm) determined by Equation 2.8, by 3D numerical simulations performed by Kashaninejad et al. (2012) and by 3D and 2D numerical simulations performed in the present study.

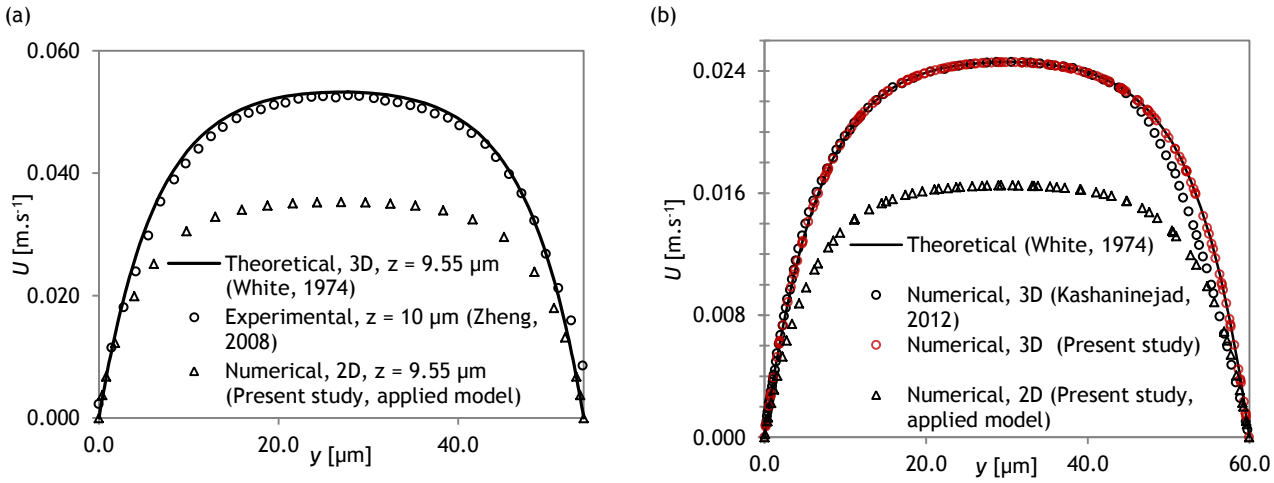

Figure 4.5 - Velocity profiles along channel width for two devices: (a) H = 19.1 μm, L = 27.9 mm, AR = 0.35, ΔP = 34000 Pa (X. Zheng and Silber-Li, 2008); (b) H = 20 μm, L = 1 mm, AR = 0.33(3), ΔP = 500 Pa (Kashaninejad et al., 2012).

In these two cases, one can observe that the 2D numerical model developed for this study underestimates the values of the real velocities along channel width (maximum relative difference between the computed velocity and the one presented by Zheng and Silber-Li of 21%, and between the

[1] The experimental velocity profile was evaluated close to the middle height plan, at z = 10 μm.

computed velocity and the one determined by Kashaninejad et al. of 33%). When the same model is adapted to 3D simulations, one obtains results consistent with the literature (Figure 4.5b). These results show that the developed model is accurate but also reveal the importance of the third dimension on the fluid flow in rectangular microchannels. However, as one of the goals of this project is a compromise between accuracy and computational cost, the use of the 2D approach is recommendable, since the computational time for the 3D approach is approximately 25 times bigger than that for the 2D approach.

This model was also tested to evaluate the ability to solve fluid flow in a device where two orthogonal streams (flowing from independent inlets) join and flow into a single channel with a rectangular cross section. A microchannel with a Y-junction inlet (Figure 4.6) was selected, with equal dimensions (W_{ent} = 750 µm, L_{ent} = 2 mm, L = 5 mm, W = 750 µm, H = 750 µm) to a device previously used by Sarkar et al. (2014) to obtain experimental data. The validation was performed by comparing the numerical and experimental values of the location of the interface between the two streams at the channel outlet ($x = L$), for different values of flow rate ratio between the two inlet streams (flow rate of the stream located at a positive y-coordinate was set to 1 ml·min^{-1}).

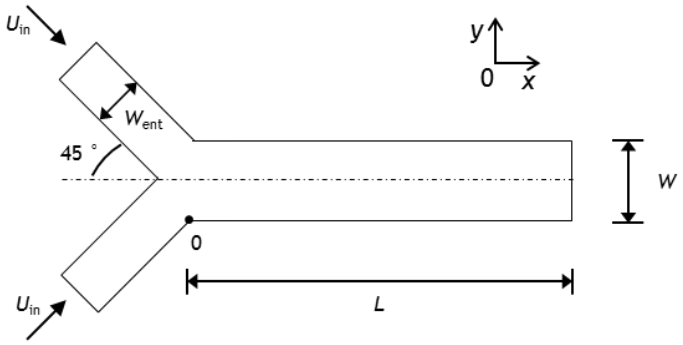

Figure 4.6 - Top view of a device with a Y-junction inlet and height *H*.

To visualize the location of the interface (distance from the wall located at $y = 0$ to the interface between the two streams), one used a Lagrangian approach by analysing the motion of a dye (i.e. a compound that does not interfere with the fluid flow), introduced in the domain by one of the inlets, along the channel. In Figure 4.7 one can observe that the numerical results are in agreement with the experimental data (relative differences less than 5%), meaning that this model is capable to solve the flow when two streams intercept.

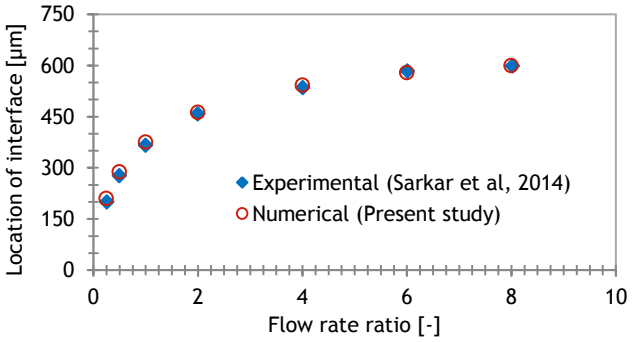

Figure 4.7 - Location of the interface between two streams, joint by a Y-junction inlet, for flow rate ratios of 0.25, 0.5, 1, 2, 4, 6 and 8.

So, regarding fluid flow, a 2D approach can be selected, as long as one keeps in mind that the velocity field is affected by the ratio between the numerical maximum velocity and the real maximum velocity, i.e. it is somewhat underestimated.

For the limit of diluted solutions and low thermal gradients, Fick's law express the mass transport by diffusion (Equation 2.9). For transient-state, Fick's second law is applicable (Equation 2.10). In a 1D domain, for example a W long line (Figure 4.8a) where the concentration at $t = 0$ on half of the geometry is 0 and on the other half is a given concentration C_1, the transient mass transfer profile is given by Equation 4.1, which is a particular solution of Equation 2.10 (Fick's second law). After a sufficiently long time, t_{ss}, the steady state is reached and the concentration in all the domain reaches half the value of C_1.

$$C_c(y,t) = \frac{C_1}{2} \times \left[1 + \operatorname{erf}\left(\frac{y}{2\sqrt{D_c t}}\right)\right] \qquad \text{Equation 4.1}$$

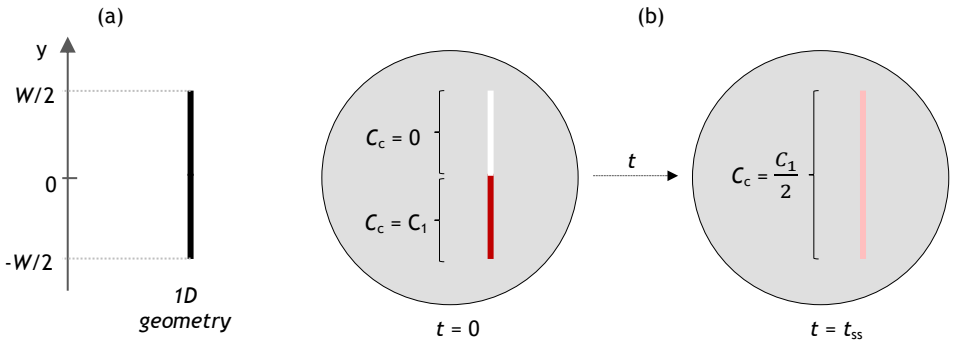

Figure 4.8 - (a) 1D geometry with width W and (b) representation of the concentration distribution at the initial time and at the stationary state.

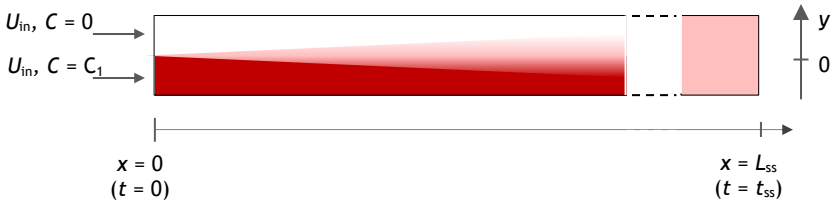

Figure 4.9 - 2D geometry with length L and width W and a scheme of the concentration field along streamwise direction.

This equation can be adapted to a diffusion-convection problem by considering a two-dimensional configuration (Figure 4.9). Instead of a vertical bar, one considers a rectangular plan, in which two separate streams flow with the same inlet velocity, one of the streams with null concentration and the other with concentration C_1. In this problem, as the species c is transported by advection, in streamwise direction, diffusion mainly occurs perpendicularly, in the y-direction. Therefore, the concentration profile changes along x-direction. By assuring a fully developed flow, the velocity profile (along y) does not depend on x. Thus, through a change of variables ($t = x/U_{in}$), Fick's second law describes the concentration field in 2D. Therefore, Equation 4.1 is able to describe transient 1D or stationary 2D problems (for similar conditions of those used in this case). The current model was validated for mass transfer in convection-diffusion problems by comparing the

numerical results obtained in the present study to a theoretical solution (Equation 4.1) and to experimental (Holden et al., 2003) and numerical (Sarkar et al., 2014) data.

A first device was studied with similar configuration to the one shown in Figure 4.6 (which has a Y-junction inlet), with dimensions previously defined by Holden et al. (2003): W_{ent} = 400 μm, L_{ent} = 7 mm, L = 21.4 mm, W = 500 μm and device height H = 6 μm. An inlet concentration of 1 mol·m^{-3} was set to the stream located at the negative y-coordinate and a diffusion coefficient of 6.5 x 10^{-11} m^2·s^{-1} was set for the diluted specie. The total flow was assumed constant and equal to 500 nl·min^{-1}. Figure 4.10 shows the concentration curves along channel width at the outlet of the device, obtained theoretically (Equation 4.1), experimentally (Holden et al., 2003) and numerically (present study). The numerical results show good agreement with the theoretical and experimental data.

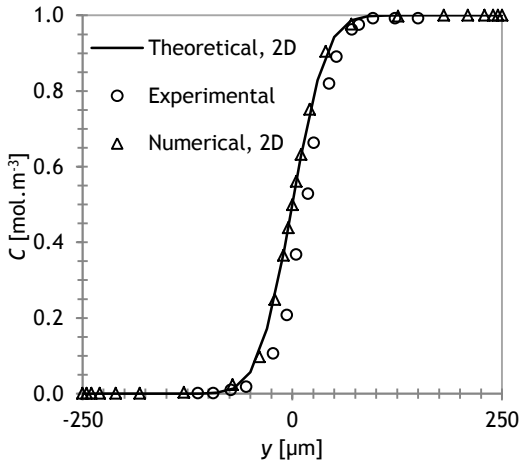

Figure 4.10 - Concentration profiles obtained theoretic-, experiment- and numerically along channel width, at the outlet, in a device previously used by Holden and co-workers.

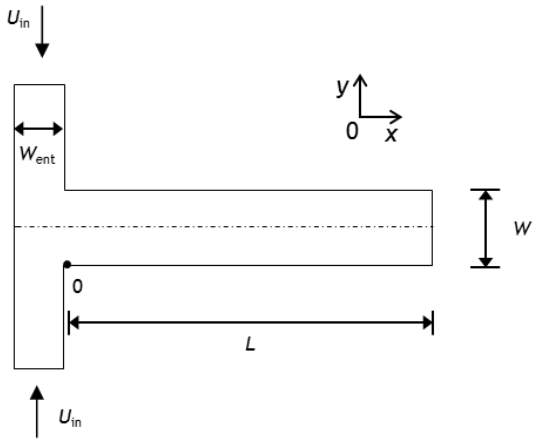

Figure 4.11 - Top view of a device with a T-junction inlet and height *H*.

Sarkar et al. (2014) performed 3D simulations in a channel with a T-junction inlet to study the transverse diffusion thickness δ, i.e. the length in y-direction of mixed solution (C_c > 0 and C_c < C_1). A 2D numerical simulation was reproduced using the current model for a similar microdevice (W_{ent} = 500 μm, L_{ent} = 1 mm, L = 5 mm, W = 500 μm, H = 500 μm). A schematic representation of the

middle plan of the channel is represented in Figure 4.11. Figure 4.12 compares the values of the diffusion thickness obtained by 3D numerical simulations (Sarkar et al., 2014) and 2D numerical simulations (model used in the present study for mass transfer studies). The numerical results show good agreement with the 3D numerical data.

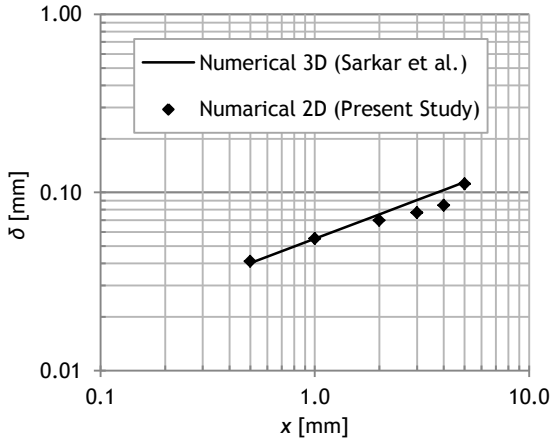

Figure 4.12 – Diffusion thickness along channel width, at the outlet, in a device previously used by Sarkar et al. (2014). Abscissa and ordinate are in logarithmic scale.

5. Results and discussion

The aim of this section is to analyse the effects of velocity ratio (U_f/U_w), feed channel inlet average velocity (U_f), feed channel width (W_f), device length with microchannels (L_μ), microchannel density (N_μ/L_μ) and microchannel length (L_m) on the motion of bacteria, on a bacteria-trapping device. Firstly, the fluid flow on the microdevice model is described and compared to that of a scaled down device. Then, the numerical results obtained for Cases I to XIX are presented and discussed. Later in this section, strategies for trapping bacteria in this type of device are suggested and the effects on the flow discussed. A preliminary analysis on the transport of nutrients and metabolic products in such a device is also discussed. Values of the variable parameters and main results for each simulation are shown in Table H.1, Table H.2, Table H.4 and Table H.5. For all the simulations the mass imbalance was inferior to 0.33% (Table H.3 and Table H.6), the molar imbalance inferior to 0.30% (Table H.6) and Reynolds number and Stokes number were inferior to 2.9×10^{-3} and 4.7×10^{-5} (Table H.3 and Table H.6), respectively.

5.1. Base model device

The fluid flow was initially solved on a microdevice equivalent to the base model, which dimensions are given in Table 2.1, for an inlet average velocity of the feed channel of 1 mm·s^{-1} and an inlet average velocity of the waste channel of 0.01 mm·s^{-1} (VR = 100). Figure 5.1a and Figure 5.1c shows a colour map of the velocity field in the device and corresponding fluid streamlines, respectively. Figure 5.2 shows the tendency curves of the pressure difference across the microchannels and the maximum fluid velocity in each microchannel, along the device length.

In Figure 5.1a one can observe that a higher inlet velocity was applied to the feed channel (main channel on the left) than to the waste channel (main channel on the right), noticeable by the colours yellow and dark blue near the corresponding inlets. The velocity difference set between feed and waste channels induces a pressure difference along the (orthogonal) microchannels which enables the fluid to flow, from the feed channel through the microchannels, to the waste channel. Thus, as the fluid (introduced in the feed inlet) flows along the device length, the fluid elements located further from the microchannels entrance gradually moves towards the right, as the fluid elements nears the microchannels escape to the waste stream. Thus, there is a decrease of the flow rate (and velocity) in the feed stream. On the other hand, the flow rate in the waste channel increases, increasing consequently the fluid velocity. After a certain device length (with microchannels) the fluid no longer flows through the following microchannels and therefore the velocity does not decrease/increase anymore in the feed/waste channel. This corresponds to null pressure difference along the microchannels and means that bacteria cannot enter those microchannels. One can see that the maximum velocity in the microchannels (Figure 5.2a) and the pressure difference along the microchannels (Figure 5.2b) decreases exponentially along the device length until it reaches zero. The bacteria motion on the microdevice was analysed through the fluid streamlines (Figure 5.1c). One can see that the released bacteria, initially ordered in the feed inlet, also enter orderly

in the microchannels, i.e. the first bacteria (the ones placed closer to the microchannels entrance) enter first in the microchannels. In this device and for the present conditions (U_f = 1 mm·s^{-1}, *VR* = 100), 48% of the released bacteria entered the microchannels.

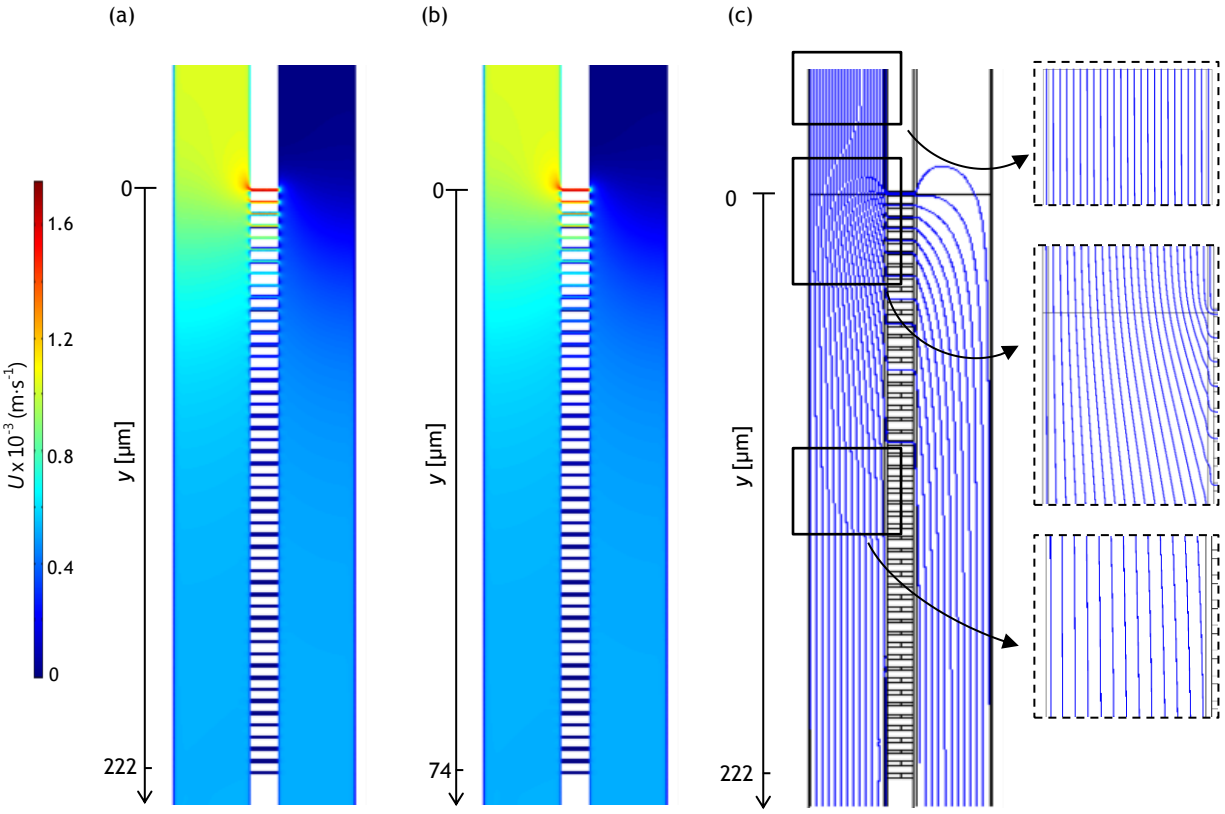

Figure 5.1 - Colour map of the velocity field (a) in the base model and (b) in the scaled down microdevices, (c) streamlines on the base model device and zoom in selected areas of the device to better visualize the behaviour of the streamlines in the feed channel.

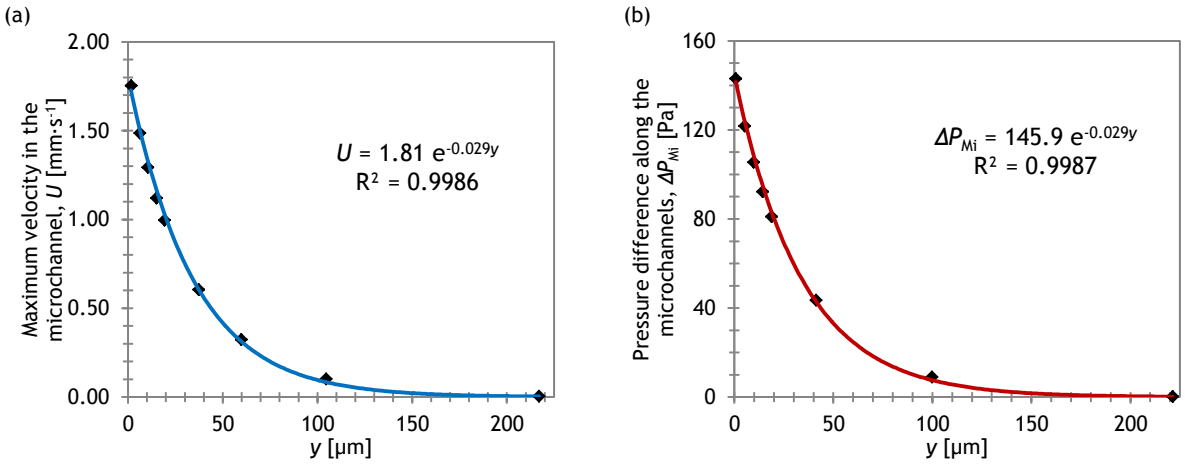

Figure 5.2 - Maximum velocity and pressure difference across the microchannels along the device length, in the base model microdevice.

The fluid flow and bacteria motion were also computed in a scaled down device with dimensions reduced to one third (W_f = W_w = 10 µm, H = 0.5 µm, L_{in} = 16.7 µm, L_{out} = 3.3 µm, L_μ = 74 µm, W_m = 0.5 µm, N_μ/L_μ = 0.68) but keeping the inlet average velocities constant (i.e. U_f = 1 mm·s^{-1},

VR = 100), which means different Reynolds in the two devices under comparison. Figure 5.1b shows the colour map of the velocity field in the scaled down device.

The applied computational model takes into consideration the influence of the wall shear stress on the fluid velocity, caused by the upper and lower walls (third dimension) in shallow channels. Since the height of the scaled down device was also lowered to one third, the aspect ratio ($AR = H/W$) of the main channels and microchannels was kept constant and one observes similar velocity fields in both devices (Figure 5.1a and Figure 5.1b). Therefore, the percentage of trapped bacteria is the same and equal to 48%. Moreover, for the ranges of parameters considered, the bacteria enter in the microchannels located at the same dimensionless *y*-coordinate, as seen in Figure 5.3b.

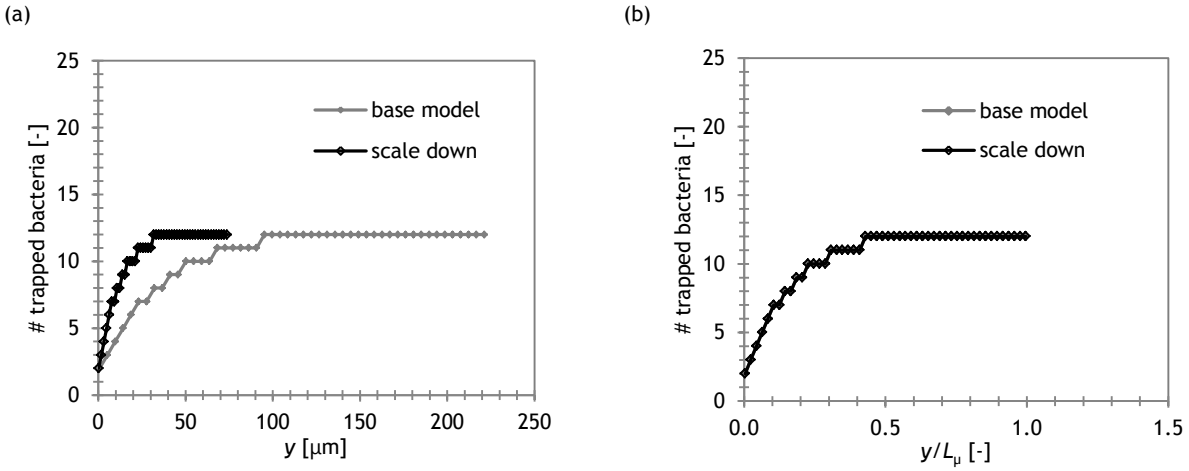

Figure 5.3 – Number of trapped bacteria (a) along *y*-coordinate and (b) along *y*-coordinate normalized by the device length, for the base model and scaled down microdevice.

5.2. Effects of feed to waste average inlet velocity ratio

As mentioned in sub-section 3.8, bacteria are expected to follow the fluid streamlines (St<<1). Therefore, it is important to analyse in which conditions the fluid flows in the microchannels, i.e. when there would be the possibility of bacteria being trapped in the microchannels.

The ratio between feed and waste channel inlet average velocity (velocity ratio, *VR*) was varied from 1 to 100, while inlet average fluid velocity of the feed channel was kept constant (U_f = 1 mm·s^{-1}). Thus, U_w (waste channel inlet average fluid velocity) varied from 1 mm·s^{-1} to 10 μm·s^{-1}. In this subsection four scenarios were studied[1]: feed channel width (W_f) equal to 30 and 10 μm, for two device lengths[2], L_μ = 42 and 222 μm.

For Case I and III, the influence of velocity ratio on the velocity field is shown in Figure 5.4 and Figure 5.5, respectively. Figure 5.6a shows the pressure difference between microchannel entrance and exit (Equation G.5) on the first five microchannels, for Case I. Moreover, the percentage of trapped bacteria, the length (in *y* direction) with microchannels where trapping can occur, L_{crit}, and

[1] Cases I, II, III and IV (Table 3.1).
[2] The device length was altered by adding microchannels spaced by 3 μm (L_μ = 42 μm corresponds to 10 microchannels and L_μ = 222 μm corresponds to 50 microchannels).

the percentage of ineffective trapping length on Cases I, II, III and IV are presented in Figure 5.6b, Figure 5.6c and Figure 5.6d, respectively. The values of the varying parameters, the obtained pressure drop on the main channels and microchannel M1, the percentage of trapped bacteria and L_{crit} values are shown in Table H.1 and Table H.2.

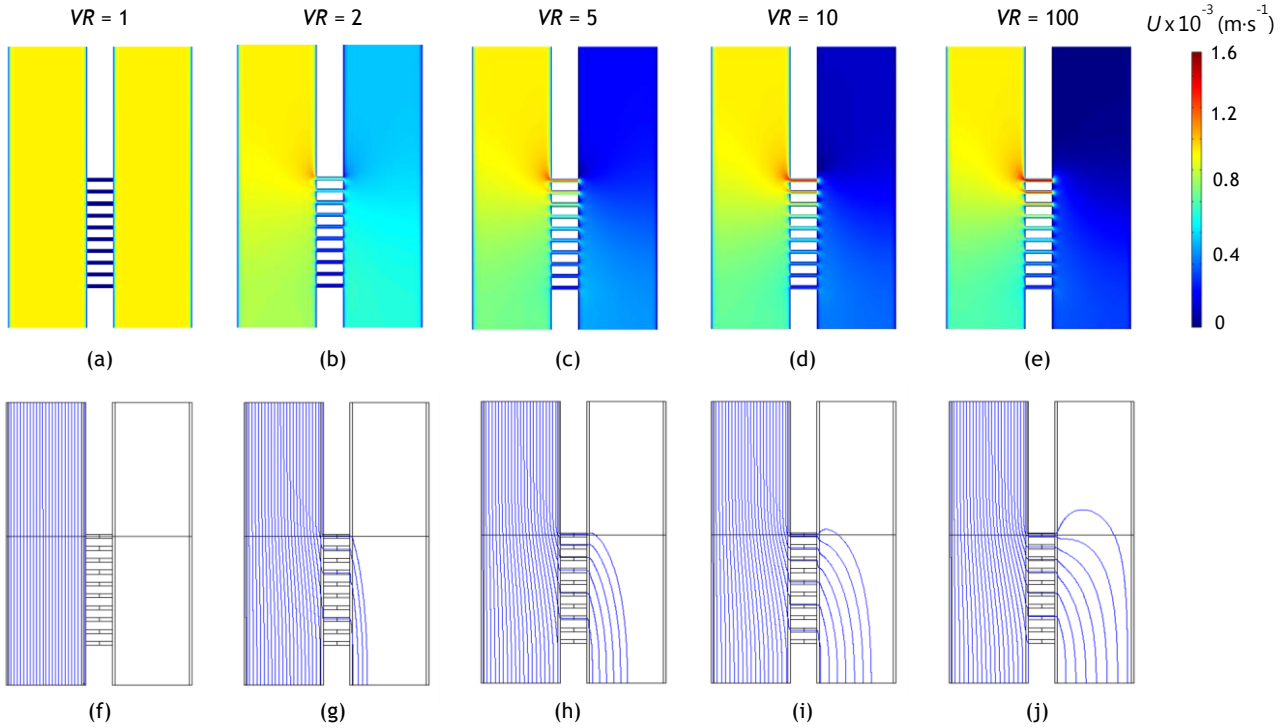

Figure 5.4 - Colour maps of the velocity field in the microdevice for selected velocity ratios of Case I, (a) to (e), and respective fluid streamlines from the feed inlet, (f) to (j).

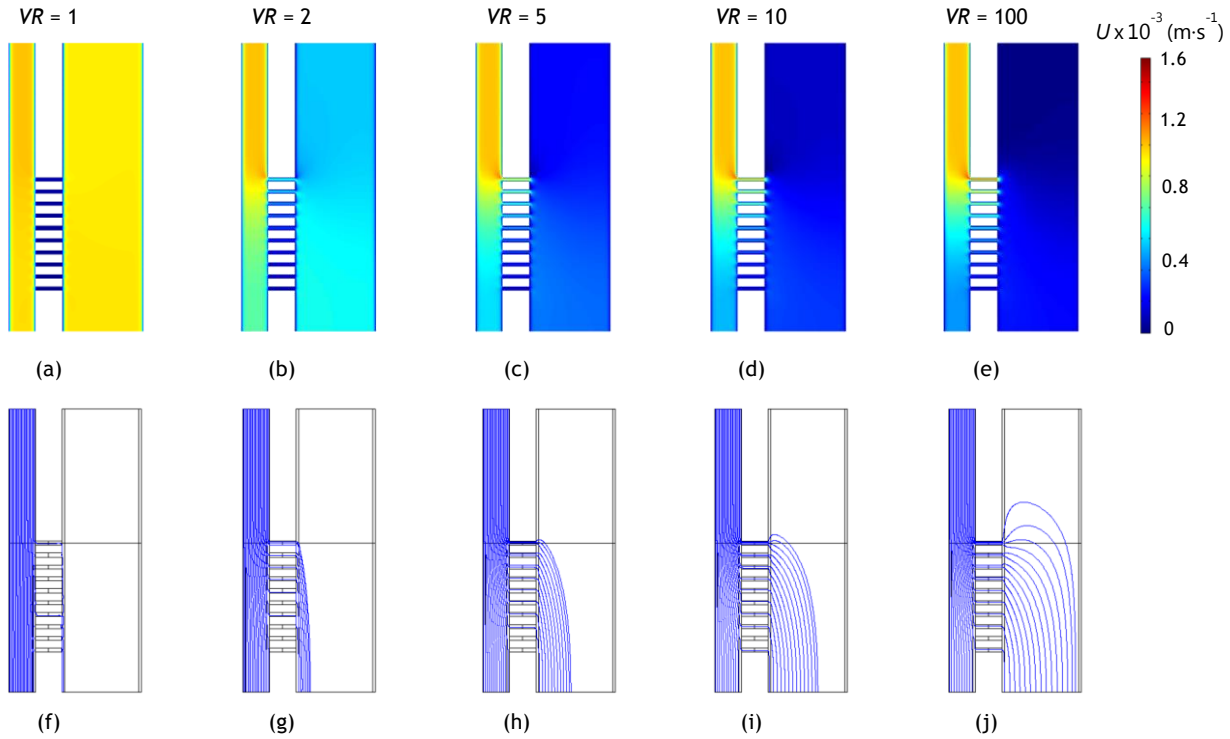

Figure 5.5 - Colour maps of the velocity field in the microdevice for selected velocity ratios of Case III, (a) to (e), and corresponding fluid streamlines from the feed inlet, (f) to (j).

In Figure 5.4 (referring to Case I) it is seen that, when feed channel inlet average velocity U_f equals the waste channel inlet average velocity U_w (*VR* = 1, Figure 5.4a), the fluid in the microchannels is stagnated. This is due to the null pressure difference between the edges of the microchannels (Figure 5.6a). When the velocity ratio increases, the pressure difference along the microchannels increases (Figure 5.6a), increasing, consequently, the fluid velocity (in Figure 5.4 the increasing velocity in the first microchannel for images a) to g) is perceptible by the colour changing from dark blue to dark red). In Cases II, III and IV the behaviour is identical.

In Figure 5.6b, one can observe the overall variation of bacteria trapping with increasing velocity ratio. Increasing *VR*, which implies bigger differences between U_f and U_w, increases the percentage of trapped bacteria (i.e. bacteria that enter the microchannels), until it levels off at *VR* = 20. Figure 5.4f-j and Figure 5.5f-j represent the fluid streamlines (that corresponds to the trajectory of 25 bacteria released from the feed inlet), for selected velocity ratios, where it is noticeable the increase on the number of streamlines that cross the microchannels to the waste channel, for increasing *VR*.

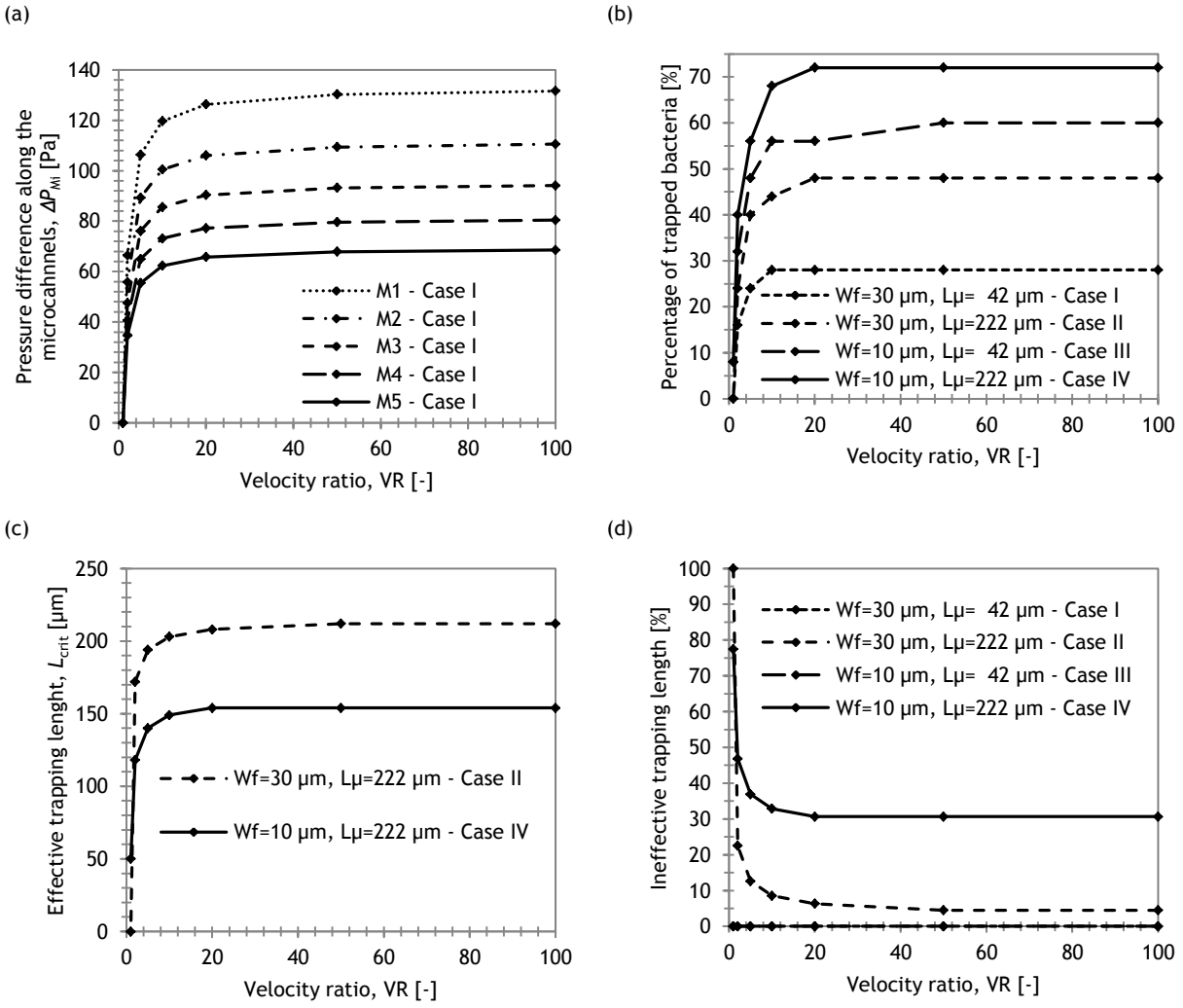

Figure 5.6 - Main results for increasing values of velocity ratio from 1 to 100: (a) pressure difference between microchannel entrance and exit, for the first five microchannels (Case I), (b) percentage of trapped bacteria for Case I to IV, (c) effective traping length (Case II and IV) and (d) percentage of device length in which trapping does not occur(Case I to IV).

For the same width of the feed channel, increasing the length with microchannels (by adding more microchannels equally spaced) increases the pressure difference along the microchannels (Table H.2). As a result, the entrance of bacteria in the microchannels is enhanced (Figure 5.6b, Cases I and II for W_f = 30 μm, and Cases III and IV for W_f = 10 μm). After a certain length L_{crit}, increasing the length with microchannels (L_μ) does not affect fluid flow and, consequently, bacteria trapping[1].

For a constant length with microchannels (L_μ), one identifies lower velocities in the microchannels for narrower feed channels (velocity maps on Figure 5.4a-e for Case I compared to matching velocity maps for Case III on Figure 5.5a-e), characteristic of lower pressure differences between the edges of the microchannels (Table H.2). Although decreasing feed channel width decreases the pressure drop along the microchannels, the percentage of trapped bacteria increases (Figure 5.6b, Cases I and III for L_μ = 42 μm, and Cases II and IV for L_μ = 222 μm). This occurs because the velocity profile in the main channels is strongly influenced by its width. For low aspect ratios of the channel (i.e. width much bigger than the height) the velocity profile is flat (constant velocity except very close to the walls). Increasing the aspect ratio *AR* (i.e. decreasing *W*), approximates the velocity profile to a parabolic curve (Lee et al., 2007, Chapter 2.5.2). As a result, for lower values of W_f (and consequently higher values of aspect ratio), the velocity near the microchannels is lower (Figure 5.7) enabling the fluid elements located in that region to change direction more easily. Thus, as bacteria follow the fluid streamlines, more bacteria are trapped for lower values of feed channel width (and lower velocity in the vicinity of microchannels inlet).

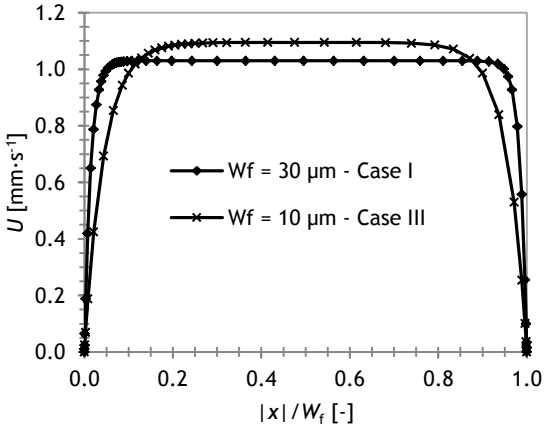

Figure 5.7 - Velocity profile at the feed inlet, along the normalized *x*-direction. x_f/W_f equal to 1 correspond to the wall closer to microchannels entrance and 0 to the opposite wall.

Because of the previous effect (different velocity profiles along a channel for different widths), one observes that when $W_f \neq W_w$ the bacteria really close to the feed channel wall (near the microchannels) can enter the microchannels even when VR = 1 (Figure 5.5f), since in that case ($W_f \neq W_w$) the pressure difference in the microchannels is not absolutely null.

In Cases II and IV, the device length is enough for the fluid in the microchannels located after L_{crit} to be stagnated. Figure 5.6c shows the device length needed to reach that point for different

[1] This effect is further discussed in section 5.4. Effects of device length.

values of velocity ratio. It is observed that, higher velocity ratios require longer devices, i.e. higher number of microchannels, until null pressure difference is observed along the microchannels (i.e. until no more bacteria trapping is observed). Additionally, wider feed channel requires longer devices to reach the state of null pressure difference. This is in agreement with Figure 5.4 and Figure 5.5: the velocity observed in the microchannels is higher for wider feed channels and for higher velocity ratios for the same *y*-coordinate, both implying longer devices (higher L_{crit}).

To sum up, in order to have flow in the microchannels and, consequently, for bacteria to be trapped, one needs to ensure a pressure difference between entrance and exit of the microchannels ($\Delta P_{Mi} \neq 0$). Therefore, above a certain device length, the existing microchannels do not produce further trapping because no bacteria will enter microchannels with stagnated fluid. For lower values of velocity ratio, shorter devices are needed to reach $\Delta P_{Mi} = 0$, but lower proportion of bacteria will be trapped. Narrower feed channels enhance bacteria trapping (i.e. entrance of bacteria in the microchannels) and reduce the device length along which trapping occurs.

5.3. Effects of feed channel width

In the previous subsection it was observed that the width of the feed channel (W_f) affects the entrance of bacteria in the microchannels. To further study this effect, W_f was varied from 3 to 30 μm for velocity ratios of 100 (Case V) and 2 (Case VI), for an inlet average velocity in the feed channel of 1 mm·s^{-1}. The influence of decreasing both feed channel and waste channel width was briefly studied in section 5.3.1. In these simulations, the selected device length[1] was 222 μm (50 microchannels), to guarantee that the results would not be influenced by device length.

For Case V, Figure 5.8a shows the pressure difference along the first five microchannels. The influence of feed channel width on the percentage of trapped bacteria and on L_{crit} is represented in Figure 5.8b and Figure 5.8c, for Cases V and VI. Figure 5.8d shows the percentage of device length that one can remove without affecting bacteria motion. The values of the varying parameters, the obtained pressure drop along the main channels and along microchannel M_1, the percentage of trapped bacteria and the effective trapping length (L_{crit}), i.e. the length from the inlet to the point where null pressure difference along the microchannels is reached, are presented in Table H.2.

By decreasing the width of the feed channel W_f (for constant inlet average velocity), the inlet flow rate also decreases ($Q_f = U_f \times A_f$, $A_f = W_f \times H$). Hence, pressure in the feed channel decreases[2]. Since, in this study, one considers higher pressure in the feed channel than in the waste channel ($U_f > U_w$), decrease of W_f (and consequently decrease of pressure in the feed channel) results in a decrease of pressure difference in the microchannels (Figure 5.8a). Despite the lower pressure difference along the microchannels of devices with narrower feed channels, more bacteria can be trapped (Figure 5.8b) due to the previously discussed[3] difference on the velocity profiles for differ-

[1] This value assures that for each set of parameters the maximum percentage of bacteria is trapped in the microchannels (5.4. Effects of device length).
[2] $\Delta P = Q \cdot R$. Pressure drop does not decrease linearly due to the increase of fluidic resistance caused by the decrease of channel width, i.e. decrease of the available space for fluid to flow (Beebe et al., 2002, p. 265).
[3] Section 5.2 Effects of feed to waste average inlet velocity ratio.

ent aspect ratios of the channels ($AR = H/W$). Figure 5.9a and Figure 5.9b show the velocity profiles on the feed channel along normalized x-coordinate, at the inlet ($y = -L_{in}$) and at the entrance of the first microchannel ($y = W_m/2$), both for Case V (W_f = 3, 5, 10, 20 and 30 µm equivalent to AR = 0.5, 0.3, 0.15, 0.075 and 0.05). Despite average velocity being the same at feed inlet, near the channel walls contiguous to the microchannel and for the same relative coordinate one observes that the velocity is lower on the narrower channels. Therefore, and as mentioned previously, the fluid elements of that zone can change direction more easily, which is confirmed, on Figure 5.8b, by the increasing percentage of trapped bacteria for lower width of the feed channels.

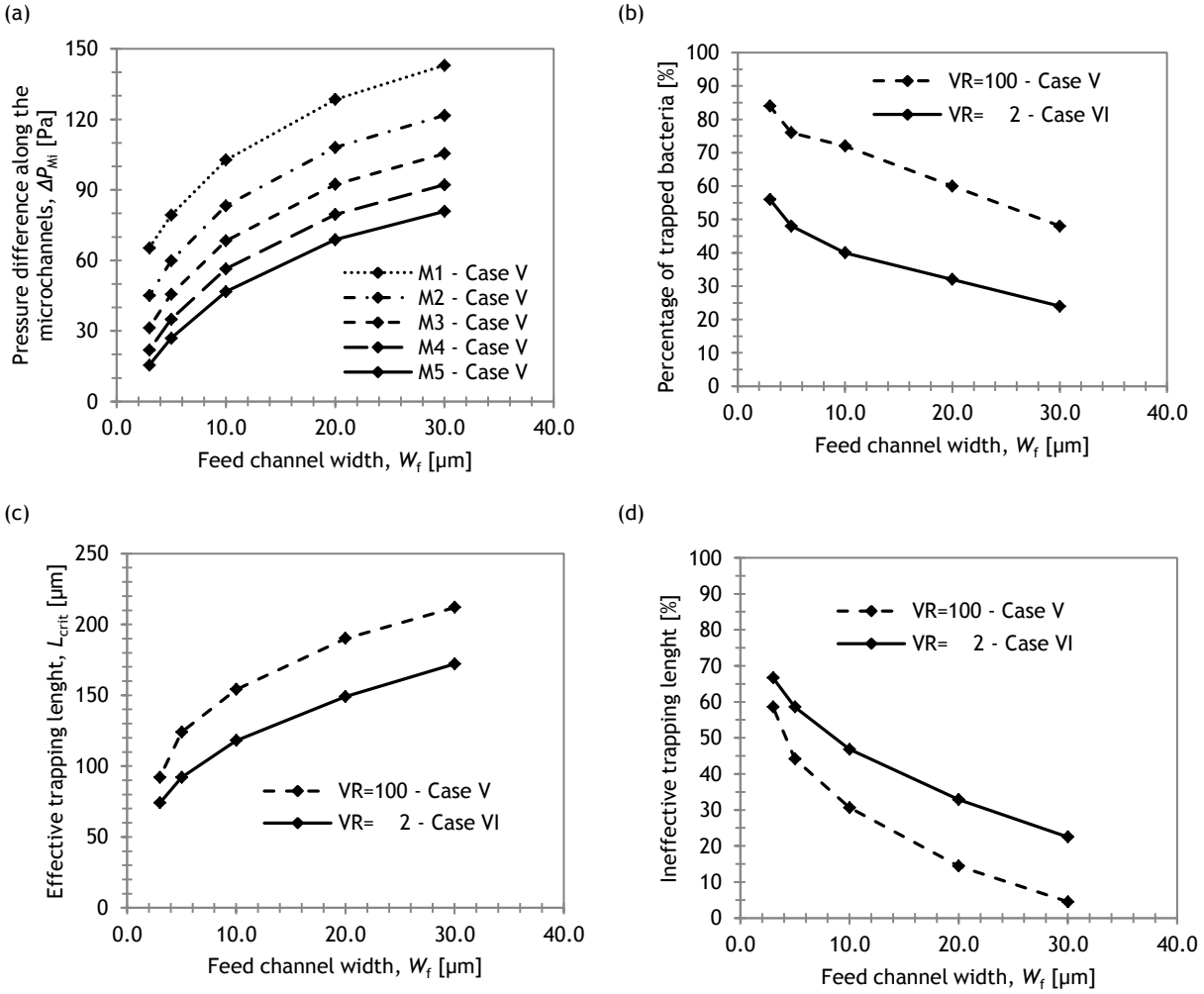

Figure 5.8 - Main results for increasing values of feed width: (a) pressure difference between microchannel entrance and exit, for the first five microchannels (Case V), (b) percentage of trapped bacteria for Case V and VI, (c) effective trapping length and (d) ineffective trapping length (where trapping does not occur) for Case V and VI.

Moreover, as bigger portion of fluid from the feed channel flows through the initial microchannels (in narrower feed channels), the equilibrium is reached more rapidly, i.e. one needs less device length to reach null pressure difference along the microchannels (Figure 5.8c). After that point, no more trapping occurs in the remaining microchannels (device length). Figure 5.8d gives the percentage of device length that does not affect bacteria trapping. By decreasing the width of the feed channel, the effective trapping length (L_{crit}) decreases and therefore the ineffective trapping length

increases. This means one can use shorter devices in order to reach the maximum amount of trapped bacteria for a given portion of released bacteria, for a given set of parameters.

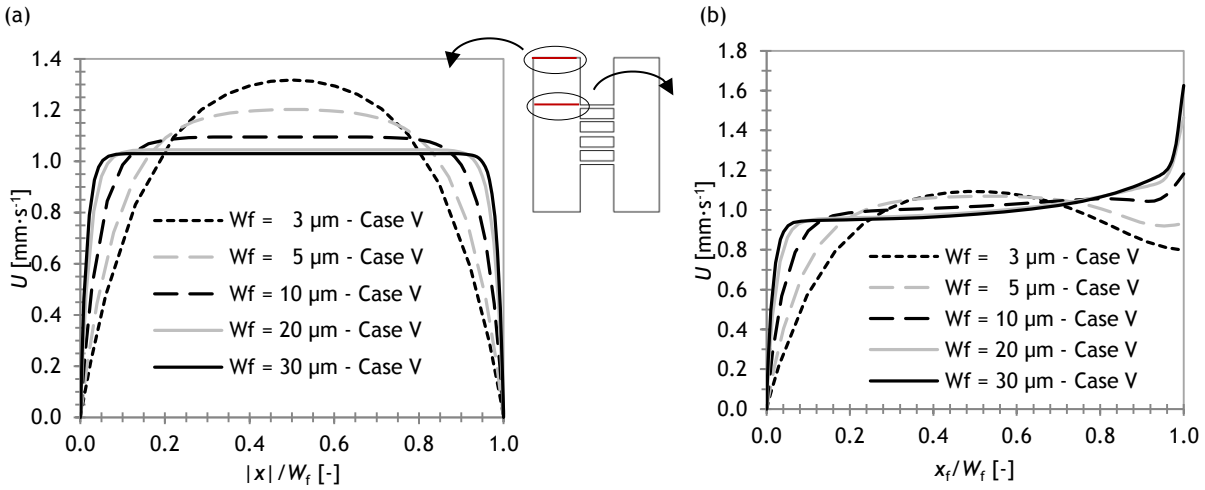

Figure 5.9 - Velocity profile it the feed channel, along the normalized x-direction (1 corresponds to the coordinate closer to the microchannels and 0 to the opposite device wall): (a) at the inlet ($y = -L_{in}$) and (b) at the first microchannel entrance ($y = W_m/2$, line C' on Figure A.1b). x_f/W_f equal to 1 correspond to the wall closer to microchannels entrance and 0 to the opposite wall.

Similar to the previously discussed Cases (sub-section 5.2) the percentage of trapped bacteria is higher for *VR* = 100 than for *VR* = 2 (Figure 5.8b), due to the higher pressure difference between the edges of the microchannels (Table H.2). The number of microchannels needed to reach null pressure difference in the microchannels is, therefore, higher for the higher velocity ratio.

5.3.1. Waste channel width

A scenario using the parameters of the base model presented in section 5.1 (*VR* = 100, U_f = 1 mm·s^{-1}, L_μ = 222 µm, N_μ/L_μ = 0.22 µm^{-1}) for a width of the feed and waste channel of 10 µm was also studied. The aim is to compare the effects of decreasing the width of the feed channel with the effects of decreasing the width of both main channels simultaneously, on bacteria trapping. Figure 5.10 shows a representation of the devices analysed. Figure 5.11a shows the cumulative number of trapped bacteria along the device length for each device, and Figure 5.11b the cumulative number of trapped bacteria along the normalized *y* positioning for the devices with feed channel width equal to waste channel width.

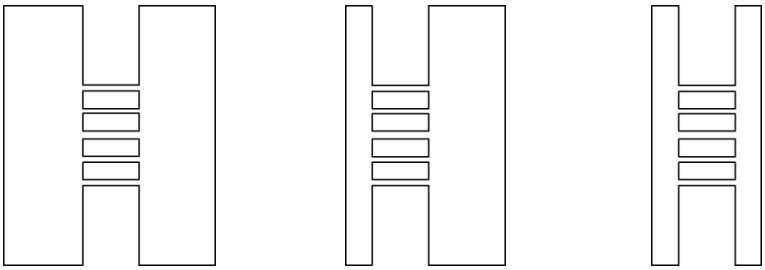

Figure 5.10 - Representative scheme of the base model microdevice (left) and identical devices with a narrower feed channel (middle) and with narrower feed and waste channels (right).

From Figure 5.11a, it is clearly visible that decreasing only the width of feed channel increases substantially the number of trapped bacteria (from 12 to 18, which corresponds to an increase of the percentage of the released bacteria from 48% to 72%). The effect of decreasing both widths to 10 μm is not so relevant, despite more bacteria entering in the upstream microchannels. For a sufficient long device, the percentage of trapped bacteria will reach the same value. In fact the curves of the number of trapped bacteria along the *y* coordinate normalized by the feed channel width, for both cases, is similar.

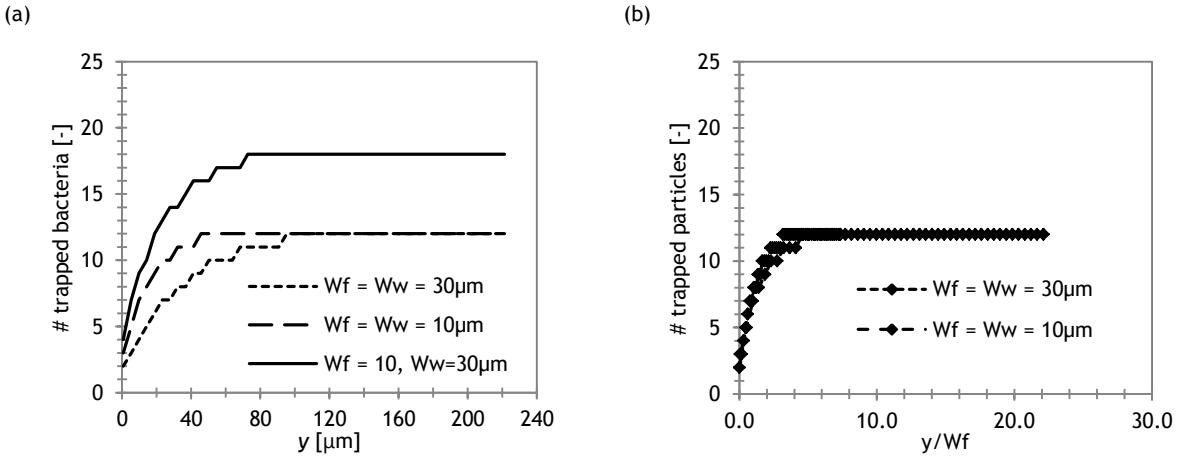

Figure 5.11 – (a) Cumulative number of bacteria that enter the microchannels along device length (left) for three different cases (scheme in Figure 5.10) and (b) cumulative number of trapped bacteria for the cases where feed and waste channel width are the same.

In this study, one observed that lower values of pressure difference in the microchannels not always indicate lower percentage of trapped bacteria. When the width of the feed channel decreases, pressure difference also decreases due to decreasing flow rate, but more bacteria enter the microchannels due to the lower velocities effect near the walls. However, lower dimensions can run into the limits of microfabrication and even cause channel obstructions. For narrower feed channels, fewer microchannels (shorter devices) are needed to trap the maximum percentage of bacteria for a given set of parameters. Moreover, one concludes that reducing only the feed channel width is more advantageous for bacteria trapping than reducing both feed and waste channel widths.

5.4. Effects of device length

In this subsection the device length was changed by adding more or less microchannels, equally spaced from each other, in order to determine the maximum percentage of trapped bacteria for a specific set of parameters. The number of microchannels was varied from 5 to 100 (L_μ = 19.5, 42, 87, 222, 447 μm), for feed to waste inlet velocity ratios of 100 (Case VII) and 2 (Case VIII).

Figure 5.12a, Figure 5.12b and Figure 5.12d show the variations of pressure drop along the first five microchannels, pressure at the entrance and at the outlet of the first microchannel and the changes on the velocity field, respectively, for different device lengths and *VR* = 100 (Case VII). Figure 5.12c gives the percentage of trapped bacteria versus the device length, for velocity ratio of

100 and 2. The effective trapping length (L_{crit}) and percentage of ineffective length are represented in Figure 5.12e and Figure 5.12f. Table H.1 and Table H.2 show the values of the varying parameters, the obtained pressure drop on the main channels and microchannel M_1, the percentage of trapped bacteria and the effective trapping length.

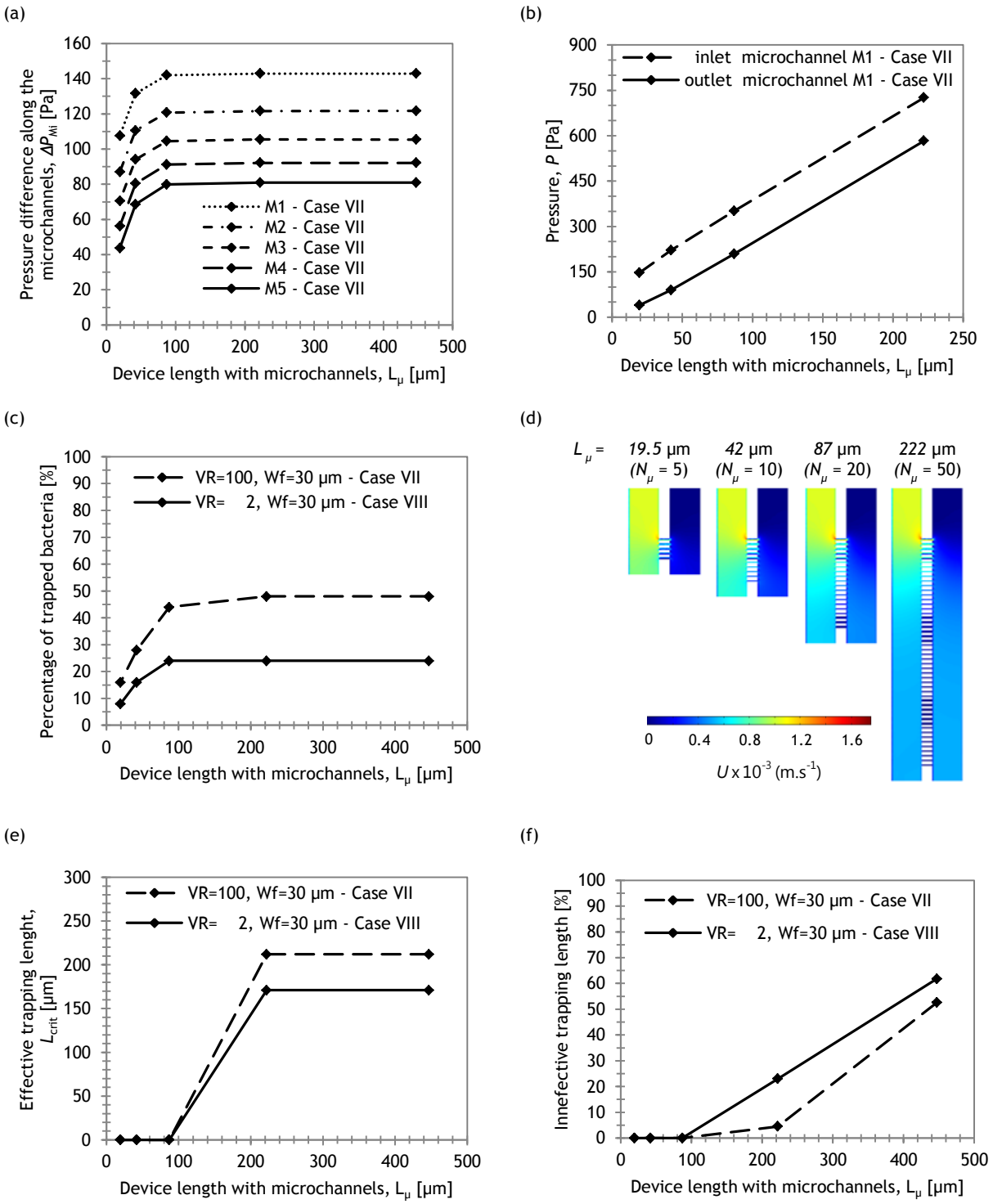

Figure 5.12 - Main results for increasing values of device length: (a) pressure difference between inlet and outlet on the main channels (Case VII); (b) pressure difference between microchannel entrance and exit, for the first five microchannels (Case VII); (c) percentage of trapped bacteria for Cases VII and VIII; (d) colour map of the velocity field (Case VII); (e) effective length; and (f) percentage of device length in which trapping does not occur (Cases VII and VIII).

In the microchannels, pressure difference between inlet and outlet increases with increasing device length (Figure 5.12a), until it reaches a plateau (ΔP_{Mi} is the same when L_μ = 222 μm and when L_μ = 447 μm). At the same *y*-coordinate, in the main channels, the pressure is higher for longer devices, due to the increased fluidic resistance. However, it is verified that the pressure increases at a higher rate in the microchannels entrance than in the microchannels outlet, for device lengths smaller than 222 μm: in Figure 5.12b, the slope of the inlet curve is bigger than the slope of the outlet curve. This occurs because the fluid did not reach the fully developed state in those cases. After a certain device length, equilibrium between the pressure in the feed and waste channel is reached. At that point ($y = L_{crit}$)[1], the fluid inside the microchannels is stagnated, which correspond to a null pressure difference between entrance and exit of the microchannel. For devices longer than L_{crit}, adding more microchannels does not affect pressure difference along the microchannels.

The evolution of the percentage of trapped bacteria for increasing device length (Figure 5.12c) is in agreement with the behaviour of pressure difference along the microchannels (Figure 5.12a): higher pressure differences along the microchannels enhance bacteria trapping. So, increasing the device length (by adding microchannels) until L_{crit}, increases the percentage of trapped bacteria. Further increase of device length with microchannels does not affect the flow/pressure of the previous microchannels, and consequently, the percentage of trapped bacteria (Figure 5.12c) reaches a plateau. Since in Case VII L_{crit} = 212 μm (Figure 5.12e), when the device length is increased from 222 to 447 μm (lengths bigger than the effective length) the number of bacteria that enter in each microchannel does not change (Figure 5.13).

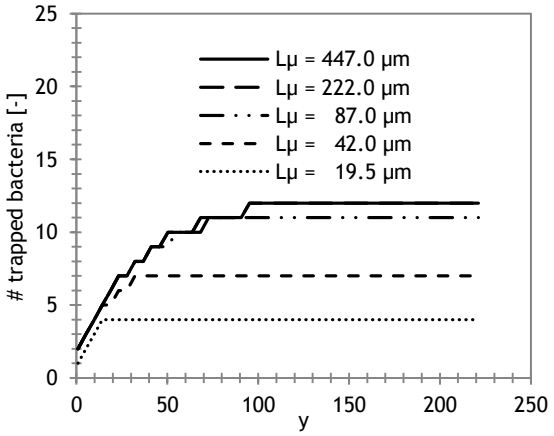

Figure 5.13 – Cumulative number of trapped bacteria that enter the microchannels along device length (right) for different device lengths (Case VII).

For the set of parameters studied in Case VII and VIII, the value of the effective trapping length is 212 and 171 μm, respectively. Since for each Case, the value of L_{crit} does not change by adding more microchannels (Figure 5.12e), it is seen that the percentage of the device that can be removed without affecting bacteria trapping (i.e. the ineffective length) is higher for longer devices (Figure 5.12f). The maximum percentage of trapped bacteria is 48 % for Case VII. The remaining

[1] Please refer to Annex F – Determination of *Lcrit*.

bacteria will acquire a rectilinear trajectory along feed channel, after passing L_{crit}. In Case VIII (lower velocity ratio), 24 % of the bacteria are trapped.

Therefore, as observed in previous parametric studies (subsection 5.2), increasing the device length increases the number of trapped bacteria. However, there is a limit on the length of the device after which further microchannels do not influence the trapping of bacteria. The evaluation of this value, for each case, is important in order to prevent unnecessary microchannels fabrication as it can increase the associated costs.

5.5. *Effects of density of microchannels*

To study the effect of microchannel density (N_μ/L_μ) on the trapping performance of the device, one selected a device length L_μ of 128 μm. Three values of microchannels density were considered: 0.22, 0.33 and 0.44, which correspond to a decrease on microchannel spacing from 3 to 0.75 and an increase on its number from 29 to 57. The parametric analysis was conducted for two values of feed channel width: W_f = 30 μm (Case IX) and W_f = 10 μm (Case X).

Figure 5.14 represents the velocity field of a selected part of the geometry (corresponding to the first 15 micrometres of device length) for Case IX. Pressure difference between inlet and outlet of the microchannels was compared as shown, for Case IX, in Figure 5.15a at the first two microchannels located at the same *y*-coordinate (1st microchannels for all microchannel densities and 3rd, 4th and 5th microchannel for N_μ/L_μ = 0.22, 0.33 and 0.44, respectively). The percentage of trapped bacteria, for Cases IX and X, and the cumulative number of bacteria trapped along the device length, for Case IX, is shown in Figure 5.15b and Figure 5.15c, respectively. The percentage of ineffective trapping length, i.e. percentage of device length in which trapping does not occur, is represented in Figure 5.15d for Cases IX and X. The values of the varying parameters, the obtained pressure drop along the main channels and along microchannel M_1, the percentage of trapped bacteria and L_{crit} are listed in Table H.1 and Table H.2.

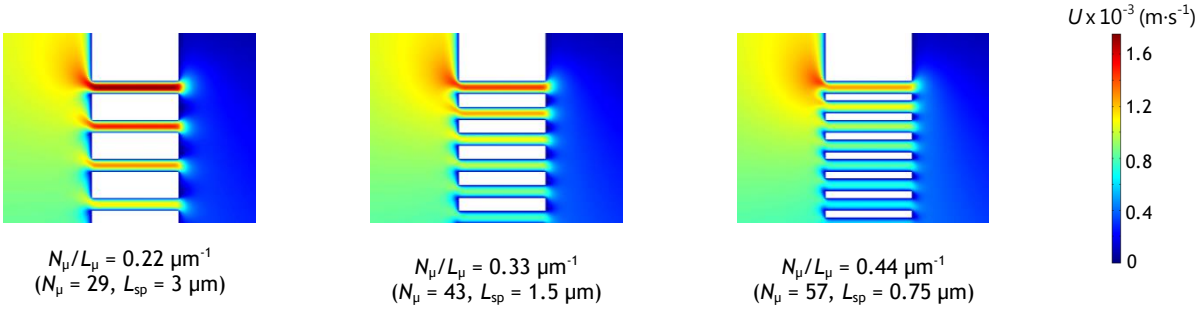

Figure 5.14 - Close-up of the colour maps of the velocity field in devices with different microchannel densities (Case IX).

As seen in Figure 5.14 (from left to right), the velocity in the microchannels, located at the same *y*-coordinate, decreases with increasing microchannel density. This is in agreement with Figure 5.15a, which shows that a denser device implies lower pressure difference along the microchannels. Therefore, devices with higher density of microchannels require lower values of effective trapping length (Figure 5.15d). It is observed (Figure 5.15b) that increasing/decreasing microchannel density does not affect the percentage of trapped bacteria when L_μ = 128 μm, both for

W_f = 30 µm and W_f = 10 µm. In addition, increasing density does not have a significant effect on the *y*-coordinate where the bacteria enter the microchannels (Figure 5.15c, Case IX).

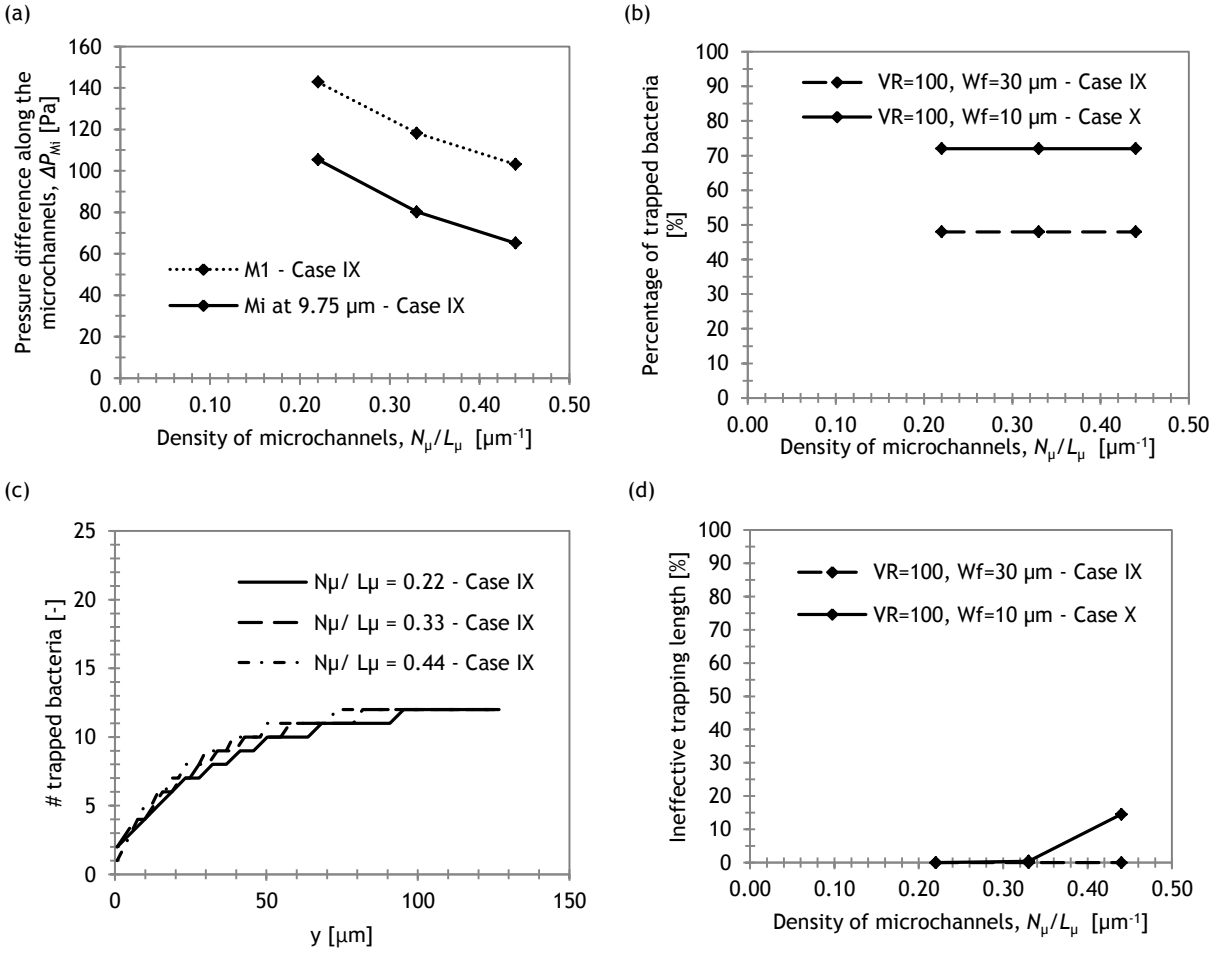

Figure 5.15 - Main results for increasing values of microchannel density: (a) pressure difference between microchannel entrance and exit, for the first five microchannels (Case IX), (b) percentage of trapped bacteria, (c) cumulative number of trapped bacteria along the device and (d) ineffective length (Case VII and VIII).

Thus, for a fixed device length, increasing microchannel density (by increasing the number of microchannels and decreasing the spacing between them) does not affect the percentage of trapped bacteria. In a practical point of view, as more microchannels are available for trapping in denser devices, there are more possibilities/locations for bacteria to be trapped and consequently monitored. A balance between the increased number of bacteria and the difficulty/costs associated to manufacturing microdevices with closer microchannels must be considered.

5.6. Effects of feed channel inlet average velocity

The effect of inlet average velocity of the feed channel on bacteria trapping was studied for velocities between 1 mm·s^{-1} and 50 µm·s^{-1}, for constant velocity ratio. This analysis was performed for two extreme values of velocity ratio, *VR* = 100 (Case XI) and *VR* = 2 (Case XIII), in a device 42 µm long (10 microchannels), with a 30 µm wide feed channel. A study of U_f was also performed for *VR* = 100 and W_f = 10 µm (Case XII). The effect of feed channel inlet average velocity on the pressure difference on the first five microchannels (for Case XI) is shown in Figure 5.16a. Figure 5.16b

presents the percentage of trapped bacteria for increasing values of feed channel velocity (Cases XI, XII and XIII). Values of the varying parameters, the obtained pressure drop on the main channels and microchannel M1 and the percentage of trapped bacteria are shown in Table H.1 and Table H.2.

For a constant velocity ratio, an increasing feed channel inlet average velocity results in a linear increase of the pressure difference across the microchannels (Figure 5.16a). However, no change of the number of trapped bacteria is observed for different values of U_f (Figure 5.16b). For Case XI (higher velocity ratio) the percentage of trapped bacteria is higher than in Case XIII (lower velocity ratio), and for Case XII (narrower feed channel) the percentage of trapped bacteria is higher than in Case XI (wider channel). For the three cases null pressure drop in the microchannels was not reached, thus, the entire length of the device is useful for bacteria trapping.

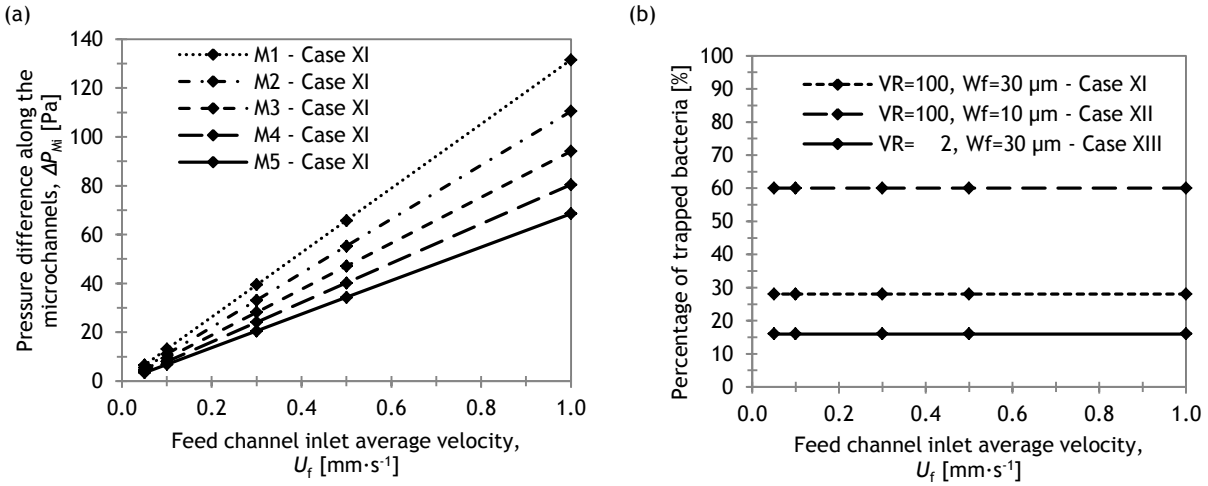

Figure 5.16 – Main results for increasing values of inlet average velocity of the feed channel: (a) pressure difference between microchannel entrance and exit, for the first five microchannels (Case XI) and (b) percentage of trapped bacteria for Cases XI, XII and XIII.

In this sub-section, one observes that the studied parameter (U_f) does not affect the trapping of bacteria, if velocity ratio is kept constant, which implies that the conclusions drawn in this project are valid for different average velocities of the feed inlet.

5.7. Effects of microchannel length

In the preceding subsections the length of the cross-channels was assumed constant and equal to 10 µm. At this point, one studied the influence of the microchannels length[1] for feed channel widths of 10 and 30 µm and velocity ratios of 1, 20 and 100 (which correspond to average inlet velocities in the waste channel of 1, 0.05 and 0.01 mm·s^{-1}).

The evolution of pressure difference and pressure difference per unit length along the first five microchannels are presented in Figure 5.17 (Case XIV). Figure 5.18 illustrates the velocity field in devices with different microchannel lengths, for Case XIV (VR = 100, W_f = 30), and Figure 5.19 shows the percentage of trapped bacteria with increasing microchannel length, for each Case from XIV to XIX.

[1] Case XIV, XV, XVI, XVII, XVIII and XIX (Table 3.1).

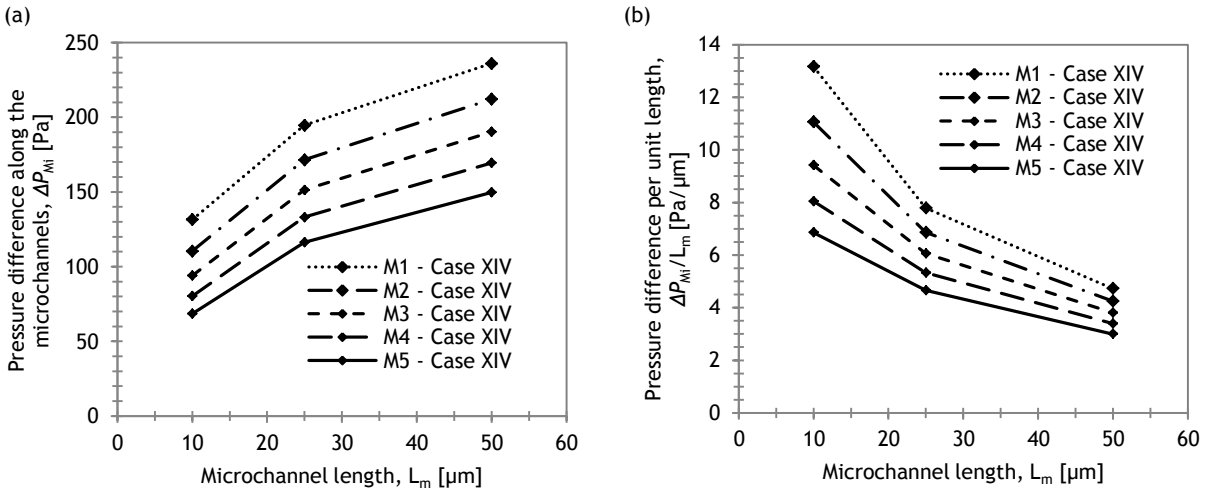

Figure 5.17 - (a) Pressure difference between microchannel entrance and exit and (b) pressure difference along the microchannels per unit length, for the first five microchannels (Case XIV).

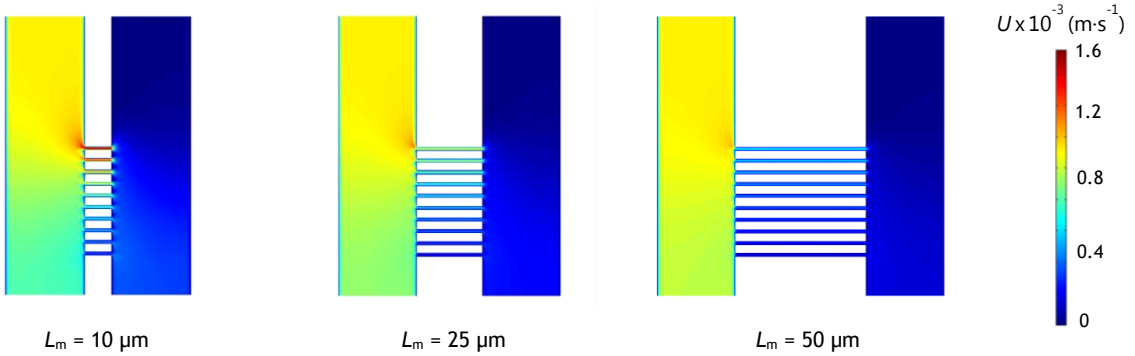

Figure 5.18 - Colour maps of the velocity field in devices with different microchannel lengths (Case XIV, *VR*=100, W_f=30 µm).

A fluid preferentially flows through places with lower fluidic resistances. Reducing the available length in the microchannel for fluid to flow (i.e. decreasing L_m), decreases the fluidic resistance[1], enabling the fluid in the feed channel to escape more easily into the microchannels, when compared to higher values of L_m. This is in agreement with pressure difference per unit length along the microchannels observed in Figure 5.17. For lower L_m, higher pressure difference per unit length is observed. Consequently, the velocity in the shorter microchannels is higher, as seen in Figure 5.18 (the colour in the first microchannel for L_m = 10 µm is red which indicates higher velocity than the blue colour observed for L_m = 25 µm and L_m = 50 µm).

Since bacteria are expected to be carried by the fluid along the streamlines, and the entrance of fluid in the microchannels is enhanced when microchannels are shorter, more bacteria are trapped for lower L_m (Figure 5.19).

In Figure 5.19 one observes that when *VR* = 1 and W_f = 30 µm (Case XVIII) the percentage of trapped bacteria is zero, but when W_f = 10 µm (Case XIX) the percentage of trapped bacteria is slightly bigger than zero (two trapped bacteria for L_m = 10 µm, and one bacteria for L_m = 25 µm and L_m = 50 µm). This occurs since $W_f \neq W_w$, which causes a difference on the velocity profiles along

[1] Fluidic resistance is directly proportional to the channel length (Beebe et al., 2002, p. 264).

feed channel width and waste channel width[1]. In narrower feed channels, the fluid near the walls/microchannel entrance flows slower than in wider feed channels (for the scenarios where velocities in the feed and waste inlet are the same, *VR* = 1), which enables the easier change of direction and the unlikely possibility of bacteria entering the microchannels. For the same reason, for higher velocity ratios, more bacteria are trapped in devices with narrower feed channels (Figure 5.19, Case XVI and VII for *VR* = 20 and Case XIV and XV for *VR* = 100). As observed in subsection 5.2 increasing the velocity ratio further than 20 does not have a relevant effect on bacteria trapping. In Figure 5.19, it is seen that the curves of the percentage of trapped bacteria for velocity ratio of 20 match those of velocity ratio of 100, both for W_f = 30 µm and W_f = 10 µm.

In this case, the device was not long enough to determine the values of the effective length. However, by analysing the velocity magnitude in the microchannels (Figure 5.18, Case XIV), for three different microchannel lengths, one can ascertain, as the velocity is higher, that the maximum length in which trapping can occur will be higher for shorter microchannels.

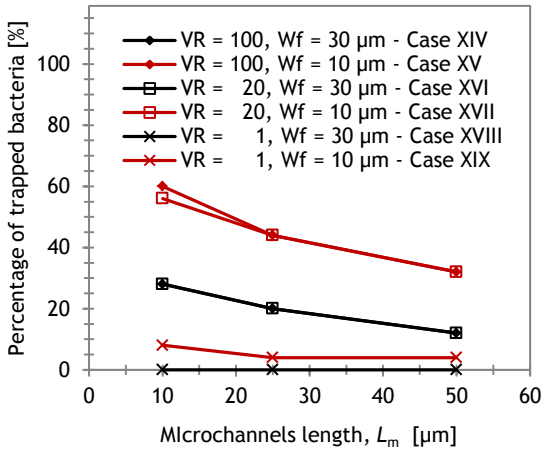

Figure 5.19 - Percentage of trapped bacteria for devices with different microchannels length, for Cases XIV to XIX.

Hence, decreasing microchannel length enhances the entrance of bacteria in the microchannels. Nevertheless, longer microchannels are suitable to monitor more bacteria per microchannel, as there is more space available for the trapped bacterium to grow, i.e. to form new bacteria by cell division.

5.8. Trapping strategies

This project gives an insight of the influence of device configuration and working conditions on the entrance of bacteria in the microchannels. However, the strategy that allows the trapping of bacteria inside the microchannels (i.e. that prevents bacteria from exit the microchannel) was not considered in the performed simulations. In this subsection trapping strategies are suggested and discussed.

[1] Please refer to subsection 5.2 for a further understanding.

In the base model device, the bacteria (1 μm diameter) released closer to the microchannels entrance, will enter the 1.5 μm wide microchannels. Then, the bacteria flow along the microchannels until they reach the waste channel since there is nothing to prevent them from leaving the microchannel. The first suggested strategy to trap bacteria consists on adding a solid barrier on the right edge of the microchannel, small enough to allow fluid to flow along the microchannels and consequently bacteria to enter the microchannels, but big enough to stop/trap the bacteria. In Figure 5.20a and Figure 5.20b cube-shaped barriers were chosen, which are represented by black squares. Another option is to block a portion of the width of the microchannel near its outlet, so the bacteria cannot pass onto the waste channel, as illustrated in Figure 5.20c. One of the goals of this microdevice is to monitor single bacteria behaviour/growth in a fixed position. Therefore, it is essential that bacteria grow in a monolayer, i.e. along *z* for a given *x*- and *y*-coordinate there is only one cell. Reducing microchannels width to 1 μm (Figure 5.20d) restricts the cells to grow in a monolayer (which allows clear analysis of single cell with the available equipment, e.g. microscopes). However, if microchannel width is equal or inferior to bacteria diameter, problems in bacteria entrance in the microchannels may arise. A strategy to avoid this is suggested in Figure 5.20e and Figure 5.20f which consists on a gradual confinement of the microchannel width. In these scenarios, if the width of the microchannel entrance is too big the bacteria can overlap, affecting the monolayer analysis. Moreover, for very narrow microchannel exits, a portion of the microchannel is unutilized for growing bacteria or newly formed bacteria will have its growth strongly restricted by microchannel width.

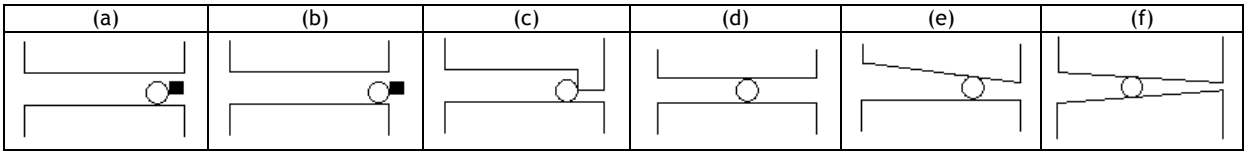

Figure 5.20 – Schematic representation of trapping strategies. Close-up of a microchannel.

Microfabrication techniques have been widely developed in the recent years to overcome size limitations. The commonly used techniques to manufacture PDMS devices (e.g. lithography[1]) have precision bigger than 0.5 μm which limits the manufacturing of devices such as the ones presented in Figure 5.20. An alternative to physical trapping is hydrodynamic trapping. As concluded in subsection 5.2, if the pressure difference between the edges of the microchannels is null, the fluid inside them is stagnated. A way to stop the bacteria inside the microchannel would be to change the velocity ratio to 1 (by equalling the velocity of the waste inlet to the one of the feed inlet) which can cause a null pressure difference along the microchannels (and possibly the bacteria will be trapped). As a change on the inlet velocities takes time to act on the entire domain (i.e. is not instantaneous), and consequently on the fluid velocity inside the microchannels, one needs to assure that the bacteria stay a sufficiently long time inside the microchannels in order to be stopped. To increase the number of trapped bacteria by this way, and regarding the numerical results presented so far, several strategies can be used to increase the residence time of the bacteria in the micro-

[1] (Tabeling, 2005, p. 247).

channels: decreasing feed channel width, which enhances the entrance of bacteria on the microchannels and decreases fluid velocities in the microchannels; decreasing the inlet average velocity in the feed channel, for a constant velocity ratio, which does not affect the entrance of bacteria in the microchannels, but allows the bacteria to cross the microchannel at a lower velocity (i.e. taking more time); last, increasing the microchannels length which increases the time of the bacteria inside the microchannels but decreases the percentage of bacteria that enters the microchannels.

5.9. Feeding of bacteria and removal of metabolic products

One of the device main goals concerning mass transport is to avoid two common problems: nutrient shortage and metabolic products accumulation, since they lead to bacteria death. In this study the transport of nutrients, without its consumption, was computed which gives a preliminary analysis of the amount of nutrients that will be available to the trapped bacteria. Further in this section, a simplified approach of bacterial metabolic conversion of nutrients in products is explained and a possible computational model to implement is proposed.

The nutrient feed was assumed to be a diluted solution of glucose in water. In a previous study, Westerwalbesloh et al. (2015) used concentrations in a range of 0.04 to 0.2 M to feed bacteria. Moreover Kazan et al. (1995) refers that a glucose concentration of approximately 0.09 M (which corresponds to 16 g/L) promotes an optimized metabolic performance of e-coli. Therefore, one selected an inlet concentration, on the feed channel, of 0.1 M and a diffusion coefficient[1] of glucose in water of 5.4×10^{-10} $m^2.s^{-1}$. In the parametric simulations performed in this project, the bacteria take 10 to 100 milliseconds to cross the microchannels, so it needs less than one second to be trapped. Thus, trapping of bacteria was not simulated since the required time is negligible compared with the time spent to monitor the growth of the (already trapped) bacteria in the microchannels (around 24 hours). It was then considered that the bacteria were immobilized in the microchannels. A bacterium[2] was placed in each microchannel, with its centre located in the geometric centre of the microchannels. Two velocity ratios, i.e. feed to waste inlet average velocity ratios, were studied in a device similar to the base model (section 5.1) but with three microchannels[3] (L_μ = 10.5 μm). The choice of velocity ratio was based on the trapping strategies. The case where the bacteria is trapped due to the sudden change of velocity ratios (hydrodynamic trapping) corresponds to the selected *VR* = 1 and the presence of a physical barrier to *VR* = 100. Figure 5.21 shows the velocity field in the first microchannel of the microdevice for both velocity ratios. Figure 5.22 and Figure 5.23 show the glucose concentration in the domain for selected, when *VR* = 1 and *VR* = 100, respectively.

[1] This value of diffusion coefficient is based on a temperature of 30 °C (Westerwalbesloh et al., 2015).

[2] Adding bacteria in the computational domain of the microchannels (represented by circumferences) increases substantially the computational time, as tighter spaces appear (similar to microchannels 0.25 μm wide) which require more mesh elements to obtain accurate results. Therefore, in a first approach one considered a single bacterium in each microchannel.

[3] A longer device would increase substantially the computational cost of the time-dependent simulations, and would not add significant information to the obtained results for the shorter device.

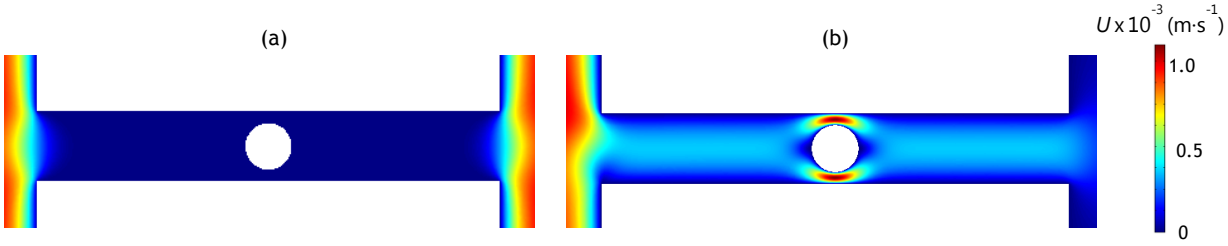

Figure 5.21 - Close-up of the velocity field colour map in the first microchannel for a device similar to the base model and L_{μ} = 10.5 µm, for (a) *VR* = 1 and (b) *VR* = 100.

For *VR* = 1, the presence of a bacteria in the microchannels does not affect the overall fluid flow behaviour because the fluid in the microchannels is stagnated (null pressure difference between entrance and exit). However, for *VR* = 100 the effects of bacteria presence on fluid velocity are visible (Figure 5.21b). Near the computed bacteria, in the gaps between the microchannel walls and the bacteria itself, the fluid elements are accelerated (due to decreasing space available for fluid to flow), which results on an increase of the local fluid velocity. When the average inlet velocity is the same in both main channels, i.e. *VR* = 1, the fluid inside the microchannels is stagnated, and therefore the Péclet number is zero. Thus, diffusion governs the mass transfer along the microchannels, as it is visible in the colour pattern from red, at the microchannel entrance, to blue, at the microchannel outlet (Figure 5.22). In the main channels, mass transfer occurs mainly by advection. In Figure 5.23 one observes that, for *VR* = 100, mass transfer in the feed channel occurs by advection. It was previously seen that for *VR* ≠ 1 the fluid flows from the feed channel to the waste channel. Therefore the mass transfer inside the microchannels is ruled by the hydrodynamic transport phenomena, i.e. diffusion does not have a significant effect when compared to advection. After the glucose reaches the end of the microchannels, mass transfer occurs mainly by diffusion in the waste channel due to the very low inlet velocity in the waste stream.

As expected, due to fluid flow behaviour in the device, the nutrients reach the bacteria in the first microchannels first, i.e. bacteria are not fed at the same time. However, after a certain time, when the stationary state is reached, all bacteria have access to the same concentration of nutrients. Figure 5.24 illustrates the evolution of average concentration along microchannel entrance, microchannel outlet and bacteria surface over time. It is shown that the steady state average concentrations are reached before 200 ms, with the exception of the microchannel outlet when VR = 100 due to the meeting of two streams with very different concentrations and velocities (microchannel stream: $C_{aver,glucose}$ = 100 mol·m^{-3}, U_{aver} = 0.245 mm·s^{-1}; waste stream: $C_{aver,glucose}$ = = 0 mol·m^{-3}, U_{aver} = 0.01 mm·s^{-1}). Moreover, one can observe that, when the ratio between feed and waste inlet average velocities is 100, the glucose spreads more efficiently across the microchannel (Figure 5.24a and b). For *VR* = 1, the concentration of glucose (in the steady state) along the microchannel varies from 93.6 to 6.4 mol·m^{-3} while for VR = 100 the concentration varies from 100.0 to 83.4 mol·m^{-3}. Therefore, the bacteria located near the edge of the microchannel closer to the waste channel will have access to more nutrients.

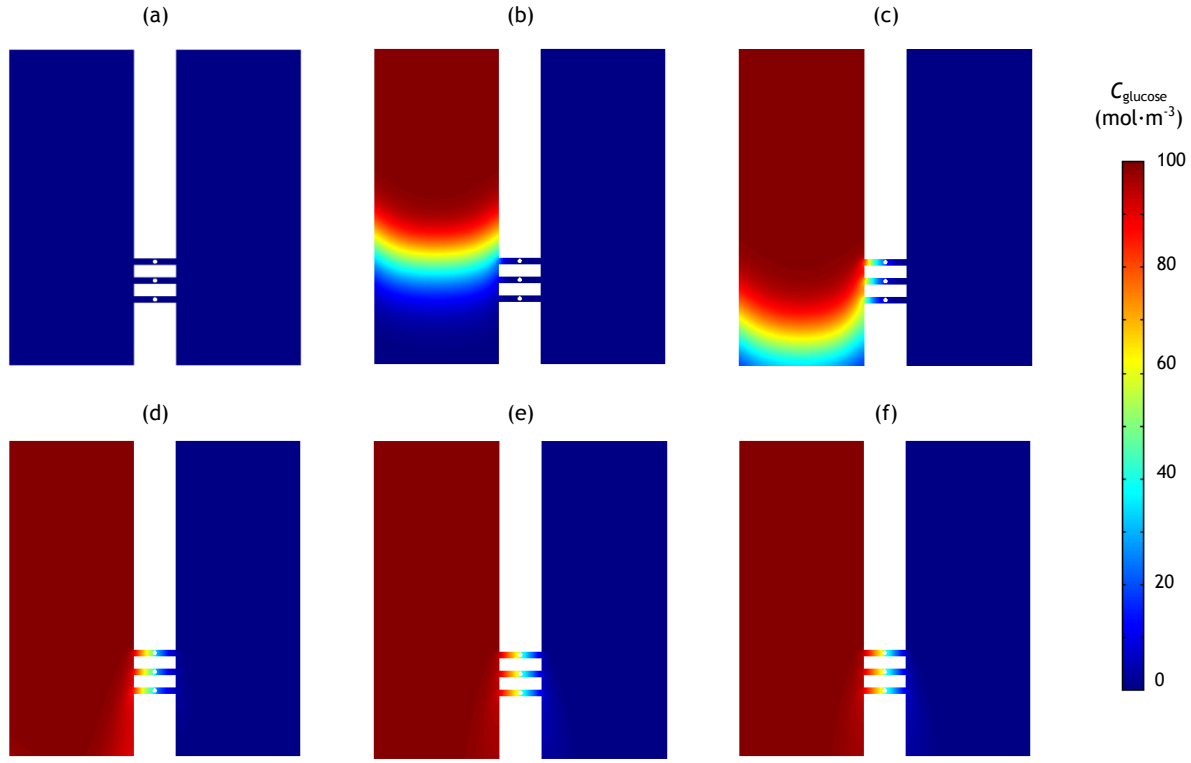

Figure 5.22 - Colour maps of the glucose concentration for a device similar to the base model and L_μ = 10.5 µm, for VR = 1, after (a) 0 ms, (b) 50 ms, (c) 70 ms, (d) 100 ms, (e) 700 ms and (f) at stationary state.

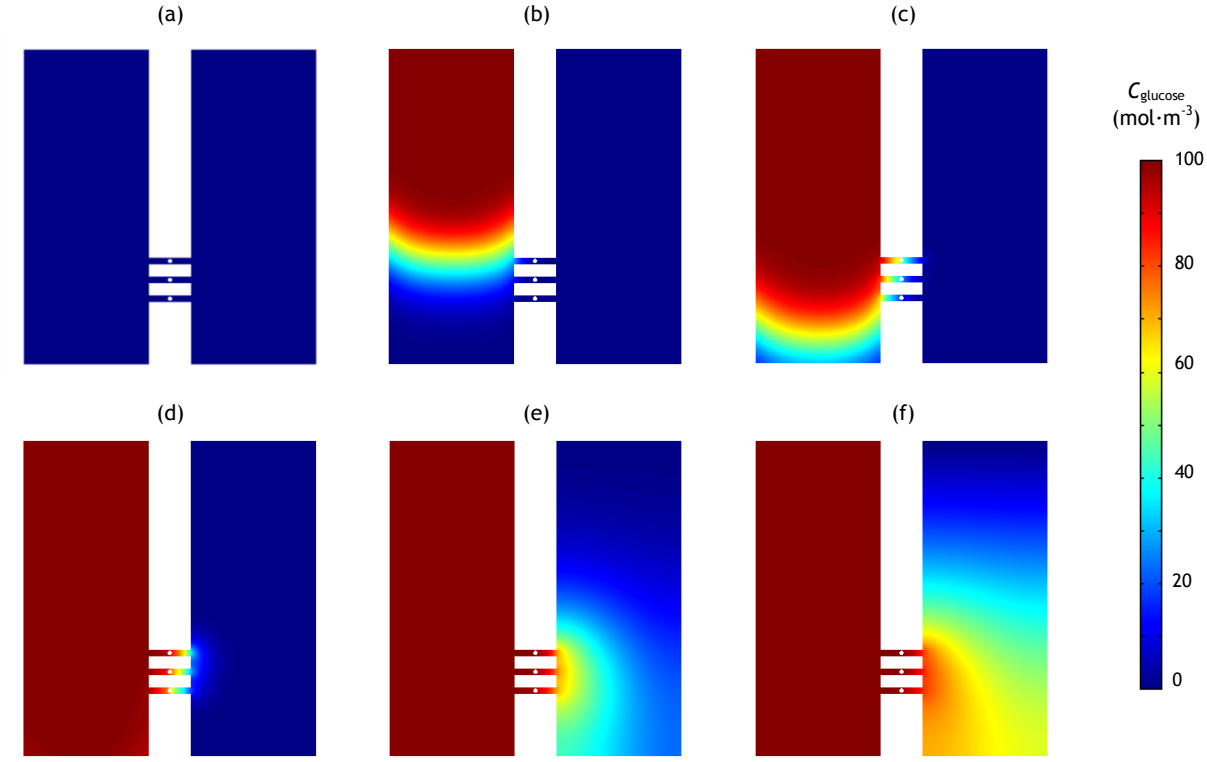

Figure 5.23 - Colour maps of the glucose concentration for a device similar to the base model and L_μ = 10.5 µm, for VR = 100, after (a) 0 ms, (b) 50 ms, (c) 70 ms, (d) 100 ms, (e) 700 ms and (f) at stationary state.

With this preliminary analysis on mass transfer one concludes that physical trapping strategies (examples shown in Figure 5.20a-f) promote a more effective feeding of the bacteria along the microchannels than hydrodynamic trapping (by equalling feed and waste inlet velocities), as long as the bacteria only partially clogs the microchannels when trapped, so that fluid flows through the microchannel and allows advection of the nutrients.

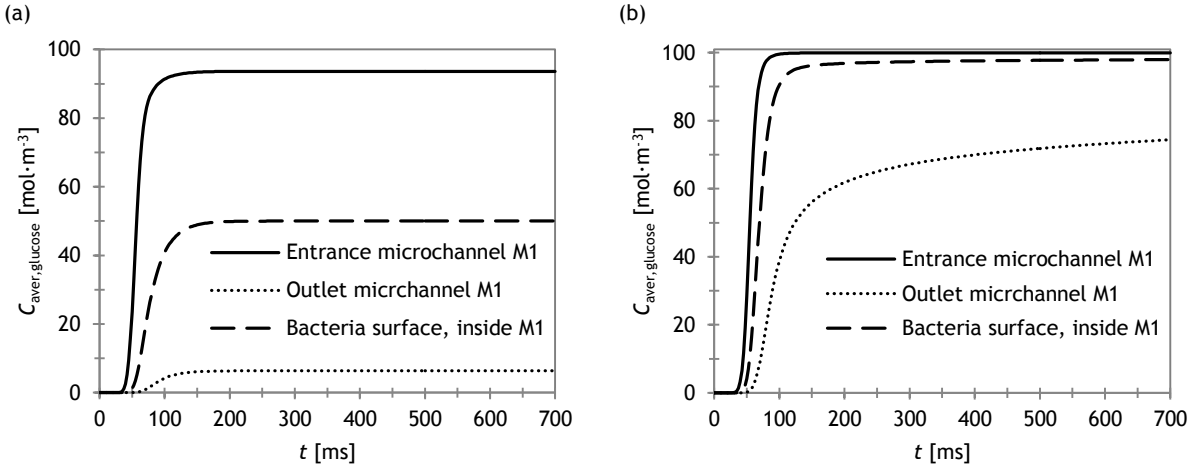

Figure 5.24 – Variation of glucose average concentration with time, at the entrance and outlet of the first microchannel and at the surface of the bacteria located in the middle of the first microchannel, for (a) *VR* = 1 and (b) *VR* = 100.

The bacterial metabolic process is many times simplified to the glycolysis reaction which converts glucose ($C_6H_{12}O_6$) into lactic acid ($C_3H_6O_3$), and can be roughly described by the following irreversible reaction: $C_6H_{12}O_6 \rightarrow 2\,C_3H_6O_3$. Assuming that the bacteria excrete the metabolic products evenly along its surface, glycolysis could be simulated by defining a surface reaction in the circumference (that represents the bacteria) which consumes the available glucose in the bacteria surface and releases lactic acid, defined as a function of the average concentration of consumed glucose. In order to apply this methodology, new settings/modules, of the FEM platform used in this project, would have to be studied to create/implement a new computational model, which would also need to be validated. Due to the limited time of the thesis, this approach was not yet developed. Nonetheless, since there is continuous flow of fresh streams in the presented device, i.e. without any metabolic products, one expects that no excessive waste will be accumulated in the microchannels.

6. Conclusions

In this project, computational fluid dynamics was used to investigate the conditions that enhance bacteria trapping and in which way these conditions affect the trajectory of bacteria in a trapping bacteria device with continuous feeding and waste removal. The effects of feed channel width (W_f), device length (L_μ), microchannel density (N_μ/L_μ), microchannel length (L_m), feed to waste inlet velocity ratio (*VR*) and average inlet velocity of the feed channel (U_f) were analysed. Trapping strategies in this type of microdevices were suggested and a preliminary analysis on the distribution of nutrients was considered.

Narrower feed channels (for constant width of the waste channel) facilitate the fluid flow from the feed channel onto the microchannels, due to the lower velocities in the vicinity of the microchannel entrance. Therefore, trapping of bacteria increases with narrower feed channels. However one must recognize that, lower dimensions can run into the limits of microfabrication and can cause an increase on manufacturing defects. Furthermore, for devices with lower feed channel width, the effective trapping length is lower. This means that the maximum percentage of trapped bacteria, for a given set of parameters, is reached in shorter device length, which may eventually imply lower fabrication cost. Changing feed and waste channel width in a similar way ($W_f = W_w$) does not produce a significant effect on bacteria trapping.

An increase of the device length, by adding microchannels equally spaced, increases the percentage of trapped bacteria until it reaches a point (L_{crit}) after which the addition of microchannels does not influence fluid flow and, consequently, bacteria trapping. When the device length is bigger than L_{crit}, the bacteria do not enter the additional microchannels because of the null pressure difference between their entrance and exit. Thus, it is important to know the value of L_{crit} (effective trapping length), for a given combination of device parameters and inlet boundary conditions, in order to avoid fabrication of unnecessarily long devices.

The density of microchannels, for a constant device length, does not affect the percentage of trapped bacteria. Therefore, a compromise between the difficulty/cost of manufacturing more confined microchannels (for the same length) and having more microchannels in which bacteria can be monitored, must be considered.

Moreover, more bacteria are trapped when the device has shorter microchannels. However, longer microchannels might be useful if one wants to monitor more bacteria per microchannel or even as an auxiliary strategy to hydrodynamic trapping, as it increases the residence time of bacteria inside the microchannel.

Regarding inlet boundary conditions, increasing the feed to waste velocity ratio *VR* (for a constant inlet feed velocity) enhances bacteria trapping, until *VR* equal to 20. Further increases of velocity ratio do not considerably influence bacteria entrance in the microchannels (i.e. trapping).

Finally, no relevant effects on bacteria trapping were found when changing the feed channel inlet average velocity for constant feed to waste velocity ratio. Therefore, the obtained results and conclusions should be valid for different velocities of the feed inlet, which is very convenient, for instance, to influence the residence time of bacteria in the microchannels.

Possible trapping strategies to implement in the future device were suggested. Hydrodynamic trapping, by equalling the inlet velocities of the main channels, does not need structural changes on the microdevice. However, the transport of nutrients inside the microchannel only occurs by diffusion, creating a concentration gradient which prevents the bacteria closer to microchannels outlet to receive sufficient nutrients. Adding physical barriers or reducing the width of the microchannels to confine the bacteria are solutions that allow advection of nutrients along the microchannel, i.e. more efficient feeding of bacteria. Nonetheless, some PDMS microdevices manufacturing methods are still not precise enough to enable these specificities.

These results will be useful for building an innovative trapping bacteria device. For its fabrication, the selection of the optimal parameters should be carefully pondered according to the experimental limitations, e.g. pressure drop/flow rate limits of the micropump, precision of the manufacturing method and biological demands of bacteria motion in a confined channel (e.g. maximum stress that a cell can sustain without occurrence of lysis, rupture of cell membrane).

6.1. Limitations and future work

This study is valid for spherical bacteria/particles with different diameters or densities as long as Stokes number is much inferior to 1, so that the assumption of bacteria following the fluid streamlines is applicable.

The next step, in computational modelling, would be to consider soft spherical bacteria (instead of the previous rigid assumption), in order to incorporate the flexible nature of cell membrane. A possible way to implement this feature would be to use the Lattice-Boltzmann method, which solves two-phase flow, and was previously used by Xiong and Zhang (2012) to model red blood cells. As many bacteria are bacillus (e.g. E. coli) it would be beneficial to assume, in a future approach, an ellipsoidal shape for the bacteria domain.

Concerning the microfabrication of the trapping device, strategies to overcome the techniques limitations should be developed, in order to enable a more precise trap fabrication among the device.

References

Ai, Y., Joo, S. W., Jiang, Y., Xuan, X. & Qian, S. Pressure-driven transport of particles through a converging-diverging microchannel. *Biomicrofluidics*, *3*, 1–14. 2009

Al Quddus, N., Moussa, W. a. & Bhattacharjee, S. Motion of a spherical particle in a cylindrical channel using arbitrary Lagrangian-Eulerian method. *Journal of Colloid and Interface Science*, *317*, 620–630. 2008

Banaeiyan, A. a., Ahmadpour, D., Adiels, C. B. & Goksör, M. Design and fabrication of high-throughput application-specific microfluidic devices for studying single-cell responses to extracellular perturbations. *Bio-MEMS and Medical Microdevices*, *8765*, 1 – 13. 2013

Bayraktar, T. & Pidugu, S. B. Characterization of liquid flows in microfluidic systems. *International Journal of Heat and Mass Transfer*, *49*, 815–824. 2006

Becker, H. & Locascio, L. E. Polymer microfluidic devices. *Talanta*, *56*, 267–287. 2002

Beebe, D. J., Mensing, G. a & Walker, G. M. Physics and applications of microfluidics in biology. *Annual Review of Biomedical Engineering*, *4*, 261–86. 2002

Boedicker, J. Q., Li, L., Kline, T. R. & Ismagilov, R. F. Detecting bacteria and determining their susceptibility to antibiotics by stochastic confinement in nanoliter droplets using plug-based microfluidics. *Lab on a Chip*, *8*, 1265–1272. 2008

Bruus, H. Acoustofluidics 1: Governing equations in microfluidics. *Lab on a Chip*, *11*, 3742–3751. 2011

Charhrouchni, I., Pallandre, A., Le Potier, I., Deslouis, C. & Haghiri-Gosnet, A.-M. Computational study of velocity profile obtained in microfluidic channel bearing a fluidic transistor: Toward highly resolved electrophoretic separation. *Electrophoresis*, *34*, 725–735. 2013

Choi, I., Yang, Y. I., Kim, Y. J., Kim, Y., Hahn, J. S., Choi, K. & Yi, J. Directed positioning of single cells in microwells fabricated by scanning probe lithography and wet etching methods. *Langmuir*, *24*, 2597–2602. 2008

COMSOL. *COMSOL Multiphysics Reference Manual*. 2013

Dechadilok, P. & Deen, W. M. Hindrance factors for diffusion and convection in pores. *Industrial and Engineering Chemistry Research*, *45*, 6953–6959. 2006

Erickson, D., Sinton, D. & Li, D. Joule heating and heat transfer in poly(dimethylsiloxane) microfluidic systems. *Lab on a Chip*, *3*, 141. 2003

Eun, Y. J., Utada, A. S., Copeland, M. F., Takeuchi, S. & Weibel, D. B. Encapsulating bacteria in agarose microparticles using microfluidics for high-throughput cell analysis and isolation. *ACS Chemical Biology*, *6*, 260–266. 2011

Faustini, M., Kim, J., Jeong, G., Kim, J. Y., Moon, H. R., Ahn, W. & Kim, D. Microfluidic approach toward continuous and ultrafast synthesis of Metal − Organic Framework crystals and hetero structures in confined microdroplets. *Journal of American Chemical Society*, *135*, 14619–14626. 2013

Figueroa-Morales, N., Miño, G. L., Rivera, A., Caballero, R., Clément, E., Altshuler, E. & Lindner, A. Living on the edge: transfer and traffic of E. coli in a confined flow. *Soft Matter*, (3), 1–11. 2015

Gerdts, C. J., Tereshko, V., Yadav, M. K., Dementieva, I., Collart, F., Joachimiak, A., … Ismagilov, R. F. Time-controlled microfluidic seeding in nL-volume droplets to separate nucleation and

growth stages of protein crystallization. *Angewandte Chemie - International Edition*, *45*, 8156–8160. 2006

Grünberger, A., Paczia, N., Probst, C., Schendzielorz, G., Eggeling, L., Noack, S., … Kohlheyer, D. A disposable picolitre bioreactor for cultivation and investigation of industrially relevant bacteria on the single cell level. *Lab on a Chip*, *12*, 2060–2068. 2012

Hardt, S. & Schönfeld, F. Microfluidics: Fundamentals and engineering concepts. In *Microfluidic Technologies for Miniaturized Analysis Systems* (pp. 1–58). 2007

Herbert, D., Elsworth, R. & Telling, R. C. The Continuous Culture of Bacteria; a Theoretical and Experimental Study. *Journal of General Microbiology*, *14*, 601–622. 1956

Holden, M. a., Kumar, S., Castellana, E. T., Beskok, A. & Cremer, P. S. Generating fixed concentration arrays in a microfluidic device. *Sensors and Actuators, B: Chemical*, *92*, 199–207. 2003

Horiuchi, K. & Dutta, P. Joule heating effects in electroosmotically driven microchannel flows. *International Journal of Heat and Mass Transfer*, *47*, 3085–3095. 2004

Hur, S. C., Mach, A. J. & Di Carlo, D. High-throughput size-based rare cell enrichment using microscale vortices. *Biomicrofluidics*, *5*, 1 – 10. 2011

Hyun, D. C., Levinson, N. S., Jeong, U. & Xia, Y. Emerging applications of phase-change materials (PCMs): Teaching an old dog new tricks. *Angewandte Chemie - International Edition*, *53*, 3780–3795. 2014

Jeon, W. & Shin, C. B. Design and simulation of passive mixing in microfluidic systems with geometric variations. *Chemical Engineering Journal*, *152*, 575–582. 2009

Junkin, M. & Tay, S. Microfluidic single-cell analysis for systems immunology. *Lab on a Chip*, *14*, 1246–60. 2014

Kashaninejad, N., Chan, W. K. & Nguyen, N. Analytical and Numerical Investigations of the Effects of Microchannel Aspect Ratio on Velocity Profile and Friction Factor (pp. 1–9). 2012

Kazan, D., Çamurdan, A. & Hortaçsu, A. The effect of glucose concentration on the growth rate and some intracellular components of a recombinant E. coli culture. *Process Biochemistry*, *30*, 269–273. 1995

Kim, M.-C. & Klapperich, C. A new method for simulating the motion of individual ellipsoidal bacteria in microfluidic devices. *Lab on a Chip*, *10*, 2464–2471. 2010

Kim, S., Kim, H. J. & Jeon, N. L. Biological applications of microfluidic gradient devices. *Integrative Biology*, *2*, 584–603. 2010

Kirby, B. J. *Micro- and Nanoscale Fluid Mechanics: Transport in Microfluidic Devices*. Cambridge University Press. 2010

Kuhn, P., Puigmartí-Luis, J., Imaz, I., Maspoch, D. & Dittrich, P. S. Controlling the length and location of in situ formed nanowires by means of microfluidic tools. *Lab on a Chip*, *11*, 753–7. 2011

Lee, H., Ham, D. & Westervelt, R. M. *CMOS Biotechnology*. Springer Science and Business Media. 2007

Li, Y., Jain, M. & Nandakumar, K. Numerical study of droplet formation inside a microfluidic flow-focusing device. In *2012 Comsol Conference in Boston* (pp. 1–6). 2012

Low, W. S., Kadri, N. A. & Wan Abas, W. A. B. Computational Fluid Dynamics Modelling of

Microfluidic Channel for Dielectrophoretic BioMEMS Application. *The Scientific World Journal*, *2014*, 1 – 11. 2014

Mckay, T. L. *A CFD model of mixing in a microfluidic device for space medicine technology*. Cleveland State University. Master Thesis 2011

Nanninga, N. Morphogenesis of Escherichia coli. *Microbiology and Molecular Biology Reviews*, *62*, 110–129. 1998

Nguyen, N.-T. & Wereley, S. T. *Fundamentals and Applications of Microfluidics*. Norwood, MA: Artech House. 2002

Nie, F., Yamada, M., Kobayashi, J. & Yamato, M. On-chip cell migration assay using microfluidic channels. *Biomaterials*, (28), 4017 – 4022. 2007

Nightingale, A. M., Bannock, J. H., Krishnadasan, S. H., O'Mahony, F. T. F., Haque, S. a, Sloan, J., … de Mello, J. C. Large-scale synthesis of nanocrystals in a multichannel droplet reactor. *Journal of Materials Chemistry A*, *1*, 4067–4076. 2013

Nightingale, A. M. & de Mello, J. C. Microscale synthesis of quantum dots. *Journal of Materials Chemistry*, *20*, 8454. 2010

Nilsson, J., Evander, M., Hammarström, B. & Laurell, T. Review of cell and particle trapping in microfluidic systems. *Analytica Chimica Acta*, *649*, 141–157. 2009

Paik, P. Y., Pamula, V. K. & Chakrabarty, K. A digital-microfluidic approach to chip cooling. *IEEE Design and Test of Computers*, *25*, 372–391. 2008

Peyman, S. a., Kwan, E. Y., Margarson, O., Iles, A. & Pamme, N. Diamagnetic repulsion-A versatile tool for label-free particle handling in microfluidic devices. *Journal of Chromatography A*, *1216*, 9055–9062. 2009

Puigmartí-Luis, J. Microfluidic platforms: a mainstream technology for the preparation of crystals. *Chemical Society Reviews*, *43*, 2253–71. 2014

Puigmartí-Luis, J., Rubio-Martínez, M., Hartfelder, U., Imaz, I., Maspoch, D. & Dittrich, P. S. Coordination polymer nanofibers generated by microfluidic synthesis. *Journal of the American Chemical Society*, *133*, 4216–4219. 2011

Puigmartí-Luis, J., Schaffhauser, D., Burg, B. R. & Dittrich, P. S. A microfluidic approach for the formation of conductive nanowires and hollow hybrid structures. *Advanced Materials*, *22*, 2255–2259. 2010

Sarkar, S., Singh, K. K., Shankar, V. & Shenoy, K. T. Numerical simulation of mixing at 1–1 and 1–2 microfluidic junctions. *Chemical Engineering and Processing: Process Intensification*, *85*, 227–240. 2014

Stone, H. a., Stroock, A. D. & Ajdari, A. Engineering flows in small devices: Microfluidics toward a Lab-on-a-chip. *Annual Review of Fluid Mechanics*, *36*, 381–411. 2004

Tabeling, P. *Introduction to Microfluidics*. Oxford University Press. 2005

Tanyeri, M., Johnson-Chavarria, E. M. & Schroeder, C. M. Hydrodynamic trap for single particles and cells. *Applied Physics Letters*, *96*, 1 – 3. 2010

Tanyeri, M., Ranka, M., Sittipolkul, N. & Schroeder, C. M. A microfluidic-based hydrodynamic trap: design and implementation. *Lab on a Chip*, *11*, 1786–1794. 2011

Tanyeri, M. & Schroeder, C. M. Manipulation and Confinement of Single Particles Using Fluid Flow. *Nano Letters*, *13*, 2357–2364. 2013

Tsai, C.-H., Chen, H.-T., Wang, Y.-N., Lin, C.-H. & Fu, L.-M. Capabilities and limitations of 2-dimensional and 3-dimensional numerical methods in modeling the fluid flow in sudden expansion microchannels. *Microfluidics and Nanofluidics*, *3*, 13–18. 2006

Vigeant, M. a & Ford, R. M. Interactions between motile Escherichia coli and glass in media with various ionic strengths, as observed with a three-dimensional-tracking microscope. *Applied and Environmental Microbiology*, *63*, 3474–3479. 1997

Vladisavljević, G. T., Shahmohamadi, H., Das, D. B., Ekanem, E. E., Tauanov, Z. & Sharma, L. Glass capillary microfluidics for production of monodispersed poly (DL-lactic acid) and polycaprolactone microparticles: Experiments and numerical simulations. *Journal of Colloid and Interface Science*, *418*, 163–170. 2014

Wehking, J. D., Chew, L. & Kumar, R. Droplet actuation in an electrified microfluidic network. *Lab on a Chip*, *15*, 793–801. 2015

Westerwalbesloh, C., Grünberger, A., Stute, B., Weber, S., Wiechert, W., Kohlheyer, D. & Lieres, E. Von. Modeling and CFD simulation of nutrient distribution in picoliter bioreactors for bacterial growth studies on single-cell level. *Lab on a Chip*, *15*, 4177–4186. 2015

White, F. M. *Viscous fluid flow*. McGraw-Hill. 1974

Whitesides, G. M. The origins and the future of microfluidics. *Nature*, *442*, 368–73. 2006

Wu, Z., Willing, B., Bjerketorp, J., Jansson, J. K. & Hjort, K. Soft inertial microfluidics for high throughput separation of bacteria from human blood cells. *Lab on a Chip*, *9*, 1193–1199. 2009

Xu, X., Li, Z. & Nehorai, A. Finite element simulations of hydrodynamic trapping in microfluidic particle-trap array systems. *Biomicrofluidics*, *7*, 1–16. 2013

Zheng, B., Tice, J. D., Roach, L. S. & Ismagilov, R. F. A droplet-based, composite PDMS/glass capillary microfluidic system for evaluating protein crystallization conditions by microbatch and vapor-diffusion methods with on-chip X-ray diffraction. *Angewandte Chemie - International Edition*, *43*, 2508–2511. 2004

Zheng, X. & Silber-Li, Z. H. Measurement of velocity profiles in a rectangular microchannel with aspect ratio α = 0.35. *Experiments in Fluids*, *44*, 951–959. 2008

Annex A – Geometry

This section is not shown because of confidentiality issues.

Annex B – One way vs two way interaction

There are two methods of solving the physics behind particle motion: considering that the fluid velocity field affects the particle trajectories but the particles do not affect the flow, known as one-way interaction, and assuming that both physics are inter-related, i.e. particle motion affects and is affected by fluid flow, known as two-way interaction. The two-way interaction is applied when particles are electrically/magnetically charged, when the number density of particles is very large or when particle size is similar to the size of the channel (since particle-particle and particle-wall interactions cannot be neglected). In this project, bacteria (that are treated as rigid spherical particles) flow in confined spaces, i.e. particle diameter is similar to the space available to move, when flowing along the microchannels.

However, both approaches were studied in a first analysis, to evaluate the need of considering two-way interaction since it implies solving fluid flow in a time-dependent study and, consequently, higher computational cost. Simulations were conducted in a device identical to the base model microdevice (Table 2.1) but with only one microchannel. One particle was released from the inlet, the average velocity at the feed inlet was set to 1 $mm \cdot s^{-1}$ and the ratio between feed and waste channel was set 100 and 10. Accordingly to the available modules in COMSOL, two models for particle motion were tested. In the first case *Laminar flow* and *Particle tracing* modules were combined for a one-way interaction approach. This approach is based in the Eulerian method that determines the velocity and the pressure field in a selected geometry and in the Lagrangian method which analyses the motion of a particle on fluid flow in space and in time. In the second case a two-way interaction approach was considered by using the *Fluid-Structure Interaction* module. For simulations of fluid-solid systems in which particle motion affects and is affected by fluid flow, arbitrary Lagrangian-Eulerian (ALE) method is widely used (Ai et al., 2009; Al Quddus et al., 2008; Xu et al., 2013).

The one-way approach is the one described in section 3.3, that consists in solving the fluid flow and particle motion independently (as the flow is not affected by the presence of the particles). The two-way model tested uses Fluid-Structure Interaction (FSI) interface that is based on three modules *Laminar flow*, *Solid mechanics* and *Moving mesh*. In this model a circle with diameter d_p is added to the geometry and then that circle, i.e. the particle, is tracked and the mesh is adapted to its location. Therefore, the fluid flow and particle motion are both solved along time.

Figure B.1a and Figure B.1b represent the trajectory of the released particle considering one-way and two-way approaches, when *VR* = 100 and *VR* = 10 respectively. The computational time needed to run the previous simulations was 37s (*VR* = 100) and 31s (*VR* = 10) for the one way approach and 1h 25min 47s (*VR* = 100) and 1h 21min 25s (*VR* = 10) for the two-way approach.

It is visible (Figure B.1) that, for both cases, the trajectory of the particle before microchannel entrance is the same when considering one-way or two-way. After the microchannel entrance, the trajectory of the particles for the two-way approach is different (from the one-way) since the particle inside the microchannel affects the local fluid velocity. In the waste channel, as the particle velocity at the microchannel outlet is different, the acquired trajectory is also different. As the goal of the project is to evaluate the entrance of the particles in the microchannels, and given the need to run an extensive series of parametric studies, the approach with lower computational cost was

selected (i.e. one-way interaction approach which considers that the fluid flow is not affected by the presence of particles). By applying the one-way approach, the particles are considered as points and therefore they do not displace the volume they occupy (i.e. it is possible, in the numerical results, that a particle centre approximates near a wall at a distance inferior to its radius).

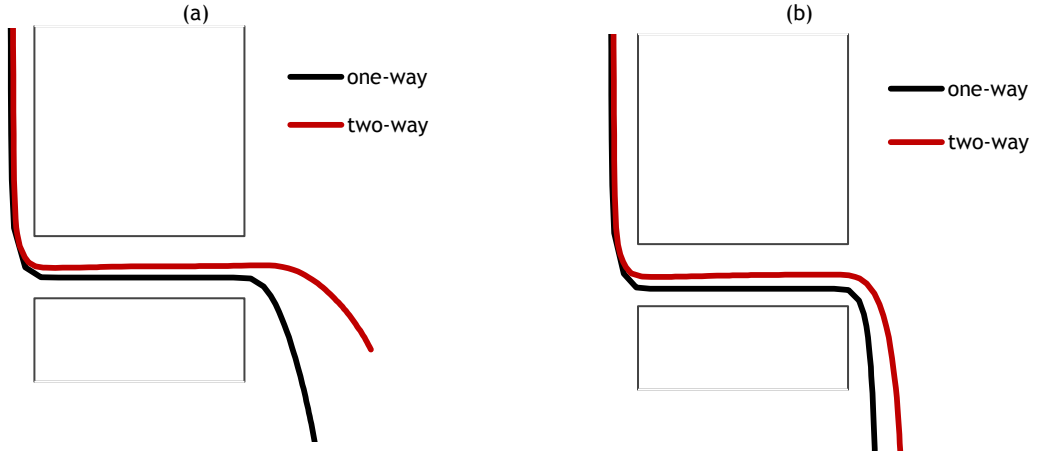

Figure B.1 – Trajectory of the released particle, in a selected part of the device, solved by an one-way and two way approach for (a) *VR* = 100 and (b) *VR* = 10.

Annex C – Grid independence test

In order to guarantee that the obtained results do not depend on the selected grid, three meshes were considered in a device with a 30 μm-wide feed channel, to study the velocity field. The time-dependent step of the simulations does not depend directly on the mesh. Therefore the model applied on this stage was simplified into a single stationary step to solve only the fluid flow.

Since the geometry repeats itself as more channels are added, the study of grid independence was performed with five microchannels. Moreover, higher gradients in the velocity field are expected for higher feed channel inlet average velocities and for higher velocity ratio (ratio between feed channel and waste channel inlet average velocity) values. Hence, one selected the highest velocity (U_f = 1 mm·s^{-1}) and the highest velocity ratio (VR = 100).

The meshes were built based on the maximum element size (MES) in each region of the device. For that reason a variable n_i (where i is feed channel, waste channel or microchannel, accordingly) was created to estimate the number of points in a specific boundary. Mesh 1, mesh 2 and mesh 3 indicate the increasing on the number of mesh elements in the domain, i.e. mesh 3 has finer elements than mesh 1. In all meshes, the maximum element size in the mesh elements near the wall boundaries was set to 0.95 x W_f/n_f, 0.95 x W_w/n_w and 0.95 x W_m/n_m on the feed channel walls, waste channel walls and microchannels walls, respectively. On the feed channel area, waste channel area and microchannels area, MES was set to W_f/n_f, W_w/n_w and W_m/n_m. Figure C.2 shows the images of the tested meshes and close-ups of the microchannel entrance area (with higher velocity gradients).

The estimated number of points on the channels was first set to 15 for the main channels and 10 for the microchannels (mesh 1). Then, two sub-regions of the main channel were created in each side of the device for further refinement of the elements (mesh 2), as seen in Figure 3.1b. In the region closer to the main channel walls (area a), maximum element size was defined as 1.5 x W_m/n_m and in the region closer to the microchannels (area c) as 2 x W_m/n_m. Additionally, n_m was increased to 15. Last, a mesh built in a similar way to mesh 2 but with n_f = n_w = 30 and n_m= 20 was tested (mesh 3). To evaluate the adequacy of the selected mesh, mass imbalance, maximum velocity of the domain, pressure difference between inlet and outlet of the main channels, pressure difference on the five microchannels, Reynolds number and Stokes number on the main and on the first microchannel, were computed (Table C.1) and velocity profiles on lines A', B', C' (Figure A.1b) and on the middle length line of microchannel M_1 were monitored (Figure C.1). From Figure C.1a one concludes that mesh 1 does not have enough elements on the feed channel, near the microchannels and from Figure C.1d that needs more elements on the feed channel, near the wall opposite to the microchannels. Moreover, mesh 1 should have more elements in the microchannels to describe the velocity profile (Figure C.1c). By analysing Figure C.1 and Table C.1 one concludes that the maximum element size relations utilized in mesh 2 are adequate for this study.

Table C.1 – Mass imbalance, global maximum velocity, pressure difference between inlet and outlet of the main channels, pressure difference on the five microchannels, Reynolds number and Stokes number on feed channel, waste channel and microchannel M1 values for meshes 1, 2 and 3, respective number of grid elements and computational time. The relative difference (ε) of the obtained variables (U_{max}, ΔP_{feed}, ΔP_{waste}, ΔP_{Mi}, Re_{feed}, Re_{waste}, Re_{Mi}, St_{feed}, St_{waste}, St_{Mi}) was determined for meshes 1 and 2 relatively to mesh 3.

–	n_f [-]	n_m [-]	MES (area a)	MES (area c)	# grid elements	t_{CPU}	Mass imbalance [%]	U_{max} [mm·s-1]	ΔP_{feed}[Pa]	ΔP_{waste} [Pa]
mesh 1	15	10	–	–	20 648	19s	0.05	1.32	441.1	27.4
ε [%]	–	–	–	–	–	–	–	*0.03%*	*0.01%*	*0.02%*
mesh 2	15	15	1.5*Wm/nm	2*Wm/nm	138 769	1min 24s	0.11	1.32	441.1	27.4
ε [%]	–	–	–	–	–	–	–	*0.01%*	*0.00%*	*0.02%*
mesh 3	35	25	1.5*Wm/nm	2*Wm/nm	339 306	8min 29s	0.11	1.32	441.1	27.4

–	ΔP_{M1}[Pa]	ΔP_{M2}[Pa]	ΔP_{M3}[Pa]	ΔP_{M4}[Pa]	ΔP_{M5}[Pa]	Re_{feed}	Re_{waste}	Re_{M1}	St_{feed}	St_{waste}	St_{M1}
mesh 1	107.5	87.0	70.5	56.2	43.7	2.9E-03	2.9E-05	1.4E-03	2.0E-05	2.0E-07	3.5E-05
ε [%]	*0.05%*	*0.06%*	*0.08%*	*0.08%*	*0.07%*	*0.00%*	*0.00%*	*0.01%*	*0.00%*	*0.00%*	*0.01%*
mesh 2	107.4	86.9	70.4	56.1	43.6	2.9E-03	2.9E-05	1.4E-03	2.0E-05	2.0E-07	3.5E-05
ε [%]	*0.06%*	*0.10%*	*0.08%*	*0.08%*	*0.12%*	*0.00%*	*0.00%*	*0.02%*	*0.00%*	*0.00%*	*0.02%*
mesh 3	107.5	87.0	70.4	56.1	43.7	2.9E-03	2.9E-05	1.4E-03	2.0E-05	2.0E-07	3.5E-05

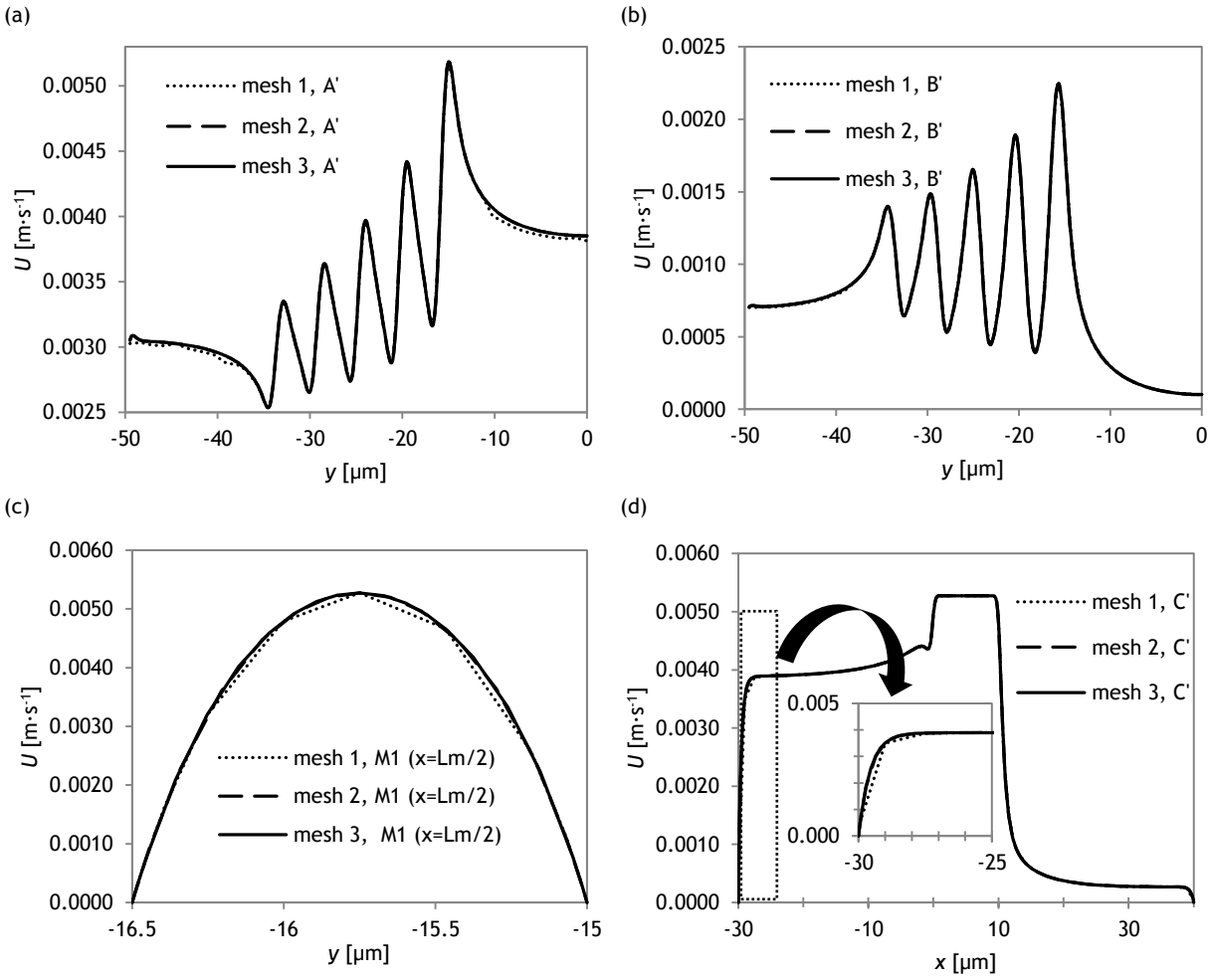

Figure C.1 – Velocity profile along *y* near the microchannel edges, (a) on the feed channel side/line A' and (b) on the waste channel side/line B', and (c) on the middle length line of microchannel M_1. Velocity (d) along *x* for line C'/line that crosses the middle width of the microchannel M_1.

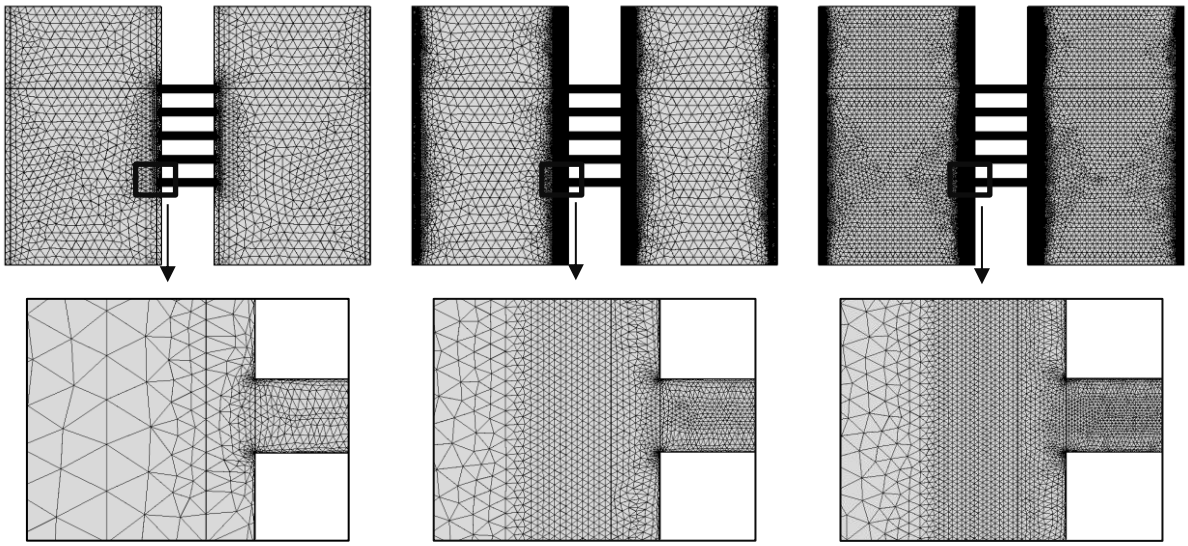

Mesh 1 Mesh 2 Mesh 3

Figure C.2 – Meshes used in the grid independence test for the stationary state study and respective close-ups of the highlighted region. Mesh refinement increases from left to right.

Annex D – Time-step dependence test

The numerical results in a transient study should be independent of the chosen space and time discretization. Particle trajectory depends on the position determined in the previous solution time. Therefore, the results might be affected by time-step selection.

In order to guarantee that the obtained results do not depend on the selected time-step, a parametric simulation of the time-step was performed for Δt = 0.05, 0.1, 0.5 and 1 ms. 5 particles were released (space between particles sp = 2 μm) from the inlet of a 30 μm feed channel into a microdevice with 5 microchannels (space between microchannels L_{sp} = 3 μm). The average fluid velocity at the inlet was set to 1 mm·s^{-1} for a ratio between inlet average velocities from feed and waste channel of 100. The trajectory of the two first particles was monitored (Figure D.1). For Δt = 0.05, 0.1, 0.5 and 1 ms the computational time for the transient step was 131, 42, 34 and 13 s, respectively. In Figure D.1a and Figure D.1b it is shown that Δt = 1 ms is too high to describe the accurate trajectory of the particle. Based on the computational cost and the trajectory of the particle, a time-step of 0.1 ms was selected.

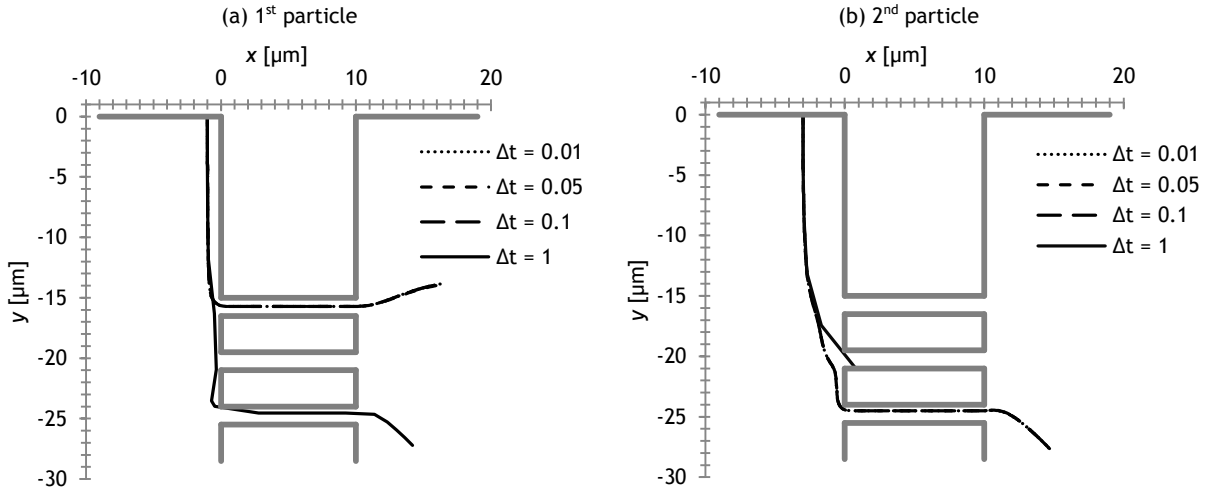

Figure D.1 – Trajectory of the (a) first and (b) second released particle on the time-step independence test for Δt = 0.05, 0.1, 0.5 and 1 ms.

Annex E – Particle motion

In the presented model, two study steps are considered, one stationary for fluid flow and one transient for particle motion. However, as Stokes number in the simulations is much inferior than 1, the particle trajectory should match the location of the fluid streamlines (Wu et al., 2009). A numeric simulation using both study steps for the base model device (presented in section 2.1.3) supports this assumption. In Figure E.1 it is shown the fluid streamlines in red and the matching particles trajectories in grey.

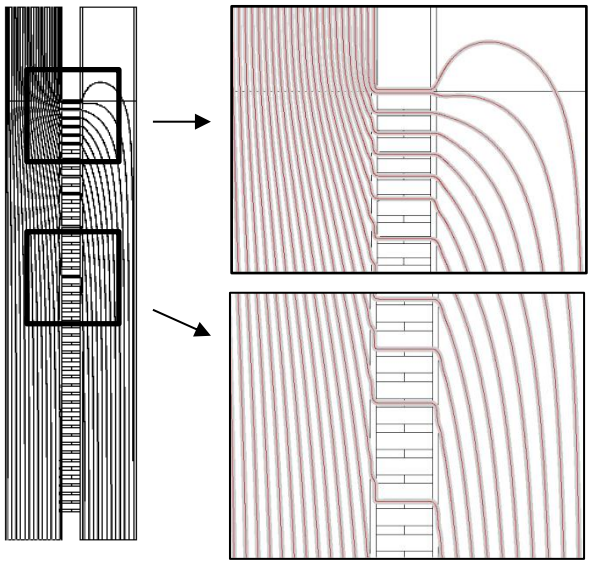

Figure E.1 – Matching fluid streamlines (red) and particles trajectories (grey) for the base device model.

By using the original model (i.e. two study steps) the number of particles that crosses the microchannels can be determined automatically. The variable "total number of particles in selection", *fpt.Nsel,* evaluates the number of particles in a domain selection. Since, on these studies, the particles are not actually trapped in the microchannels (they carry on to the waste channel), one selected the domains microchannel and waste channel to evaluate the number of particles that pass through the microchannels. If the model is resumed to the single stationary step, one has to count the particles manually (by counting the number of flow streamlines).

Despite the original model being more automated, each simulation takes more time. For example, for the base device model, and a solution time of 900 ms for the transient step, the simulation time was of 23min and 34s while the simplified model took 9min to solve the fluid flow.

In this study the simplified model was selected considering the time of the project. For other studies an evaluation between simulation time and post-processing effort must be done.

Annex F – Determination of L_{crit}

In this study, it was considered that when the pressure difference between microchannels edges was zero, the velocity near the microchannels on the feed and waste sides were approximately the same. Therefore the equivalent *y*-coordinate was determined by comparing the velocity between the lines A' and B' (FigureA.1b); a relative difference of 1% was assumed. L_{crit} corresponds to the value of the y-coordinate. In Figure F.1a (relative to Case I) one can observe that equality of velocities in both lines is not reached. Therefore there is possibility of trapping in all the microchannels. However, in Figure F.1b (relative to Case II) on sees that after a certain device length, velocities are the same, i.e. velocity in line A' is smaller than the velocity plus 1% in line B'.

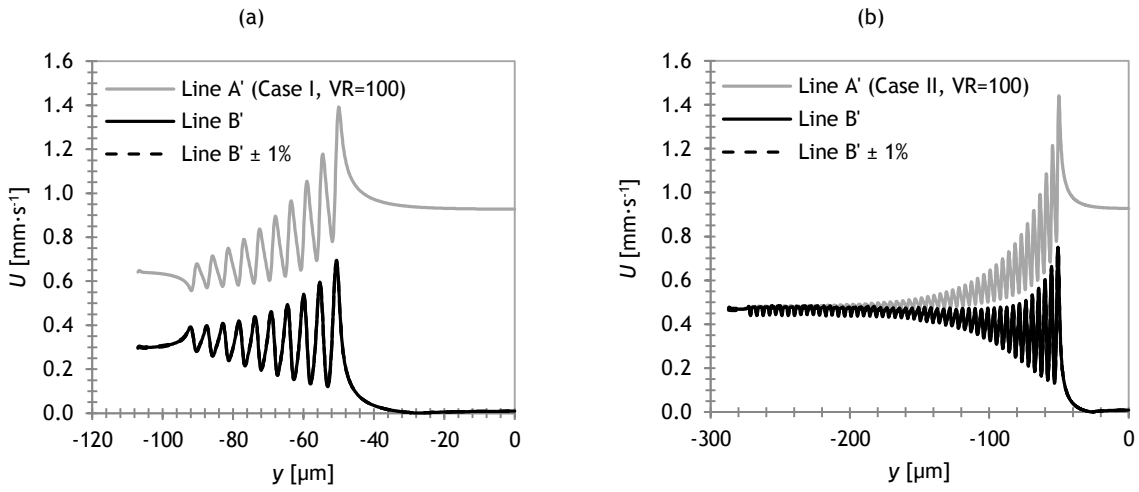

Figure F.1 – Velocity along A' and B' lines for (a) Case I and (b) Case II. Labelling of lines according to Figure A.1b.

Annex G – Formulae

The equations applied throughout this study to evaluate mass flow rates, mass and molar imbalances, pressure differences, Reynolds number and Stokes number are given in this section.

Mass flow rate is given by the surface integral in the cross-sectional area of the fluid velocity times its density. Since 2D simulations were performed, the integrals were evaluated along lines, in the width direction. Therefore mass flow rate was determined by:

$$Q = \iint \rho U \, \mathrm{d}A \equiv \int_0^{w_i} \rho U H \, \mathrm{d}x = \rho H \int_0^{w_i} U \, \mathrm{d}x \qquad \textbf{Equation G.1}$$

In order to ensure conservation of mass, the difference between inlet total mass flow rate and outlet total mass flow rate should be negligible. Thus, mass imbalance (Equation G.2) was determined for each simulation. For the conservation of species quantity, molar imbalances were determined by Equation G.3.

$$\text{mass imbalance } (\%) = \frac{|Q_{\text{in}} - Q_{\text{out}}|}{Q_{\text{in}}} \times 100 \qquad \textbf{Equation G.2}$$

$$\text{molar imbalance } (\%) = \frac{|C_{\text{in}} Q_{\text{in}} - C_{\text{out}} Q_{\text{out}}|}{C_{\text{in}} Q_{\text{in}}} \times 100 \qquad \textbf{Equation G.3}$$

The pressure drop along the main channels was evaluated by the difference between the average relative pressure on the inlet and the average relative pressure on the outlet (Equation G.4). In the microchannels, the pressure drop was determined by the difference between average relative pressure on the edge near the feed channel and the average relative pressure on the opposite edge (Equation G.5).

$$\Delta P_i = \int_0^{w_i} P_{y=-L_{\text{in}}} \, \mathrm{d}x - \int_0^{w_i} P_{y=L_{\mu}+L_{\text{out}}} \, \mathrm{d}x \,, \quad \mathrm{i} = \text{feed, waste} \qquad \textbf{Equation G.4}$$

$$\Delta P_{M_i} = \int_{(W_m+L_{sp})\times(i-1)}^{W_m\times\, i+L_{sp}\times(i-1)} P_{x=0} \, \mathrm{d}y - \int_{(W_m+L_{sp})\times(i-1)}^{W_m\times\, i+L_{sp}\times(i-1)} P_{x=L_m} \, \mathrm{d}y \,, \qquad \textbf{Equation G.5}$$

$$i = 1, 2, \ldots, num$$

Reynolds number (Equation G.6) and Stokes number (Equation G.7) on the main channels and on the microchannels were determined based on the inlet average velocity and middle length line average velocity, respectively.

$$\mathrm{Re} = \frac{\rho_{\mathrm{f}} U_{\text{aver}} D_{\mathrm{h}}}{\mu} \qquad \textbf{Equation G.6}$$

$$\mathrm{St} = \frac{\rho_{\mathrm{p}} (d_{\mathrm{p}})^2 U_{\text{aver}}}{18 \mu D_{\mathrm{h}}} \qquad \textbf{Equation G.7}$$

Annex H – Data

After each simulation, the automatically generated data (varying parameters values, pressure difference, Reynolds number, Stokes number, time range, mass and molar imbalances and percentage of trapped bacteria) was exported to an excel file. Manually, one registered the simulation times and, when applicable, the length from inlet to the point where null pressure in the microchannels is reached (effective trapping length). The obtained data is presented in Table H.1, Table H.2 and Table H.3 for the parametric studies and in Table H.4, Table H.5, Table H.6 for the mass transfer study.

Table H.1 – Values of inlet average velocities of the feed and waste channel, feed channel width, number of microchannels space between them, device length, density of microchannels and global maximum velocity for Cases I to XIX and base model, scaled down and narrower microdevice. [continues]

Case	Studied Parameter	*VR* [-]	U_f [mm·s^{-1}]	U_w [mm·s^{-1}]	W_f [µm]	N_μ [-]	L_{sp} [µm]	L_μ [µm]	N_μ/L_μ [µm^{-1}]	U_{max} [mm·s^{-1}]
		100	1	0.01	30	10	3	42	0.22	1.61
		50	1	0.02	30	10	3	42	0.22	1.59
		20	1	0.05	30	10	3	42	0.22	1.55
I	*VR*	10	1	0.10	30	10	3	42	0.22	1.46
		5	1	0.20	30	10	3	42	0.22	1.32
		2	1	0.50	30	10	3	42	0.22	1.16
		1	1	1.00	30	10	3	42	0.22	1.03
		100	1	0.01	30	50	3	222	0.22	1.75
		50	1	0.02	30	50	3	222	0.22	1.73
		20	1	0.05	30	50	3	222	0.22	1.68
II	*VR*	10	1	0.10	30	50	3	222	0.22	1.59
		5	1	0.20	30	50	3	222	0.22	1.41
		2	1	0.50	30	50	3	222	0.22	1.18
		1	1	1.00	30	50	3	222	0.22	1.03
		100	1	0.01	10	10	3	42	0.22	1.26
		50	1	0.02	10	10	3	42	0.22	1.25
		20	1	0.05	10	10	3	42	0.22	1.24
III	*VR*	10	1	0.10	10	10	3	42	0.22	1.22
		5	1	0.20	10	10	3	42	0.22	1.20
		2	1	0.50	10	10	3	42	0.22	1.14
		1	1	1.00	10	10	3	42	0.22	1.10
		100	1	0.01	10	50	3	222	0.22	1.27
		50	1	0.02	10	50	3	222	0.22	1.26
		20	1	0.05	10	50	3	222	0.22	1.25
IV	*VR*	10	1	0.10	10	50	3	222	0.22	1.23
		5	1	0.20	10	50	3	222	0.22	1.20
		2	1	0.50	10	50	3	222	0.22	1.14
		1	1	1.00	10	50	3	222	0.22	1.10
		100	1	0.01	30	50	3	222	0.22	1.75
		100	1	0.01	20	50	3	222	0.22	1.57
V	W_f	100	1	0.01	10	50	3	222	0.22	1.27
		100	1	0.01	5	50	3	222	0.22	1.22
		100	1	0.01	3	50	3	222	0.22	1.32
		2	1	0.50	30	50	3	222	0.22	1.18
		2	1	0.50	20	50	3	222	0.22	1.15
VI	W_f	2	1	0.50	10	50	3	222	0.22	1.14
		2	1	0.50	5	50	3	222	0.22	1.20
		2	1	0.50	3	50	3	222	0.22	1.32
		100	1	0.01	30	100	3	447	0.22	1.75
		100	1	0.01	30	50	3	222	0.22	1.75
VII	L_μ	100	1	0.01	30	20	3	87	0.22	1.74
		100	1	0.01	30	10	3	42	0.22	1.61
		100	1	0.01	30	5	3	20	0.22	1.32
		2	1	0.5	30	100	3	447	0.22	1.18
		2	1	0.5	30	50	3	222	0.22	1.18
VIII	L_μ	2	1	0.5	30	20	3	87	0.22	1.18
		2	1	0.5	30	10	3	42	0.22	1.16
		2	1	0.5	30	5	3	20	0.22	1.12

Table H.1 - Values of inlet average velocities of the feed and waste channel, feed channel width, number of microchannels space between them, device length, density of microchannels and global maximum velocity for Cases I to XIX and base model, scaled down and narrower microdevice. [continued]

Case	Studied Parameter	VR [-]	U_f [mm·s^{-1}]	U_w [mm·s^{-1}]	W_f [μm]	N_μ [-]	L_{sp} [μm]	L_μ [μm]	N_μ/L_μ [μm^{-1}]	U_{max} [mm·s^{-1}]
		100	1	0.01	30	29	3	128	0.22	1.75
IX	N_μ/ L_μ	100	1	0.01	30	43	1.5	128	0.33	1.45
		100	1	0.01	30	57	0.75	128	0.44	1.43
		100	1	0.01	10	29	3	128	0.22	1.27
X	N_μ/ L_μ	100	1	0.01	10	43	1.5	128	0.33	1.23
		100	1	0.01	10	57	0.75	128	0.44	1.23
		100	1	0.010	30	10	3	42	0.22	1.61
		100	0.5	0.005	30	10	3	42	0.22	0.81
XI	U_f	100	0.3	0.003	30	10	3	42	0.22	0.48
		100	0.1	0.001	30	10	3	42	0.22	0.16
		100	0.05	0.001	30	10	3	42	0.22	0.08
		100	1	0.010	10	10	3	42	0.22	1.26
		100	0.5	0.005	10	10	3	42	0.22	0.63
XII	U_f	100	0.3	0.003	10	10	3	42	0.22	0.38
		100	0.1	0.001	10	10	3	42	0.22	0.13
		100	0.05	0.001	10	10	3	42	0.22	0.06
		2	1	0.500	30	10	3	42	0.22	1.16
		2	0.5	0.250	30	10	3	42	0.22	0.58
XIII	U_f	2	0.3	0.150	30	10	3	42	0.22	0.35
		2	0.1	0.050	30	10	3	42	0.22	0.12
		2	0.05	0.025	30	10	3	42	0.22	0.06
		100	1	0.01	30	10	3	42	0.22	1.61
XIV	L_m	100	1	0.01	30	10	3	42	0.22	1.20
		100	1	0.01	30	10	3	42	0.22	1.11
		100	1	0.01	10	10	3	42	0.22	1.26
XV	L_m	100	1	0.01	10	10	3	42	0.22	1.16
		100	1	0.01	10	10	3	42	0.22	1.12
		20	1	0.05	30	10	3	42	0.22	1.55
XVI	L_m	20	1	0.05	30	10	3	42	0.22	1.19
		20	1	0.05	30	10	3	42	0.22	1.11
		20	1	0.05	10	10	3	42	0.22	1.24
XVII	L_m	20	1	0.05	10	10	3	42	0.22	1.15
		20	1	0.05	10	10	3	42	0.22	1.12
		1	1	1.00	30	10	3	42	0.22	1.03
XVIII	L_m	1	1	1.00	30	10	3	42	0.22	1.03
		1	1	1.00	30	10	3	42	0.22	1.03
		1	1	1.00	10	10	3	42	0.22	1.10
XIX	L_m	1	1	1.00	10	10	3	42	0.22	1.10
		1	1	1.00	10	10	3	42	0.22	1.10
base model	W_f	100	1	0.01	30	50	3	222	0.22	1.75
scaled down	W_f	100	1	0.01	10	50	1	74	0.67	1.75
narrower device	W_f	100	1	0.01	10 (=W_w)	50	3	222	0.22	1.19

Table H.2 – Values of the inlet flow rates in the feed and waste channel, pressure drop in the feed channel, waste channel and microchannel M1, percentage of trapped b, effective and ineffective length values for Cases I to XIX and base model, scaled down and narrower microdevice. [continues]

Case	Studied Parameter		Q_f [nl·min^{-1}]	Q_w [nl·min^{-1}]	ΔP_f [Pa]	ΔP_w [Pa]	ΔP_{M1} [Pa]	% trap. bacteria	L_{crit} [µm]	$(L_\mu - L_{crit})/L_\mu$ x100
		100	2.70	0.027	519.3	73.8	131.6	28	-	0.0
		50	2.70	0.054	520.0	79.0	130.2	28	-	0.0
		20	2.70	0.135	522.0	94.6	126.3	28	-	0.0
I	*VR*	10	2.70	0.27	525.5	120.5	119.6	28	-	0.0
		5	2.70	0.54	532.3	172.3	106.3	24	-	0.0
		2	2.70	1.35	552.9	327.9	66.5	16	-	0.0
		1	2.70	2.7	587.2	587.2	0.0	0	-	0.0
		100	2.70	0.027	1025.3	564.6	142.9	48	212	4.5
		50	2.70	0.054	1030.9	574.8	141.5	48	212	4.5
		20	2.70	0.135	1047.5	605.4	137.2	48	208	6.3
II	*VR*	10	2.70	0.27	1075.2	656.4	129.9	44	203	8.6
		5	2.70	0.54	1130.7	758.4	115.5	40	194	12.6
		2	2.70	1.35	1297.0	1064.3	72.2	24	172	22.5
		1	2.70	2.7	1574.2	1574.2	0.0	0	0	100.0
		100	0.90	0.027	471.8	53.5	101.1	60	-	0.0
		50	0.90	0.054	473.3	58.9	100.2	60	-	0.0
		20	0.90	0.135	477.6	75.2	97.3	56	-	0.0
III	*VR*	10	0.90	0.27	484.8	102.3	92.5	56	-	0.0
		5	0.90	0.54	499.2	156.5	82.8	48	-	0.0
		2	0.90	1.35	542.5	319.0	54.0	32	-	0.0
		1	0.90	2.7	614.7	590.0	5.8	8	-	0.0
		100	0.90	0.027	731.2	310.8	102.7	72	154	30.6
		50	0.90	0.054	740.1	323.7	101.7	72	154	30.6
		20	0.90	0.135	766.9	362.5	98.8	72	154	30.6
IV	*VR*	10	0.90	0.27	811.6	427.2	93.9	68	149	32.9
		5	0.90	0.54	901.0	556.5	84.1	56	140	36.9
		2	0.90	1.35	1169.0	944.4	54.8	40	118	46.8
		1	0.90	2.7	1615.8	1591.0	5.9	8	50	77.5
		30	2.70	0.027	1025.3	564.6	142.9	48	212	4.5
		20	1.80	0.027	910.2	467.1	128.5	60	190	14.4
V	W_f	10	0.90	0.027	731.2	310.8	102.7	72	154	30.6
		5	0.45	0.027	611.4	191.0	79.3	76	124	44.1
		3	0.27	0.027	585.0	130.0	65.3	84	92	58.6
		30	2.70	1.35	1297.0	1064.3	72.2	24	172	22.5
		20	1.80	1.35	1245.2	1018.3	65.8	32	149	32.9
VI	W_f	10	0.90	1.35	1169.0	944.4	54.8	40	118	46.8
		5	0.45	1.35	1131.0	888.0	45.6	48	92	58.6
		3	0.27	1.35	1148.9	859.2	41.2	56	74	66.7
		447	2.70	0.027	1648.4	1187.7	142.9	48	212	52.6
		222	2.70	0.027	1025.3	564.6	142.9	48	212	4.5
VII	L_μ	87	2.70	0.027	650.8	191.5	142.0	44	-	0.0
		42	2.70	0.027	519.3	73.8	131.6	28	-	0.0
		20	2.70	0.027	441.1	27.4	107.5	16	-	0.0
		447	2.70	1.35	2222.3	1989.6	72.2	24	171	61.7
		222	2.70	1.35	1297.0	1064.3	72.2	24	171	23.0
VIII	L_μ	87	2.70	1.35	741.5	509.5	71.7	24	-	0.0
		42	2.70	1.35	552.9	327.9	66.5	16	-	0.0
		20	2.70	1.35	452.3	243.4	54.3	8	-	0.0
		0.22	2.70	0.027	763.6	303.0	142.8	48	-	0.0
IX	N_μ / L_μ	0.33	2.70	0.027	750.0	316.1	118.2	48	-	0.0
		0.44	2.70	0.027	741.9	323.6	103.1	48	-	0.0
		0.22	0.90	0.027	595.9	175.4	102.7	72	-	0.0
X	N_μ / L_μ	0.33	0.90	0.027	580.9	179.8	85.3	72	127	0.4
		0.44	0.90	0.027	571.9	182.3	74.6	72	109	14.5
		1.00	2.70	0.027	519.3	73.8	131.6	28	-	0.0
		0.50	1.35	0.014	259.6	36.9	65.8	28	-	0.0
XI	U_f	0.30	0.81	0.008	155.8	22.1	39.5	28	-	0.0
		0.10	0.27	0.003	51.9	7.4	13.2	28	-	0.0
		0.05	0.14	0.001	26.0	3.7	6.6	28	-	0.0
		1.00	0.90	0.027	471.8	53.5	101.1	60	-	0.0
		0.50	0.45	0.014	235.9	26.8	50.6	60	-	0.0
XII	U_f	0.30	0.27	0.008	141.5	16.1	30.3	60	-	0.0
		0.10	0.09	0.003	47.2	5.4	10.1	60	-	0.0
		0.05	0.05	0.001	23.6	2.7	5.1	60	-	0.0

Table H.2 - Values of the inlet flow rates in the feed and waste channel, pressure drop in the feed channel, waste channel and microchannel M1, percentage of trapped b, effective and ineffective length values for Cases I to XIX and base model, scaled down and narrower microdevice. [continued]

Case	Studied Parameter		Q_f [nl·min^{-1}]	Q_w [nl·min^{-1}]	ΔP_f [Pa]	ΔP_w [Pa]	ΔP_{M1} [Pa]	% trap. bacteria	L_{crit} [µm]	$(L_\mu - L_{crit})/L_\mu$ x100
XIII	U_f	1.00	2.70	1.35	552.9	327.9	66.5	16	-	0.0
		0.50	1.35	0.675	276.5	164.0	33.2	16	-	0.0
		0.30	0.81	0.405	165.9	98.4	19.9	16	-	0.0
		0.10	0.27	0.135	55.3	32.8	6.6	16	-	0.0
		0.05	0.14	0.0675	27.6	16.4	3.3	16	-	0.0
XIV	L_m	10	2.7	0.027	519	74	132	28	-	0.0
		25	2.7	0.027	543	50	195	20	-	0.0
		50	2.7	0.027	560	34	236	12	-	0.0
XV	L_m	10	0.9	0.027	472	54	101	60	-	0.0
		25	0.9	0.027	513	41	163	44	-	0.0
		50	0.9	0.027	547	30	213	32	-	0.0
XVI	L_m	10	2.7	0.135	522	95	126	28	-	0.0
		25	2.7	0.135	545	71	187	20	-	0.0
		50	2.7	0.135	561	56	227	12	-	0.0
XVII	L_m	10	0.9	0.135	478	75	97	56	-	0.0
		25	0.9	0.135	517	63	157	44	-	0.0
		50	0.9	0.135	549	53	205	32	-	0.0
XVIII	L_m	10	2.7	2.700	587	587	0	0	-	0.0
		25	2.7	2.700	587	587	0	0	-	0.0
		50	2.7	2.700	587	587	0	0	-	0.0
XIX	L_m	10	0.9	2.700	615	590	6	8	-	0.0
		25	0.9	2.700	617	589	9	4	-	0.0
		50	0.9	2.700	619	589	12	4	-	0.0
base model	W_f	30	2.70	0.027	1025	564	142	48	212	4.5
scaled down	W_f	10	0.30	0.003	3076	1693	428	48	64	13.1
narrower device	W_f	10 (=W_w)	0.90	0.009	1038	647	82	48	109	50.9

Table H.3 – Simulation time, computation time, mass imbalance, Reynolds number and Stokes number for feed channel, waste channel and microchannel M1, and respective studied parameter for Cases I to XIX and base model, scaled down and narrower microdevice. [continues]

Case	Studied Parameter		t_{CPU}	Mass imbalance [%]	Re_{feed}	Re_{waste}	Re_{M1}	St_{feed}	St_{waste}	St_{M1}
I	*VR*	100	19min 20s	0.11	2.9E-03	2.9E-05	1.7E-03	2.0E-05	2.0E-07	4.3E-05
		50		0.11	2.9E-03	5.7E-05	1.7E-03	2.0E-05	4.0E-07	4.3E-05
		20		0.11	2.9E-03	1.4E-04	1.6E-03	2.0E-05	1.0E-06	4.1E-05
		10		0.11	2.9E-03	2.9E-04	1.5E-03	2.0E-05	2.0E-06	3.9E-05
		5		0.11	2.9E-03	5.7E-04	1.4E-03	2.0E-05	4.0E-06	3.5E-05
		2		0.10	2.9E-03	1.4E-03	8.5E-04	2.0E-05	1.0E-05	2.2E-05
		1		0.10	2.9E-03	2.9E-03	1.7E-09	2.0E-05	2.0E-05	4.5E-11
II	*VR*	100	1h 0min 29s	0.10	2.9E-03	2.9E-05	1.8E-03	2.0E-05	2.0E-07	4.7E-05
		50		0.10	2.9E-03	5.7E-05	1.8E-03	2.0E-05	4.0E-07	4.6E-05
		20		0.10	2.9E-03	1.4E-04	1.8E-03	2.0E-05	1.0E-06	4.5E-05
		10		0.10	2.9E-03	2.9E-04	1.7E-03	2.0E-05	2.0E-06	4.3E-05
		5		0.10	2.9E-03	5.7E-04	1.5E-03	2.0E-05	4.0E-06	3.8E-05
		2		0.10	2.9E-03	1.4E-03	9.2E-04	2.0E-05	1.0E-05	2.4E-05
		1		0.10	2.9E-03	2.9E-03	5.0E-08	2.0E-05	2.0E-05	1.3E-09
III	*VR*	100	18min 39s	0.19	2.6E-03	2.9E-05	1.3E-03	2.2E-05	2.0E-07	3.3E-05
		50		0.19	2.6E-03	5.7E-05	1.3E-03	2.2E-05	4.0E-07	3.3E-05
		20		0.19	2.6E-03	1.4E-04	1.2E-03	2.2E-05	1.0E-06	3.2E-05
		10		0.18	2.6E-03	2.9E-04	1.2E-03	2.2E-05	2.0E-06	3.0E-05
		5		0.18	2.6E-03	5.7E-04	1.1E-03	2.2E-05	4.0E-06	2.7E-05
		2		0.17	2.6E-03	1.4E-03	6.9E-04	2.2E-05	1.0E-05	1.8E-05
		1		0.16	2.6E-03	2.9E-03	7.4E-05	2.2E-05	2.0E-05	1.9E-06
IV	*VR*	100	1h 0min 23s	0.16	2.6E-03	2.9E-05	1.3E-03	2.2E-05	2.0E-07	3.4E-05
		50		0.16	2.6E-03	5.7E-05	1.3E-03	2.2E-05	4.0E-07	3.3E-05
		20		0.16	2.6E-03	1.4E-04	1.3E-03	2.2E-05	1.0E-06	3.2E-05
		10		0.16	2.6E-03	2.9E-04	1.2E-03	2.2E-05	2.0E-06	3.1E-05
		5		0.16	2.6E-03	5.7E-04	1.1E-03	2.2E-05	4.0E-06	2.8E-05
		2		0.16	2.6E-03	1.4E-03	7.0E-04	2.2E-05	1.0E-05	1.8E-05
		1		0.16	2.6E-03	2.9E-03	7.5E-05	2.2E-05	2.0E-05	1.9E-06
V	W_f	30	-	0.10	2.9E-03	2.9E-05	1.8E-03	2.0E-05	2.0E-07	4.7E-05
		20	12min 38s	0.13	2.8E-03	2.9E-05	1.6E-03	2.1E-05	2.0E-07	4.2E-05
		10	-	0.16	2.6E-03	2.9E-05	1.3E-03	2.2E-05	2.0E-07	3.4E-05
		5	8min 14s	0.18	2.3E-03	2.9E-05	1.0E-03	2.5E-05	2.0E-07	2.6E-05
		3	6min 46s	0.18	2.0E-03	2.9E-05	8.4E-04	2.9E-05	2.0E-07	2.1E-05
VI	W_f	30	-	0.10	2.9E-03	1.4E-03	9.2E-04	2.0E-05	1.0E-05	2.4E-05
		20	14min 46s	0.13	2.8E-03	1.4E-03	8.4E-04	2.1E-05	1.0E-05	2.2E-05
		10	-	0.16	2.6E-03	1.4E-03	7.0E-04	2.2E-05	1.0E-05	1.8E-05
		5	17min 23s	0.18	2.3E-03	1.4E-03	5.8E-04	2.5E-05	1.0E-05	1.5E-05
		3	13min 12s	0.18	2.0E-03	1.4E-03	5.3E-04	2.9E-05	1.0E-05	1.4E-05
VII	L_μ	447	16min 37s	0.10	2.9E-03	2.9E-05	1.8E-03	2.0E-05	2.0E-07	4.7E-05
		222		0.10	2.9E-03	2.9E-05	1.8E-03	2.0E-05	2.0E-07	4.7E-05
		87		0.10	2.9E-03	2.9E-05	1.8E-03	2.0E-05	2.0E-07	4.7E-05
		42		0.11	2.9E-03	2.9E-05	1.7E-03	2.0E-05	2.0E-07	4.3E-05
		20		0.10	2.9E-03	2.9E-05	1.4E-03	2.0E-05	2.0E-07	3.5E-05
VIII	L_μ	447	23min 45s	0.10	2.9E-03	1.4E-03	9.2E-04	2.0E-05	1.0E-05	2.4E-05
		222		0.10	2.9E-03	1.4E-03	9.2E-04	2.0E-05	1.0E-05	2.4E-05
		87		0.10	2.9E-03	1.4E-03	9.2E-04	2.0E-05	1.0E-05	2.4E-05
		42		0.10	2.9E-03	1.4E-03	8.5E-04	2.0E-05	1.0E-05	2.2E-05
		20		0.10	2.9E-03	1.4E-03	6.9E-04	2.0E-05	1.0E-05	1.8E-05
IX	N_μ/ L_μ	0.22	26min 53s	0.10	2.9E-03	2.9E-05	1.8E-03	2.0E-05	2.0E-07	4.7E-05
		0.33		0.10	2.9E-03	2.9E-05	1.5E-03	2.0E-05	2.0E-07	3.9E-05
		0.44		0.10	2.9E-03	2.9E-05	1.3E-03	2.0E-05	2.0E-07	3.4E-05
X	N_μ/ L_μ	0.22	23min 1s	0.16	2.6E-03	2.9E-05	1.3E-03	2.2E-05	2.0E-07	3.4E-05
		0.33		0.16	2.6E-03	2.9E-05	1.1E-03	2.2E-05	2.0E-07	2.8E-05
		0.44		0.16	2.6E-03	2.9E-05	9.5E-04	2.2E-05	2.0E-07	2.5E-05
XI	U_f	1.00	13min 41s	0.11	2.9E-03	2.9E-05	1.7E-03	2.0E-05	2.0E-07	4.3E-05
		0.50		0.11	1.4E-03	1.4E-05	8.4E-04	1.0E-05	1.0E-07	2.2E-05
		0.30		0.11	8.6E-04	8.6E-06	5.0E-04	6.1E-06	6.1E-08	1.3E-05
		0.10		0.11	2.9E-04	2.9E-06	1.7E-04	2.0E-06	2.0E-08	4.3E-06
		0.05		0.11	1.4E-04	1.4E-06	8.4E-05	1.0E-06	1.0E-08	2.2E-06
XII	U_f	1.00	14min 4s	0.19	2.6E-03	2.9E-05	1.3E-03	2.2E-05	2.0E-07	3.3E-05
		0.50		0.19	1.3E-03	1.4E-05	6.5E-04	1.1E-05	1.0E-07	1.7E-05
		0.30		0.19	7.8E-04	8.6E-06	3.9E-04	6.6E-06	6.1E-08	1.0E-05
		0.10		0.19	2.6E-04	2.9E-06	1.3E-04	2.2E-06	2.0E-08	3.3E-06
		0.05		0.19	1.3E-04	1.4E-06	6.5E-05	1.1E-06	1.0E-08	1.7E-06

Table H.3 - Simulation time, computation time, mass imbalance, Reynolds number and Stokes number for feed channel, waste channel and microchannel M1, and respective studied parameter for Cases I to XIX and base model, scaled down and narrower microdevice. [continued]

Case	Studied Parameter		t_{CPU}	Mass imbalance [%]	Re_{feed}	Re_{waste}	Re_{M1}	St_{feed}	St_{waste}	St_{M1}
XIII	U_f	1.00	13min 45s	0.10	2.9E-03	1.4E-03	8.5E-04	2.0E-05	1.0E-05	2.2E-05
		0.50		0.10	1.4E-03	7.1E-04	4.2E-04	1.0E-05	5.1E-06	1.1E-05
		0.30		0.10	8.6E-04	4.3E-04	2.5E-04	6.1E-06	3.0E-06	6.5E-06
		0.10		0.10	2.9E-04	1.4E-04	8.5E-05	2.0E-06	1.0E-06	2.2E-06
		0.05		0.10	1.4E-04	7.1E-05	4.2E-05	1.0E-06	5.1E-07	1.1E-06
XIV	L_m	10	69min 9s	0.11	2.9E-03	2.9E-05	1.7E-03	2.0E-05	2.0E-07	4.3E-05
		25		0.10	2.9E-03	2.9E-05	1.0E-03	2.0E-05	2.0E-07	2.6E-05
		50		0.10	2.9E-03	2.9E-05	6.1E-04	2.0E-05	2.0E-07	1.6E-05
XV	L_m	10		0.19	2.6E-03	2.9E-05	1.3E-03	2.2E-05	2.0E-07	3.3E-05
		25		0.22	2.6E-03	2.9E-05	8.4E-04	2.2E-05	2.0E-07	2.1E-05
		50		0.26	2.6E-03	2.9E-05	5.5E-04	2.2E-05	2.0E-07	1.4E-05
XVI	L_m	10		0.11	2.9E-03	1.4E-04	1.6E-03	2.0E-05	1.0E-06	4.1E-05
		25		0.10	2.9E-03	1.4E-04	9.6E-04	2.0E-05	1.0E-06	2.5E-05
		50		0.10	2.9E-03	1.4E-04	5.8E-04	2.0E-05	1.0E-06	1.5E-05
XVII	L_m	10		0.19	2.6E-03	1.4E-04	1.2E-03	2.2E-05	1.0E-06	3.2E-05
		25		0.21	2.6E-03	1.4E-04	8.0E-04	2.2E-05	1.0E-06	2.1E-05
		50		0.24	2.6E-03	1.4E-04	5.3E-04	2.2E-05	1.0E-06	1.4E-05
XVIII	L_m	10		0.10	2.9E-03	2.9E-03	1.7E-09	2.0E-05	2.0E-05	4.5E-11
		25		0.10	2.9E-03	2.9E-03	1.8E-09	2.0E-05	2.0E-05	4.7E-11
		50		0.10	2.9E-03	2.9E-03	3.1E-09	2.0E-05	2.0E-05	7.9E-11
XIX	L_m	10		0.16	2.6E-03	2.9E-03	7.4E-05	2.2E-05	2.0E-05	1.9E-06
		25		0.16	2.6E-03	2.9E-03	4.8E-05	2.2E-05	2.0E-05	1.2E-06
		50		0.16	2.6E-03	2.9E-03	3.2E-05	2.2E-05	2.0E-05	8.1E-07
base model	W_f	30	9min 20s	0.10	2.9E-03	2.9E-05	1.8E-03	2.0E-05	2.0E-07	4.7E-05
scaled down	W_f	10	12min 13s	0.10	9.5E-04	9.5E-06	6.1E-04	6.1E-05	6.1E-07	1.4E-04
narrower device	W_f	10 (=W_w)	14min 50s	0.33	2.6E-03	2.6E-05	1.0E-03	2.2E-05	2.2E-07	2.7E-05

Table H.4 – Values of inlet average velocities of the feed and waste channel, feed channel width, number of microchannels and space between them, device length, density of microchannels and glucose concentration at the feed inlet for mass transfer studies, considering hydrodynamic trapping (*VR* = 1) and physical trapping (*VR* = 100).

Case	*VR* [-]	U_f [mm·s-1]	U_w [mm·s-1]	W_f [μm]	N_μ [-]	L_{sp} [μm]	L_μ [μm]	N_μ/L_μ [μm^{-1}]	$C_{in,feed}$ [M]
hydrodynamic trapping	1	1.00	1.00	30	3	3.00	10.5	0.22	100
physical trapping	100	1.00	0.01	30	3	3.00	10.5	0.22	100

Table H.5 – Values of the inlet flow rates in the feed and waste channel, pressure drop in the feed channel, waste channel and microchannel M1, average concentration at microchannel inlet, average concentration at microchannel outlet and average concentration at bacteria surface, for the case considering hydrodynamic trapping (*VR* = 1) and physical trapping (*VR* = 100).

Case	Q_f [nl·min^{-1}]	Q_w [nl·min^{-1}]	ΔP_f [Pa]	ΔP_w [Pa]	ΔP_{M1} [Pa]	$C_{aver,\mu entrance}$ (t_{ss}) [M]	$C_{aver,\mu outlet}$ (t_{ss}) [M]	$C_{aver,bacteriasurface}$ (t_{ss}) [M]
hydrodynamic trapping (*VR* = 1)	2.70	2.70	414.5	414.5	0.0	93.6	6.4	50.0
Physical trapping (*VR* = 100)	2.70	0.027	411.1	7.5	120.0	100.0	83.4	98.7

Table H.6 – Simulation time for transient studies (time step of 2.5 ms and time range of 700 ms) and stationary studies, mass and molar imbalances and Reynolds number for feed channel, waste channel and microchannel M1, for the case considering hydrodynamic trapping (*VR* = 1) and physical trapping (*VR* = 100).

Case	$t_{CPU,\ transient}$	$t_{CPU,\ stationary}$	Mass Imbalance [%]	Molar Imbalance [%]	Re_{feed} [-]	Re_{waste} [-]
hydrodynamic trapping (*VR* = 1)	1h 41min 52s	14min 35s	0.10	0.10	2.9E-03	2.9E-03
Physical trapping (*VR* = 100)			0.10	0.30	2.9E-03	2.9E-05